Technical Report

TR-06-16

Geochemical evolution of the near field of a KBS-3 repository

David Arcos, Fidel Grandia, Cristina Domènech
Enviros, Spain

September 2006

Svensk Kärnbränslehantering AB
Swedish Nuclear Fuel
and Waste Management Co
Box 5864
SE-102 40 Stockholm Sweden
Tel 08-459 84 00
+46 8 459 84 00
Fax 08-661 57 19
+46 8 661 57 19

Geochemical evolution of the near field of a KBS-3 repository

David Arcos, Fidel Grandia, Cristina Domènech
Enviros, Spain

September 2006

This report concerns a study which was conducted for SKB. The conclusions and viewpoints presented in the report are those of the authors and do not necessarily coincide with those of the client.

A pdf version of this document can be downloaded from www.skb.se

Abstract

The Swedish concept developed by SKB for deep radioactive waste disposal, envisages an engineered multi-barrier system surrounding the nuclear waste (near field). In the present study we developed a numerical model to assess the geochemical evolution of the near field in the frame of the SKB's safety assessment SR-Can. These numerical models allow us to predict the long-term geochemical evolution of the near field system by means of reactive-transport codes and the information gathered in underground laboratory experiments and natural analogues. Two different scenarios have been defined to model this near field evolution, according to the pathway used by groundwater to contact the near field: a) through a fracture in the host rock intersecting the deposition hole; and b) through the material used to backfill the deposition tunnel. Moreover, we also modelled the effect of different groundwater compositions reaching the near field, as the up-rise of deep-seated brines and the intrusion of ice-melting derived-groundwater. We also modelled the effect of the thermal stage due to the heat generated by spent fuel on the geochemical evolution of the bentonite barrier.

Sammanfattning

I det svenska systemet för slutförvaring av radioaktivt avfall, som har utvecklats av SKB, förutsätts ett tekniskt konstruerat multibarriär system runt avfallet (närområdet). I den här studien har vi utvecklat en numerisk modell för att beskriva den geokemiska utvecklingen i närområdet inom ramen för SKB:s säkerhetsanalys SR-Can. Den numeriska modellen medger oss att prediktera den långsiktiga geokemiska utvecklingen i närområdet med hjälp av ett reaktiv-transport datorprogram och information från underjordsexperiment och naturliga analogier. Två olika scenarier har definierats för att beskriva närområdesutvecklingen med avseende på hur grundvattnet kommer I kontakt med närområdet: a) genom en spricka som skär deponeringshålet; b) genom återfyllnadsmaterialet i tunnel. Utöver detta har vi också studerat effekten av att olika grundvattensammansättningar når närområdet, såsom intrång av salta vatten från djupet eller smältvatten från inlandsisar. Vi har också studerat vilken effekt den termiska perioden orsakad av värmen från avfallet har på den geokemiska utvecklingen i bentonitbarriären.

Contents

1 Introduction

Engineered barriers in deep geological repositories of high level nuclear waste (HLNW) are designed, among other mechanical aspects, to retard the intrusion of groundwater to the canisters and, in case of canister failure, to retard radionuclides in their way to the geosphere. Groundwater interaction with the components of the barrier will modify the composition of the groundwater that will eventually reach the canister. Knowledge of such a composition, especially of the master variables, pH and Eh, is very relevant in the repository performance assessment (PA), since it would control the solubility of radionuclides in case of isolation failure.

The Swedish Nuclear Fuel and Waste Management Co. (SKB) engineered a system for the deep final storage of the spent nuclear fuel (KBS-3). At present two sites in Sweden have been investigated as potential repository emplacements, Forsmark and Oskarshamn. Site investigations have focused mainly on the geological characterisation of host rocks (lithologies, structural patterns) and the hydrological and hydrogeochemical description of groundwater at different depths, their past evolution and present-day conditions /SKB 2004a/. These investigations are conducted to ensure that deep emplacements present low hydraulically conductivity, as well as to characterise the composition of the deep groundwaters.

In this study, we assess the processes that would affect the near field geochemistry in a deep HLNW repository hypothetically sited at Forsmark or Simpevarp. However, as both sites correspond to granitic environments, no significant differences are expected, and we will focus on the Forsmark site.

1.1 Objectives

Hydrological and geological information of the emplacement is implemented in a geochemical model that will help to evaluate the behaviour of the bentonite barrier. The model includes a set of geochemical processes of importance for the interaction between groundwater and the bentonite barrier, such as precipitation/dissolution of solid phases, cation exchange and surface acidity reactions in the clay fraction of the bentonite. The analysis of the results will allow the determination of the processes controlling the chemistry of the system.

Modelling results are expected to give information on the evolution of the following geochemical parameters and processes:

- Evolution of the pH of the system and the processes that govern such evolution.
- Evolution of the redox capacity of the system.
- Evolution of the cation occupancy in exchange sites of smectite fraction in bentonite.
- Role of the surface acidity reactions on the overall pH-buffering capacity of the bentonite.
- Behaviour of bentonite accessory minerals, mainly carbonate minerals (calcite, dolomite, and siderite), sulphates (gypsum and anhydrite), silica phases, sulphides (pyrite and amorphous FeS) and Fe(III) oxi-hydroxides (amorphous $Fe(OH)_3$ and hematite), in terms of dissolution-precipitation, redistribution, and the effect on the pH and Eh of the system.
- Effect of dramatic changes in the chemical composition of the groundwater reaching the near field system.

There are other processes that are not being evaluated in the present modelling exercise, as:

- Montmorillonite stability.
- Canister corrosion.
- Water saturation of bentonite.

2 Geological background

2.1 Geology of the Forsmark area

The Forsmark site covers an area of 6×2 km in northern Uppland, located about 170 km north of Stockholm, in Sweden. Geologically, the Forsmark area belongs to the Fennoscandian shield, and it is made up predominantly with metagranitoids (metadiorites, metatonalites and metagranites) and associated metavolcanics that crystallised ca 1,900 Ma (Figure 2-1).

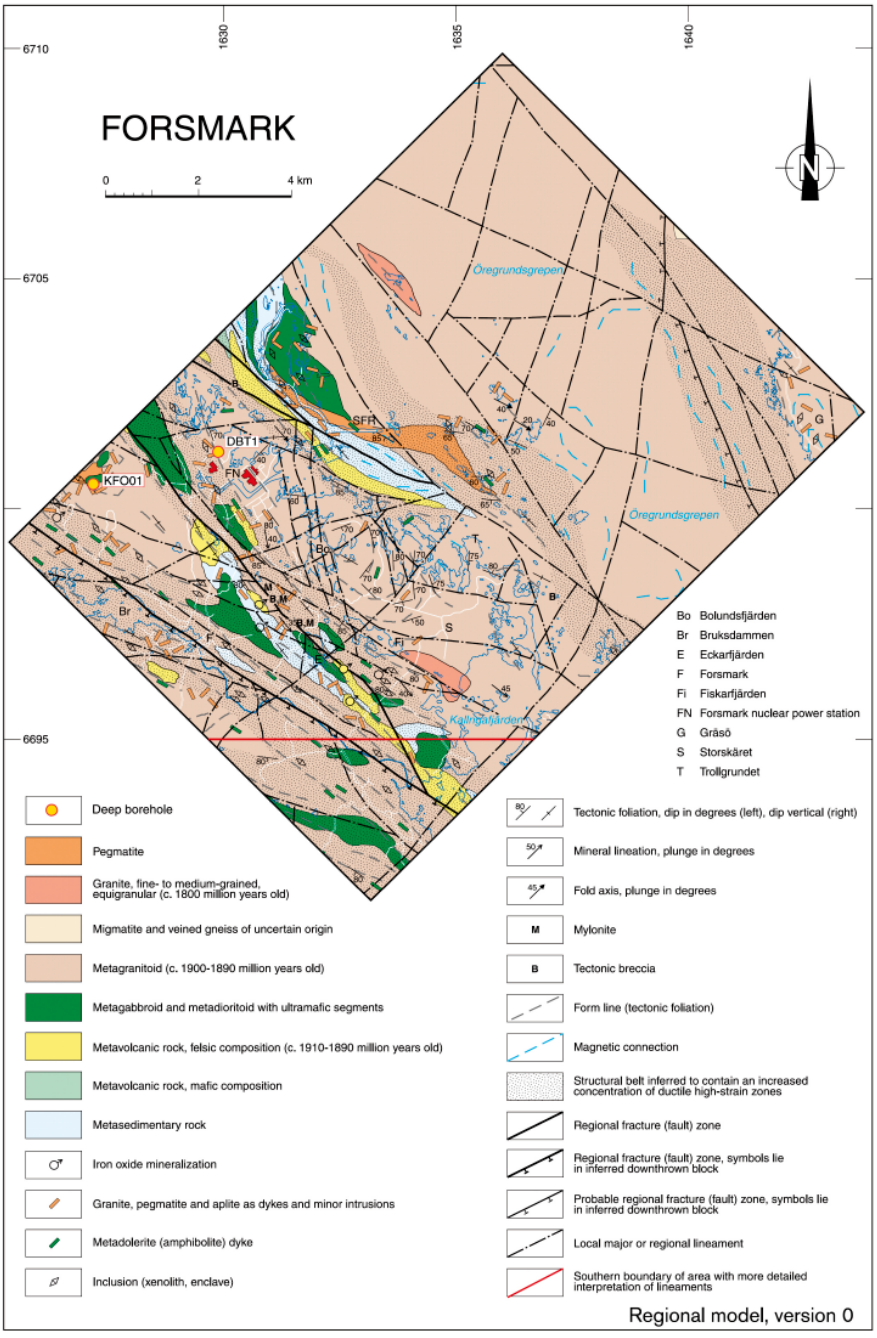

Figure 2-1. *2D cartographic model for the bedrock geology at the surface, both onshore and offshore in Forsmark area. After /SKB 2002/.*

The metamorphic character of the rocks was caused by subsequent episodes of both brittle and ductile deformation /SKB 2004a/. The most relevant feature related to these periods of deformation is a set of tectonic lenses of high strain. Equigranular textures are dominant, except for areas with major deformation where mylonitic to cataclastic rocks occur. Mineralogically, these rocks are rich in quartz (40–50%), plagioclase (30–40%), and K-feldspar (10–30%). Biotite is present in lesser amounts.

Other rocks occurring close to the studied area includes sedimentary units (mainly shales and limestones) of early Palaeozoic age.

It is noteworthy that recent glaciation periods has resulted in the reworking of the lithologies above mentioned, resulting in Quaternary units covering more than 80% of the surface of the Forsmark site area.

In addition to ductile structures, a dense fracture network has been described in the Forsmark area, likely associated with the Caledonian Orogeny, which took place during the Early Palaeozoic. Data from surface outcrops and geophysical methods revealed the existence of several sets of fractures, although the information at repository depths (–500 m) is still being recorded /SKB 2004a/. At surface, the maximum fracture frequency is 4.5 m^{-1}, and mean values range from 1.1 to 1.6 m^{-1} /Stephens et al. 2003/. Most fractures are steeply dipping, predominantly NE striking, but sub-horizontal fractures also occur. At depth, it seems that sub-horizontal fractures are more frequent. The frequency of open fractures below –400 m is 0.14 m^{-1}.

In shallower fractures, fracture-filling minerals have been identified to be calcite, chlorite, quartz, epidote, magnetite, hematite, feldspar, laumontite and sulphides /Nordman 2003/. At depth, data from core-drilled borehole /Petersson et al. 2004, Sandström et al. 2004/ show that quartz, calcite, hematite, pyrite, albite and chlorite/corrensite are the most abundant fracture-filling minerals.

2.2 Hydrology and hydrochemistry

The nature of surface waters in the Forsmark area has changed through time since the Holocene. During the last 2,500 years, the area was covered by seawater, with salinities close to those found today in the Baltic Sea (around 7 per mil). However, the salinity of the Baltic Sea increased significantly from –2,000 years to –6,500 years (Litorina stage), reaching values close to 14 per mil /Westman et al. 1999/. Previous to these marine stages, glacial and lacustrine stages predominated in the region (at least in the last 15,000 years). Formation of permafrost in brackish environments could contribute to the formation of relatively high-salinity waters /Bein and Arad 1992/.

All these types of water could potentially infiltrate down through the bedrocks, specially those with higher salinity (i.e. higher density), leading to a regional groundwater flow. In fact, it is reasonable to assume that present-day groundwaters at Forsmark represent a mixture of water of different origin, whose composition may be modified by water-rock interactions. /Laaksoharju 1999/ provides a number of possible end-members of this mixture in Fennoscandian sites, which are modern meteoric water, pore water of marine sediments, ancient Litorina seawater, glacial melt water and deep brines.

It is important to keep in mind that groundwater composition may change through time due to local and global climatic changes that modify the relative proportions of the end members that contribute to groundwater. The long time considered in many numerical simulations of the repository chemistry (typically from 10^4 to 10^5 years) makes unlikely that the composition of the inflow groundwater remains unaltered. Intrusion of groundwaters with distinct composition may lead to substantial changes in the evolution of the near field geochemistry. Moreover, such changes could be different depending on the time elapsed between the closure of the repository and the intrusion.

Groundwater at repository levels from Forsmark is relatively saline (data from SICADA database, Table 2-1) compared with present-day Baltic Sea (0.0073 mol·kg^{-1} Cl^-). The ultimate origin of such water is unknown but it has been suggested that it could be brackish water from the ancient Litorina Sea, as proposed for the Olkiluoto (Finland) deep groundwaters /Laaksoharju et al. 2004/. There is evidence of more saline fluids in the Fennoscandian shield, as in Laxemar /Laaksoharju et al. 1995/, with salinities up to 1.28 mol·kg^{-1} Cl^- at depths down to 1,700 m (KLX02 drill hole, Table 2-1). In addition, it seems reasonable to expect the intrusion of more diluted waters resulting from glacial melting in cooler climatic periods. For modelling purposes (see Chapter 5), a very diluted water derived from ice melting at Grimsel site /Hoehn et al. 1998/ has been also considered in this work to simulate the intrusion of glacial waters down to repository depths.

Speciation-solubility calculations using PHREEQC /Parkhurst and Appelo 1999/ show that the Forsmark groundwater is saturated with respect to calcite and quartz, indicating equilibration with the host rock and fracture-filling minerals. On the other hand, the saline water is undersaturated in calcite and gypsum, and in equilibrium with silica, whereas the ice-melting water is saturated with calcite and silica, but undersaturated with gypsum (see Sections 5.3.5.3 and 5.3.5.4).

The migration of fluids in the Forsmark area is mainly channelled through fracture zones. Data from pumping tests reveal that open fractures are the most conductive structures, with transmissivities ranging from 5×10^{-4} to 5×10^{-5} m s^{-1} in the studied sections (0–200 m depth) /Ludvigson and Jönsson 2003/. At depth (300–500 m), hydraulic conductivity for fractures ranges from 5×10^{-7} to 5×10^{-5} m·s^{-1}. These values are calculated from data of intrinsic permeabilities reported by /Hartley et al. 2004/. Transmissivity of metagranite is believed to be much lower, about 1.5×10^{-10} m s^{-1}. No data for deeper zones are available.

Table 2-1. Chemical composition of the groundwaters considered in this work.

Moles/L	Forsmark	Laxemar saline[1]	Grimsel Ice-melting
pH	7.2	7.9	9.6
pe	–2.42	–5.08	–3.38
HCO_3^-	2.20×10^{-3}	1.00×10^{-4}	4.50×10^{-4}
Ca	2.33×10^{-2}	4.64×10^{-1}	1.40×10^{-4}
Cl	1.53×10^{-1}	1.28	1.60×10^{-4}
Fe tot	3.31×10^{-5}	8.00×10^{-6}	3.00×10^{-9}
K	8.75×10^{-4}	7.00×10^{-4}	5.00×10^{-6}
Mg	9.30×10^{-3}	1.00×10^{-4}	6.20×10^{-7}
Na	8.88×10^{-2}	3.49×10^{-1}	6.90×10^{-4}
SO_4^{2-}	6.80×10^{-3}	9.00×10^{-3}	6.10×10^{-5}
Si	1.85×10^{-4}	8.00×10^{-5}	2.05×10^{-4}

[1] Data for saline water as reported in /SKB 2004b/, except for pe and silica, which come from /Laaksoharju et al. 1995/.

3 The KBS-3 concept

The KBS-3 concept for storage of High Level Nuclear Waste (HLNW) designed by SKB consists of copper canisters with a cast iron insert containing the spent nuclear fuel. Each canister is deposited in a hole excavated in a granitic rock at depths around 500 m, and are surrounded by compacted bentonitic clays that work as a chemical and hydraulic barrier (Figure 3-1).

3.1 Bentonite barrier in the near field

The bentonite barrier in the KBS-3 repository design has to meet certain requirements in order to protect the canister from mechanical and chemical degradation:

- maintain a very low hydraulic conductivity, in order to isolate the canister from groundwater flow and enhancing diffusion as the main transport process in the near field,
- meet a swelling pressure high enough to seal the gaps between the bentonite and the host rock and canister respectively, and
- maintain a certain degree of plasticity to absorb small rock movements, but avoiding canister to shift due to loading effect.

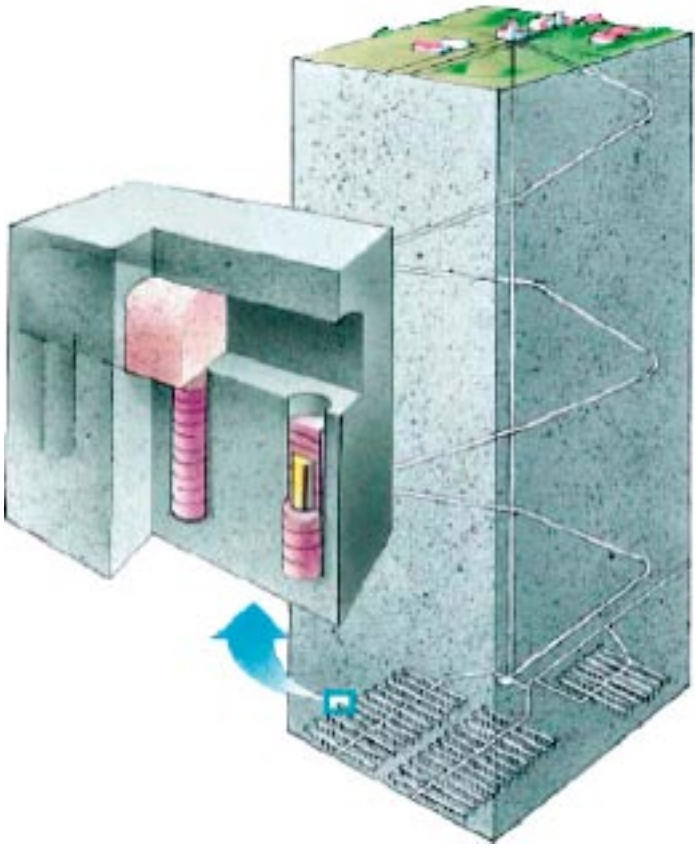

Figure 3-1. *KBS-3 concept for storage of HLNW designed by SKB. Spent nuclear fuel will be stored in copper canisters buried at depth and surrounded by compacted bentonite blocks.*

In addition, if the canister loses its containment function, the buffer may also provide:

- a favourable chemical environment promoting retention of radionuclides released from the spent fuel,
- a permeability to gas flow that is high enough to allow any gases generated by corrosion of the canister's iron insert to pass through the buffer without forming permanent permeable channels or cavities, and
- a filtration capacity that effectively stops the migration of potential radionuclide bearing colloids.

Bentonites have a large swelling capacity when they are in contact with water resulting in an important reduction of porosity. This property makes these clays a very effective barrier to isolate the copper canisters from the potential advective flow in the repository. In addition, radionuclides can be retarded by sorption onto reactive clay surfaces. Both physical and chemical properties of bentonite are mainly provided by montmorillonite, which is its major mineral (65–90 wt %). This mineral is a phyllosilicate with a TOT (tetrahedral-octahedral-tetrahedral) layer structure. Polar molecules, as water, may occupy interlayer positions leading to the swelling mentioned above.

Isomorphous substitution of lattice cations by cations of a lower valence results in a negative charge of the montmorillonite surfaces, which is compensated by the presence of interlayer cations. These cations may be exchanged by other cations from the pore water. The total negative charge is defined as the cation exchange capacity (CEC). Since solid/pore water ratios are very high in compacted bentonite, the exchange process will play an essential role in the composition of the water equilibrating with the bentonite clays. Another relevant process in montmorillonite is the deprotonation/protonation associated with surface hydroxyl groups.

For the KBS-3 concept, a number of commercially available bentonites have been tested, although only one, the "Wyoming-type" MX-80, has been extensively studied. The MX-80 bentonite consists mainly of Na-Montmorillonite, and includes other minerals in minor concentrations such as quartz, feldspar, gypsum, and pyrite (Table 3-1). Another bentonite under testing is the "Milos-type" Deponit CA-N, which has a Ca-Montmorillonite as the dominant clay mineral and is relatively rich in carbonate minerals (up to 13% of calcite + siderite + dolomite, Table 3-1).

Table 3-1. Mineralogical composition and the cation exchange capacity of the clay fraction of bentonites MX-80 and Deponit CA-N, based on /SKB 2004b/.

Mineral (wt %)	MX-80	Deponit CA-N
Montmorillonite	87	81
Quartz	5	2
Feldspar + mica	7	2
Dolomite	0	3
Calcite + siderite	0	10
Pyrite	0.07	0.5
Gypsum	0.7	1.8
CEC (meq/100 g)	75	70
NaX (%)	72	24
KX (%)	2	46
CaX_2 (%)	18	29
MgX_2 (%)	8	2

The presence of carbonate minerals (calcite and siderite), even in low concentrations, is of special relevance due to their pH buffer capacity. Similarly, pyrite may also control the O_2 consumption by oxidation and the availability of aqueous sulphide for copper corrosion in the canister.

The CEC of bentonites is still under debate, and a number of values have been reported in literature. For the present work, we used the data provided by /SKB 2004b/ (Table 3-1).

An even more controversial issue is that referring to the porosity in the bentonite after swelling. Due to electrostatic repulsion between anions and charged clay surfaces, effective porosity for solute transport could be largely reduced. In contrast, cations access more easily to interlayer porosity and participate to exchange in clay surfaces. From a literature review, /Ochs et al. 2001/ calculated the dependence of the bentonite density on the physical porosity (ε), which follows:

$$\varepsilon = 1 - (\rho/\rho s)$$

where ρ is the dry density and ρ_s the specific density of bentonite (2,750 kg·m^{-3}).

/Ochs et al. 2001/ recommended a value of total physical porosity (diffusion-available porosity) of 0.43 for all elements except Cs and non-sorbing anions, in bentonites with dry density of 1,570 kg·m^{-3}.

The hydraulic conductivity of bentonite clays is very low (lower than 10^{-12} m·s^{-1}), and thus, it can be considered that diffusion rules the solute transport and advection is negligible /SKB 1999/. Like porosity, effective diffusion coefficients (D_e) are also affected by electrostatic phenomena and different values must be adopted for anions and cations. /Ochs and Talerico 2004/ proposed an equation to calculate the D_e in MX-80 bentonite for tritiated water (HTO) as a function of dry density:

$$D_e = 6.7785 \times 10^{-9} \times e^{-0.0025671 \times \rho}$$

For a dry density of 1,570 kg·m^{-3} previous equation yields a D_e of 1.2×10^{-10} m^2·s^{-1}. These authors also recommended this value for all cations except Cs.

3.2 The backfill in the deposition tunnels

In the KBS-3 concept, the deposition holes, where canisters are emplaced, are excavated at the deposition tunnels ground (see Figure 3-1). In the closure of these deposition tunnels, two backfilling systems have been tested. Especial attention has been paid to two materials: 1) the Friedland-type clay /SKB 2004b/, and 2) a mixture consisting of 70% crushed rock derived from the excavation itself and 30% bentonite clay (MX-80 or Deponit CA-N).

3.2.1 The Friedland Clay

The Friedland Clay is a rock of Tertiary age from the Friedland area in Germany, which is extensively exploited for ceramic and isolation uses, and it has also been tested as buffer material in HLNW repositories. Compositionally, this clay is characterised by a lower content of the clay fraction relative to other clay rocks studied for nuclear waste storage (especially bentonite; Table 3-2). The mineral composition of the Friedland Clay has been investigated in several studies. These studies indicate that the smectite content in the rock is about 45–50 wt % /Pusch 1998, Pusch and Schomburg 1999, SKB 2004b, Carlson 2004, Ochs 2006/. /Pusch et al. 2003/ propose that the structure of the clay is a system of alternating layers of irregular sequences of montmorillonite and muscovite (Figure 3-2).

Table 3-2. Mineral composition of the Friedland Clay. Composition of MX-80 and Deponit CA-N bentonites are also shown for comparison. Data from /Pusch 1998, Ochs 2006/.

Mineral (wt %)	Friedland Clay	MX-80	Deponit CA-N
Montmorillonite*	44	87	81
Illite	4	0	0
Quartz	28	5	2
Feldspar + mica	12	7	2
Dolomite	0	0	3
Calcite + siderite	0	0	10
Pyrite	0.62	0.07	0.5
Gypsum	0.8	0.7	1.8

* In the case of the Friedland Clay, the montmorillonite layers are mixed with illite layers (I/S = 1/3).

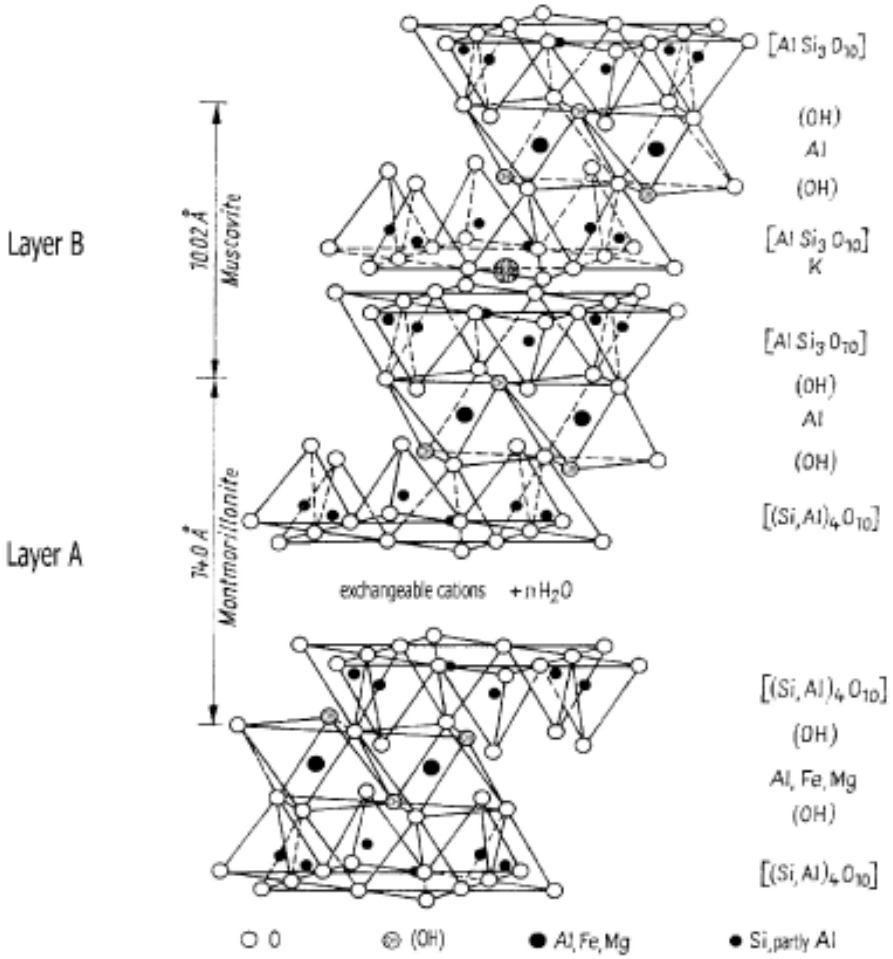

Figure 3-2. *Structure of the Friedland Clay, alternating muscovite and montmorillonite layers. From /Pusch et al. 2003/.*

The exchange properties of the Friedland Clay are not well determined as indicated by the wide ranges in CEC reported in literature (Table 3-3). In any case, though, the CEC is significantly smaller than other clays with higher smectite content. The CEC value ranges from 25 to 51 meq·100g^{-1} and the distribution of the exchanged cations also differs between samples. Data from Pusch and co-workers show that the exchanger is rich in potassium (66% of the CEC), whereas sodium (22%) and calcium (8%) have lower concentrations. In contrast, all experiments from /Carlson 2004/ yield a Na-rich composition (from 52 to 70%), whereas potassium has much lower concentrations (from 8 to 16%). The variability in the data from /Carlson 2004/ is interpreted by the author to be controlled by extra supply of calcium due to dissolution of accessory minerals, mainly calcite. This conclusion is derived from the correlation between the total CEC and the measured calcium concentration (the higher CEC the higher Ca). Consequently, it was concluded that data provided from methods yielding lower Ca concentrations could be more representative of the true exchanger composition. In a recent report, /Ochs 2006/ proposed a CEC value of 22 meq·100g^{-1}.

On the other hand, neither data for the surface complexation nor reactive surface area exist in literature.

Unlike bentonites, which have been deeply studied, the physical and hydraulic properties of the Friedland Clay have only been partially determined. Hydraulic conductivity is by far the best-known parameter. /Pusch and Schomburg 1999, Pusch 2001/ carried out a set of experiments aimed to determine, among other purposes, the dependence of the hydraulic conductivity on the salinity of the pore fluid. They found values of hydraulic conductivity ranging from 5×10^{-12} m·s^{-1} when the percolating water was distilled and with a clay density of 2,050 kg·m^{-3} to 2×10^{-8} m·s^{-1} at very high salinities (20% NaCl) and lower densities (1,750–1,800 kg·m^{-3}) (Figure 3-3). These values have been derived from oedometer tests /Johannesson and Nilsson 2006/.

On the other hand, /Börgesson and Fälth 2004/ used in a resaturation modelling a hydraulic conductivity of 7×10^{-12} m·s^{-1} in unsaturated Friedland clay samples. This conductivity was inferred to a compacted clay of a dry density (ρ) of 1.59 g·cm^{-3} and a void ratio (e) of 0.70. e and porosity (ε) are related from the next equality:

$$\varepsilon = \frac{e}{1+e}$$

Therefore, a porosity of 0.41 is obtained.

Table 3-3. Cation exchange capacity (CEC) and concentration of exchanged cations in meq·100g–1 of the Friedland Clay found in literature. NR = not reported.

Source	Na^+	Ca^{2+}	Mg^{2+}	K^+	CEC
/Jacobsson and Pusch 1978/	11	4	2	34	51
/Pusch et al. 2003/	11	4	2	*NR*	50
/Carlson 2004/					
$BaCl_2$ method	25.9	4.4	3.0	3.5	36.8
LiCl method	24.7	6.2	4.3	3.2	38.4
NH_4-Acetate method	22.8	6.3	3.9	2.3	35.3
Cu(II) ethylenediamine method	22.2	11	6.9	2.2	42.3
/SKB 2004d/					
Whole rock	*NR*	*NR*	*NR*	*NR*	25
Clay fraction	*NR*	*NR*	*NR*	*NR*	35
/Ochs 2006/					22

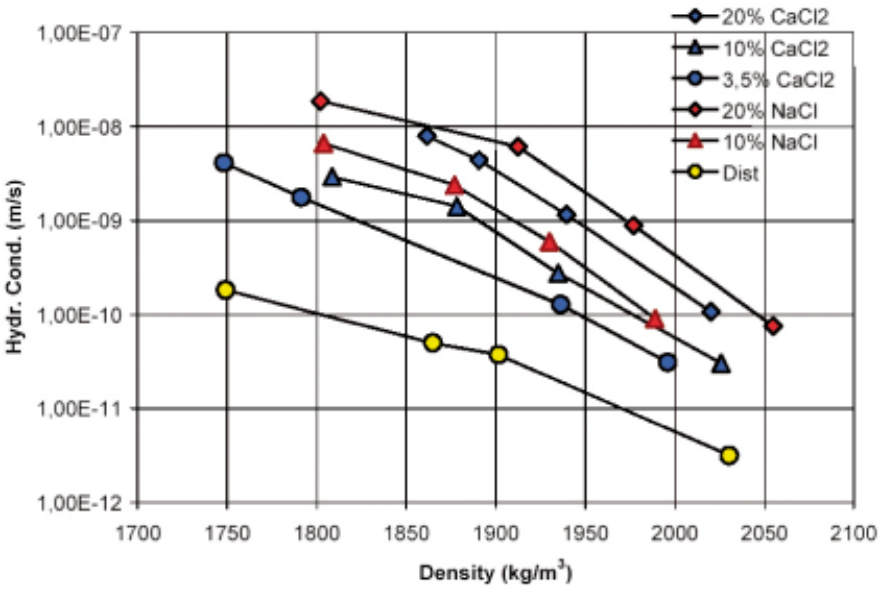

Figure 3-3. *Hydraulic conductivity vs. clay density in experiments where water with variable salinity is percolated. From /Pusch et al. 2003/.*

In SR-Can safety assessment /Ochs 2006/ a dry density of 1,780 kg·m^{-3} for Friedland clay has been selected. This value will lead to a hydraulic conductivity of 10^{-12} m·s^{-1}, which is the value we will use in the calculations.

As for the bentonite buffer, we can calculate the diffusion-available porosity through the following equation:

$\varepsilon = 1 - (\rho/\rho s)$

The values used were those to be considered in SR-Can safety assessment /Ochs 2006/: ρ = 1,780 kg·m^{-3} and ρ_s = 2,780 kg·m^{-3}. From the above equation, a porosity of 0.36 is obtained. This value is also assumed the total porosity for all elements except for non-sorbing anions. Diffusion-available porosity for non-sorbing anions is 0.14.

Other parameters such as diffusivity, heat conductivity and capacity or those referring to rheological properties are unknown so far. For diffusivity, as in the case of the bentonite buffer, we can calculate a D_e from the dry density. Then, for a dry density of a 1,780 kg·m^{-3}, the D_e value for all elements except for non-sorbing anions and Cs is 7.0×10^{-11} m^2·s^{-1}.

3.2.2 30/70 mixture

The mineral and cation exchange compositions considered are those of the corresponding bentonite type, assuming that the minerals from the crushed rock have a very low reactivity (low kinetic dissolution rate).

Hydraulic properties, such as hydraulic conductivity, of the bentonite-host rock backfill depend mainly on the heterogeneities of the mixture, which in turn are controlled by the grain size distribution and on the mixing procedure. /Börgesson and Fälth 2004/ found that the hydraulic conductivity ranged from 4×10^{-10} to 5.5×10^{-12} m·s^{-1}, using a conductivity value of 5×10^{-11} m·s^{-1} and a porosity of 36.3% to model the saturation process of the backfill.

The low hydraulic conductivity difficults advective transport versus diffusion. Effective diffusion coefficients in the backfill are not well known; /Lindgren and Lindström 1999/ used in their numerical simulations a value of 1.0×10^{-10} m^2·s^{-1} for a backfill with 15% bentonite and 85% crushed rock.

4 Conceptual model for the near field

In this section, we describe the main transport and geochemical processes involved in the geochemical evolution of the near field. Although most of these processes occur at the near field (i.e. bentonite + canister), some other processes occurring in its vicinity could also affect the geochemical evolution of the near field (i.e. processes in the near-far field transition zone). For this reason, these processes must be included in the model.

4.1 Transport processes

The main transport mechanism through the bentonite buffer is diffusion, given the very low hydraulic conductivity of high compacted bentonite under repository conditions. However, as bentonite blocks will be deposited under unsaturated conditions with respect to water content, advective transport due to negative capillary pressure could be important until full water saturation of bentonite, which can occur between 10 and more than 100 years after bentonite deposition /SKB 2004c/. In the present study, only the saturated stage will be considered. Additionally, during the thermal stage, transport will be affected by the thermal gradient imposed on the near field due to the heat generated by radioactive decay of the waste. This effect on the transport processes will be more pronounced during the water saturation stage of the buffer /SKB 2004c/.

The crystalline host rock surrounding the near field is, by definition, impervious. However, due to the geologic history of the rock (magma cooling, hydrothermal events, or tectonic movements), a fracture network can be formed, allowing advective flow of groundwater. In the present study we consider the scenario where one of these fractures has been intersected during the excavation of the deposition hole. Thus, groundwater flowing through the fracture can reach the near field of the repository (Figure 4-1).

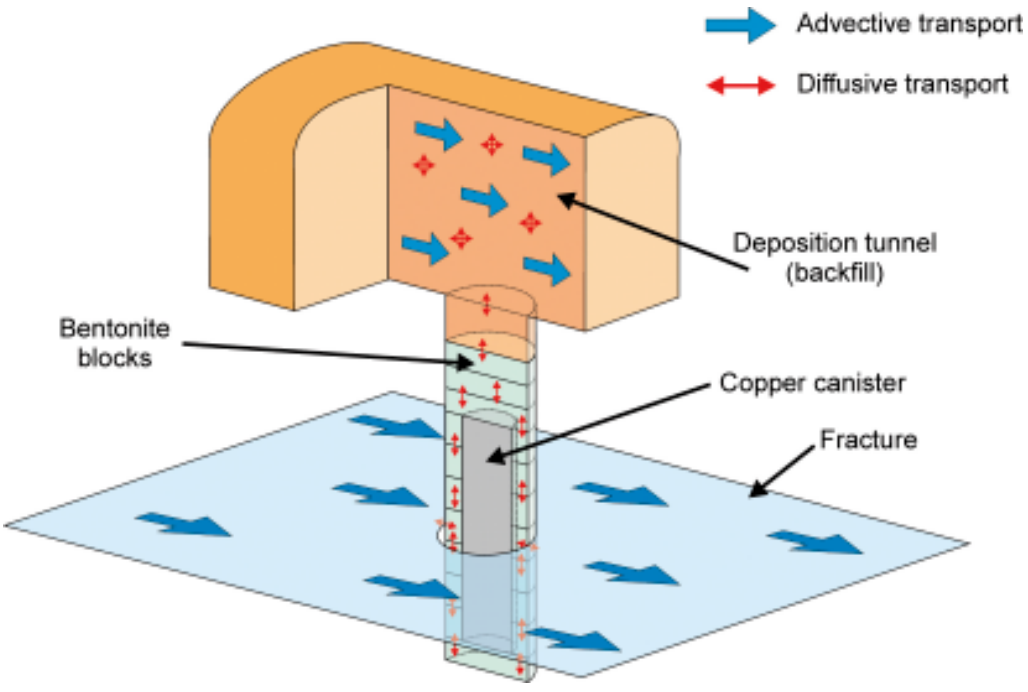

Figure 4-1. *Schematic view of the near field of a KBS-3 repository showing the transport mechanisms in the different parts of the system.*

The transport mechanism in the backfill is somewhat more complex. In order to prevent the deposition tunnels from being conductive pathways for groundwater, the backfill shall have a hydraulic conductivity in the same order of magnitude as that of the surrounding rock, or low enough to ensure that transport is dominated by diffusion /Gunnarsson et al. 2004/. However, it is possible that in some cases advection could dominate over diffusion as the main transport mechanism.

4.2 Geochemical processes

Different geochemical processes are expected to occur in the different components of the system under consideration, given the different mineralogical composition. Bentonite is the major component of both, the bentonite buffer and the backfill. Thus, similar water-rock interaction processes must be considered in these two zones of the system. The mineralogy of the fracture filling material is different from the previous one, therefore allowing for different geochemical processes to take place in the fractures.

4.2.1 Bentonite and backfill

The main mineral in both these components of the system is smectite, as it constitutes more that 75% of the bentonite. The smectite dissolution or its replacement by other clay minerals could result in a decrease of the swelling capacity of bentonite. The process of smectite dissolution is, nevertheless, very slow /Cama et al. 2000/. Thus, it seems reasonable to consider smectite dissolution as a process of minor importance in the geochemical evolution of the system.

Therefore, the interaction of pore water with accessory minerals as well as montmorillonite surface reaction will be the processes controlling the geochemical evolution of the system. Such reactions are /Bruno et al. 1999/:

Dissolution-precipitation of carbonates. Although the carbonate content in bentonite tends to be relatively small, the dissolution-precipitation reactions are of paramount importance to buffer the alkalinity of bentonite pore waters.

$CaCO_3(s) + H^+ \leftrightarrow Ca^{2+} + HCO_3^-$

$CaMg(CO_3)_2(s) + 2H^+ \leftrightarrow Ca^{2+} + Mg^{2+} + 2HCO_3^-$

$FeCO_3(s) + H^+ \leftrightarrow Fe^{2+} + HCO_3^-$

The last reaction has also a clear effect on the redox capacity of the bentonite.

Cation exchange reactions. The control exerted by this process on the calcium and magnesium concentrations in pore water directly affects the dissolution-precipitation of carbonate accessory minerals in the bentonite. The main cation exchange reactions can be expressed by the following equations:

$NaX + K^+ \leftrightarrow KX + Na^+$

$2NaX + Ca^{2+} \leftrightarrow CaX_2 + 2Na^+$

$2NaX + Mg^{2+} \leftrightarrow MgX_2 + 2Na^+$

The initial composition of the exchanger as well as the exchange coefficients depend on the bentonite type selected as buffer.

Protonation-deprotonation surface reactions. Surface edge groups of smectite may experiment protonation and deprotonation processes. These processes can contribute to the pH buffering:

$\equiv sOH + H^+ \leftrightarrow \equiv sOH_2^+$

$\equiv sOH \leftrightarrow \equiv sO^- + H^+$

Some of the parameters associated to these reactions (initial composition, protonation-deprotonation constants, surface area, etc.) depend on the bentonite type, thus a careful examination of the selected bentonite must be conducted prior to their inclusion in any geochemical model.

Sulphate dissolution-precipitation. Precipitation or dissolution of gypsum (and/or anhydrite) may control the calcium availability in the system, leading to an indirect buffering due to its effect on the carbonate dissolution-precipitation reactions.

$CaSO_4 \leftrightarrow Ca^{2+} + SO_4^{2-}$

However, this process can be affected by other cations competing for sulphate to form other sulphate minerals. In addition, the precipitation of gypsum or anhydrite is dependent on temperature, thus leading to a strong dependency of this process on the thermal gradient expected during early times of the repository life.

Oxidation-reduction processes in the bentonite. The reducing capacity of bentonite is an essential parameter for the repository stability. The redox state in the bentonite barrier will be controlled by:

Pyrite oxidation. Pyrite oxidation consumes oxygen and produces Fe(III) and sulphate. Fe(III) can precipitate in the form of Fe(III) oxy-hydroxides in the pH range of interest. The oxidation reaction can be expressed by the following equation:

$FeS_2(s) + 3.75O_2(g) + 3.5H_2O \rightarrow Fe(OH)_3(s) + 2SO_4^{2-} + 4H^+$

If there is no pyrite in the bentonite, then the oxidation of sulphide to sulphate will not occur and the redox of the system will be buffered by the redox pair Fe(II)/Fe(III).

Amorphous iron sulphide (FeS) could precipitate in case of saturation, considering the increase in concentration of aqueous sulphide and/or iron due to diffusion from host rock.

Siderite dissolution/amorphous Fe(III) oxy-hydroxide precipitation. This is likely to be the most relevant redox process in the bentonite in the absence of pyrite. If a significant fraction of carbonates in bentonite contains Fe(II), the equilibrium between Fe(II) carbonates and Fe(III) oxy-hydroxides can readily buffer the redox state of the bentonite:

$FeCO_3(s) + 2.5H_2O + 0.25O_2(g) \leftrightarrow Fe(OH)_3(s) + H^+ + HCO_3^-$

During the thermal stage (thermal gradient induced by heat generation from the waste), the precipitation of hematite instead of the one of amorphous $Fe(OH)_3(s)$ is expected, given the higher stability of the more crystalline material (hematite) at higher temperatures.

Other processes. Other geochemical processes that can occur in the barrier are the dissolution-precipitation of silica phases (quartz, cristobalite and amorphous SiO_2) and chlorides, especially in the presence a thermal gradient:

$SiO_2(s) \leftrightarrow SiO_2$

$NaCl(s) \leftrightarrow Na^+ + Cl^-$

The dissolution of accessory aluminosilicate minerals in the bentonite, such as plagioclase or K-feldspar can be also considered.

$CaAl_2Si_2O_8 + 8H_2O \rightarrow Ca^{2+} + 2Al(OH)_4^- + 2Si(OH)_4$

$KAlSi_3O_8 + 8H_2O \rightarrow K^+ + Al(OH)_4^- + 3Si(OH)_4$

The rate of aluminosilicate dissolution is very slow and it will be an efficient chemical buffer only when the most readily occurring reactions are no further active, due to the depletion of the minerals involved.

4.2.2 Fracture-filling in the host rock

Minerals filling the open fractures are suitable to interact with groundwater. Some of these fracture-filling minerals in the Forsmark area are of metamorphic or hydrothermal origin, such as albite, adularia, epidote, chlorite and corrensite, among others /Sandström et al. 2004/. Most of these hydrothermal minerals are metastable and present slow dissolution kinetics. According to /Sandström et al 2004/ these minerals formed from one or several hydrothermal events occurred more than 6×10^8 years ago. Their total dissolution will not occur before one million years. Present-day groundwaters can be in equilibrium with some of the lower temperature forming minerals (illite, illite-smectite mixed layers, saponite, calcite, and hematite /Sandström et al. 2004/, as well as pyrite and quartz.

However, groundwater composition can be modified due to its interaction with near field materials, leading to the possible dissolution of some of these phases and the precipitation of new secondary phases (mainly gypsum). This modified groundwater composition could be found in the surroundings of the near field, given that farther away, mixing processes with other groundwater compositions will mask these changes. Thus, dissolution of primary fracture-filling minerals and precipitation of new phases will only be evident at the vicinity of the near field. Special attention should be paid to redox reactions in the host rock, as they can affect the properties of the near field. The processes described below following the energetic yield as described in natural systems /Stumm and Morgan 1981/ will control the redox capacity of the host rock formation.

Oxidation of the host rock formation organic matter. This process is exemplified by the following reaction:

$CH_2O + O_2(aq) \rightarrow CO_2(g) + H_2O$

The CO_2 generated in this process is involved in the carbonate (calcite) dissolution-precipitation reactions and thus, affecting the pH buffering capacity of the system.

In addition, groundwaters from host rock formations with a high concentration of sulphate can gather the activity of sulphate-reducing bacteria (SRB) oxidising organic matter through the following reaction:

$CH_2O + ½SO_4^{2-} \rightarrow HCO_3^- + ½HS^- + ½H^+$

This process can lead to the formation of sulphide minerals (mainly pyrite) and will contribute to the acidity of the system.

Pyrite oxidation. The next electron donor in the host rock formation is sulphide, mainly in the form of pyrite. Most clay rocks and fracture-fillings in granitic rocks have certain amounts of pyrite. The pyrite oxidation process is exemplified by the following reaction:

$FeS_2(s) + 3.75O_2(g) + 3.5H_2O \rightarrow Fe(OH)_3(s) + 2SO_4^{2-} + 4H^+$

This oxidative process has some limitations from the kinetic point of view and, consequently, it is necessary to discuss which are the main factors affecting the oxidation rate in order to assess whether it could be treated as an equilibrium process at the repository conditions.

The pyrite oxidation rate is affected by three main factors: a) the pyrite grain size, b) the oxygen content in the interaction waters, and c) the pH value of these waters.

4.3 Boundary conditions: Limitations and validity

The system is arbitrarily defined as a hydraulic conductive fracture intersecting a deposition hole. Therefore, transport boundary conditions will be constrained by the transport properties of the host rock, including the fracture. However, changes in some of the transport parameters could modify the modelling results:

- Number of fractures intersecting the deposition hole.
- Fracture geometry (hydraulic aperture, intersection angle, shape of the fracture plane and presence of subordinated fractures).
- Hydraulic parameters of the fracture (head gradient and hydraulic conductivity).
- Diffusive transport through the bentonite – non-fractured granite boundary.

The consideration of more than one fracture intersecting the deposition hole at different parts of the deposition hole could speed up the alteration of the bentonite (i.e. dissolution of accessory minerals). Whereas, if no fractures intersect the deposition hole, water can only contact the buffer through the backfill in the deposition tunnel or by diffusion through the bentonite – non-fractured granite boundary. However, despite the case considered, the geochemical process governing the system will be the same. For this reason, the selection of a single fracture intersecting the deposition hole is a reasonable assumption to obtain information on the relevance of the different geochemical processes and their effect on the evolution of the system.

Other parameters affecting the groundwater flow through the fracture (i.e. fracture geometry and hydrodynamic parameters) can also affect the results of the models. However, as we will see in Section 5.3.2, the set of parameters used result in a groundwater flow, which is in agreement with that considered in the SR-Can safety assessment /SKB 2006/.

Boundary conditions have been validated with the LOT experiment /Karnland et al. 2000/ conducted at Äspö Hard Rock Laboratory /Arcos et al. 2003, Domènech et al. 2004/, although more work is needed to refine those boundary conditions by adding the water saturation process of the bentonite coupled with the thermal gradient.

5 Modelling

5.1 Introduction: Modelled cases

This study focuses on the chemical evolution of the buffer when groundwater enters the near field system. Such evolution will depend on the path followed by groundwater and on its composition. Therefore, several cases have been evaluated in order to cover a relatively wide range of possible situations, Table 5-1.

Table 5-1. Modelling cases and variants considered.

			VARIANTS		
			Forsmark groundwater	**Ice-melting intrusion**	**High-salinity intrusion**
MODELLING CASES	MX-80 bentonite	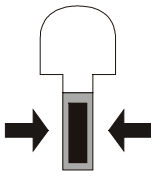	CASE-I (Reference case)	Variant 1.1	Variant 1.2
	Deponit CA-N bentonite				
	MX-80 bentonite buffer + Friedland clay backfill	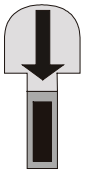	CASE-II (Reference case)	Variant 2.1	Variant 2.2
	Deponit CA-N bentonite buffer + Friedland clay backfill				
	MX-80 bentonite buffer + 30/70 mixture backfill				
	Deponit CA-N bentonite buffer + 30/70 mixture backfill				
	Thermal gradient (MX-80 and Deponit CA-N bentonite)	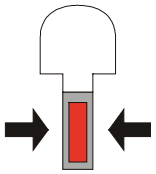	CASE-III		

- **CASE-I: Groundwater-buffer interaction**. Reference case. This case assumes that groundwater with the composition of the Forsmark sampled at depth (see Table 2-1) can reach the bentonite buffer. Since the most conductive structures in the Forsmark metagranite are unsealed fractures, we considered that one fracture intersects the deposition hole (Figure 4-1). We have simulated two additional scenarios that are likely to occur in the Scandinavian Shield: 1) the brine up-rise from depth, and the intrusion of ice-melting water at the repository level. We selected the chemical composition of these waters as equivalent to high-salinity water from Laxemar and diluted water from Grimsel respectively (Table 2-1). The reference case and the other two scenarios have been simulated using two different compositions of bentonite in terms of accessory minerals: MX-80 and Deponit CA-N. The simulation will assume isothermal conditions (i.e. 15°C).
- **CASE-II: Groundwater-backfill-buffer interaction**. In this case, we evaluated the buffering effect of the backfill and the changes on the composition of pore water before interacting with the buffer in the deposition hole. We considered the same water types and bentonite compositions as in the previous case and the two backfill types as previously described in Section 3.2. Groundwater enters into the modelled domain only through the deposition tunnel (Figure 5-1).
- **CASE-III: Thermal effect**. In this third case, a detailed analysis of the thermal effect on MX-80 and Deponit CA-N bentonite buffers caused by the radionuclide decay in the spent fuel is evaluated by assuming a thermal gradient on a two-dimensional section of the bentonite buffer. Two different approaches have been considered: 1) a bentonite section in contact with a hydraulically conductive fracture, and 2) a bentonite section far away from the conductive fracture to minimise the effect of groundwater on the geochemical evolution of the system, which will be mainly affected by the thermal gradient in the bentonite.

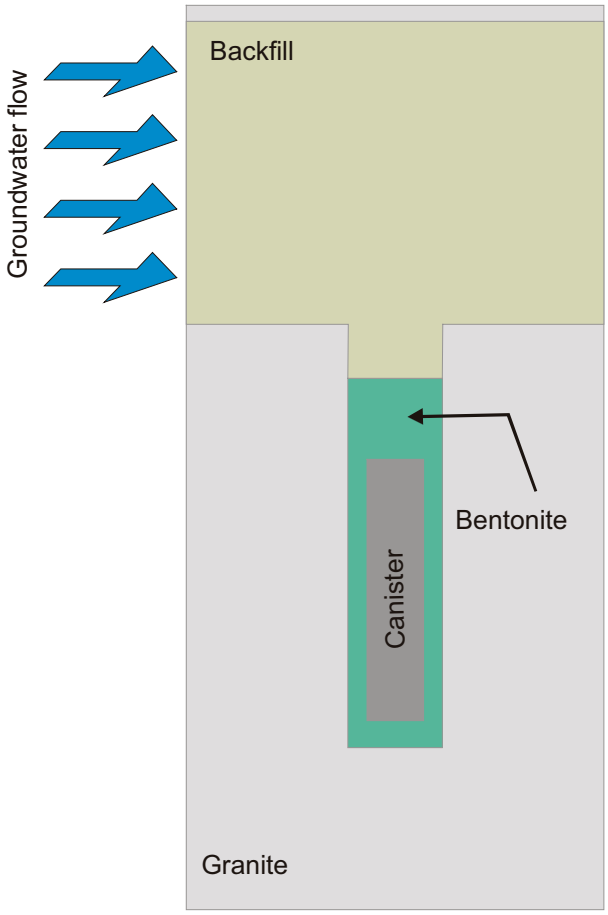

Figure 5-1. *Modelled domain in the CASE-II.*

5.2 The reactive-transport code

The geochemical simulations have been performed with the reactive transport code PHAST /Parkhurst et al. 2004/. This code is the result of coupling a transport code, HST3D /Kipp 1997/ and a geochemical code, PHREEQC /Parkhurst and Appelo 1999/. It is able to simulate multi-component, reactive solute transport in three-dimensional saturated groundwater flow systems. A number of boundary conditions are available (specified-head, flux and leaky conditions), and chemical reactions include homogeneous equilibria using an ion-association thermodynamic model, heterogeneous equilibria between the aqueous solution and minerals, gases, surface complexation sites, ion exchange sites, solid solutions, and kinetic reactions. The reaction and transport equations are solved by sequential approach in which solute transport and chemical reaction are divided into separate calculations for each time step. First, the components are transported into a cell and, then, the outcome of the geochemical reactions occurring in the cell is calculated. PHAST uses porous media properties and boundary conditions defined by zones for a point-distributed-finite-difference grid.

5.3 CASE-I: Groundwater-buffer interaction

5.3.1 The modelled domain and boundary conditions

The simulations have been performed on a three-dimensional domain that reproduces a half of the deposition hole system defined in the KBS-3 concept. This domain has been divided into four different zones: the granite host rock, the fracture plane, the bentonite barrier and the canister. Both the canister and the granite host rock have been considered as no-flow domains. The domain has been discretised into 43,370 elements (47,880 nodes), with a maximum $\Delta X = \Delta Y = \Delta Z = 300$ mm and a minimum of 116 mm, and total X = 7,740 mm, Y = 3,928 and Z = 9,844. The model assumes that groundwater flows through the fracture plane from the left boundary to the right boundary. The fracture has a width equivalent to one grid cell, which is 116 mm. A prescribed hydraulic head has been imposed at both boundaries and a fixed solution composition at the left boundary. At the right boundary, the solution composition is allowed to change because of the chemical reactions considered. Upper and lower boundaries of the domain are no flow boundaries.

The time period of simulation is 60,000 years, with a time step varying from 1 to 250 years.

5.3.2 Hydraulic properties

We assume that water in the granite host rock can only flow through the fracture, and therefore, the granite host rock is considered as an inactive zone from the point of view of transport and chemical reactions. The cast iron insert and copper canister are considered impervious (i.e. not even diffusive transport can occur) and, therefore, we also considered this domain as an inactive region.

A value of 5×10^{-7} m·s^{-1} for the hydraulic conductivity in the fracture has been adopted, which is the lowest value calculated from the data of /Hartley et al. 2004/ (see Section 2.2). No available data of fracture porosity at Forsmark have been reported so far. For the present simulation, a value of 20% has been assumed, which is the value reported by /Dershowitz et al. 2003/ for some fractures at Äspö. The hydraulic conductivity for the bentonite buffer is much lower, 1×10^{-14} m·s^{-1} and the effective diffusion coefficient (D_e) and the porosity have values of 1.2×10^{-10} m·s^{-1} and 0.43, respectively, as recommended in /Ochs and Talerico 2004/. As mentioned in Section 2.2, such values for both porosity and effective diffusion coefficient are valid for water and cations, and therefore, an error is assumed for calculations of anion concentrations. In the model we use the diffusion coefficient in water (D_w), which is $D_w = D_e/\varepsilon$, resulting in a diffusion coefficient for water of 2.8×10^{-10} m^2·s^{-1}. Table 5-2 summarizes the data of the hydraulic properties used in CASE-I.

Table 5-2. Hydraulic properties considered in the simulations performed in CASE-I.

Material	Porosity (unitless)	D_e ($m^2 \cdot s^{-1}$)	K ($m \cdot s^{-1}$)
Granite	Inactive		
Bentonite	0.43	1.2×10^{-10}	1×10^{-14}
Fracture	0.20	–	5×10^{-7}
Canister	Inactive		

Hydraulic head gradients at repository depths are unknown at Forsmark. In the Äspö area, which shares many geological and hydrologic features with Forsmark, head gradients ranges from 5×10^{-4} to 2×10^{-3} $m \cdot m^{-1}$ /SKB 1999/. In the present study, the upper value of 0.002 $m \cdot m^{-1}$ has been selected for the simulations.

The selected parameters can be used to calculate the equivalent flow (Q_{eq}) through the fracture according to /Moreno and Gylling 1998/, which can be used in calculations of mass transfer from the COMP23 compartment into the far-field. To calculate the Q_{eq}, the following expression can be used:

$$Q_{eq,i} = 2W_i\sqrt{4D_w q_i L_i \varepsilon_i / \pi}$$

where W_i is the width of the fracture surface in contact with the flowing water, D_w the diffusivity in water, q_i is the Darcy velocity, L_i the length of the pathway in contact with water and ε_i the flow porosity. Using the selected parameters for the model gives a $Q_{eq} = 5.44\times10^{-3}$ m^3/yr, which is within the range of values considered for the equivalent flow in a fracture intersecting the deposition hole /SKB 2006/ and references therein.

5.3.3 Initial calculations

We performed some calculations to obtain the initial chemical composition of pore water in bentonite using the PHREEQC code /Parkhurst and Appelo 1999/. These calculations have been done by equilibrating the Forsmark groundwater with bentonite with a porosity of 43%, including equilibrium with bentonite accessory minerals as gypsum and quartz (equilibrium with carbonate minerals have also been calculated when considering the Deponit CA-N bentonite), and exchange and surface reactions. Table 5-3 and Table 5-4 shows the thermodynamic data used. Oxidative dissolution of pyrite has been considered as a kinetic reaction, following the rate law described by /Williamson and Rimstidt 1994/:

$$R_{py}(\text{moles}\cdot\text{m}^{-2}\text{s}^{-1}) = 10^{-8.19(\pm0.10)}\frac{[O_2 aq]^{0.50(\pm0.04)}}{[H^+]^{0.11(\pm0.01)}}$$

In the reference case, carbonate minerals (calcite and siderite), amorphous FeS and $Fe(OH)_3$ are allowed to precipitate as secondary minerals if the resulting solution is supersaturated in these phases. FeS is preferred because precipitates easily than pyrite, which is formed only after ageing and/or sulfidation of FeS following the Ostwald's rule /Stumm 1992/. In addition, the sulphate to sulphide transformation in the bentonite buffer has not been allowed, as this reaction can only proceed in the presence of sulphate reducing bacteria (SRB). However, it has been demonstrated /Pedersen 2000/ that such bacteria cannot survive in bentonite at repository conditions, and therefore, the only source for sulphide in the bentonite (and eventually contacting the canister) is diffusion from groundwater into the near field or the dissolution of pyrite initially present in the bentonite.

On the other hand, due to the low kinetic rate of dissolution of montmorillonite by granitic water under near-neutral pH /Cama et al. 2000, Huertas et al. 2001/, the calculations do not include the potential dissolution-precipitation of montmorillonite. Moreover, illitisation

Table 5-3. Thermodynamic data used in the mineral, exchange and surface reactions. Also, the reactive surface for the pyrite used for kinetic oxidative dissolution is indicated.

Mineral phase: reaction	Log K	Reference
Calcite: $CaCO_3 = Ca^{2+} + CO_3^{2-}$	–8.48	/Allison et al. 1991/
Quartz: $SiO_2 + 2H_2O = H_4SiO_4$	–4.00	/Allison et al. 1991/
Gypsum: $CaSO_4{\cdot}2H_2O = Ca^{2+} + SO_4^{2-} + 2H_2O$	–4.85	/Allison et al. 1991/
Siderite: $FeCO_3 = Fe^{2+} + CO_3^{2-}$	–10.80	/Allison et al. 1991/
Dolomite: $CaMg(CO_3)_2 = Ca^{2+} + Mg^{2+} + 2CO_3^{2-}$	–17.90	/Allison et al. 1991/
FeS(am): $FeS + H^+ = Fe^{2+} + HS^-$	–3.92	/Falck et al. 1996/
$Fe(OH)_3$(am): $Fe(OH)_3 + 3H^+ = Fe^{3+} + 3H_2O$	–4.89	/Johnson 2000/
Cation exchange reactions	**Log K**	**Reference**
$X^- + Na^+ = NaX$	0.00	/Bradbury and Baeyens 2002/
$X^- + K^+ = KX$	0.60	/Bradbury and Baeyens 2002/
$2X^- + Ca^{2+} = CaX_2$	0.41	/Bradbury and Baeyens 2002/
$2X^- + Mg^{2+} = MgX_2$	0.34	/Bradbury and Baeyens 2002/

Protonation/deprotonation reactions	Log K	Surface capacity	Reference
$ZOH + H^+ = ZOH_2^+$	4.50	4.0×10^{-2} mol/kg	/Bradbury and Baeyens 2002/
$ZOH = ZO^- + H^+$	–7.90		/Bradbury and Baeyens 2002/
$YOH + H^+ = YOH_2^+$	6.00	4.0×10^{-2} mol/kg	/Bradbury and Baeyens 2002/
$YOH = YO^- + H^+$	–10.50		/Bradbury and Baeyens 2002/
Parameters used in pyrite kinetic rate			
Surface area ($m^2{\cdot}dm^{-3}$)	2.7		

Table 5-4. Calculated chemical composition of bentonite pore waters for the reference case. Forsmark groundwater is also reported for comparison.

Moles/L	MX-80	Deponit CA-N	Forsmark
pH	7.08	7.09	7.2
pe	–2.19	–2.30	–2.42
HCO_3^-	2.14×10^{-3}	2.33×10^{-3}	2.20×10^{-3}
Ca	9.97×10^{-3}	2.37×10^{-2}	2.33×10^{-2}
Cl	1.53×10^{-1}	1.53×10^{-1}	1.53×10^{-1}
Fe tot	3.31×10^{-5}	1.72×10^{-4}	3.31×10^{-5}
K	1.14×10^{-3}	1.34×10^{-3}	8.75×10^{-4}
Mg	4.97×10^{-3}	2.39×10^{-2}	9.30×10^{-3}
Na	1.69×10^{-1}	7.11×10^{-2}	8.88×10^{-2}
SO_4^{2-}	2.94×10^{-2}	1.32×10^{-2}	6.80×10^{-3}
Si	6.60×10^{-5}	6.64×10^{-5}	1.85×10^{-4}

(montmorillonite transformation to illite) is believed to have minor influences to pore water chemistry at repository conditions /Karnland 1995, Benbow et al. 2000/.

Selectivity coefficients for cation exchange reactions and surface acidity reaction data (BET surface area, surface sites concentrations and surface complexation constants) are taken from the work of /Bradbury and Baeyens 2002/ on MX-80 bentonite. These data have also been considered in simulations when using the Deponit CA-N bentonite, given the lack of characterization of this type of bentonite.

The initial inflow groundwater composition has been calculated by equilibrating it with reactive minerals present in the fractures: quartz, pyrite and calcite. No information on the quantity of these minerals in fractures is reported in /Petersson et al. 2004/, therefore, data from /Dershowitz et al. 2003/ obtained in the Äspö fractures were used.

5.3.4 Results

Calculations of steady-state fluid heads show that advective flow is restricted to fracture plane area, as expected by the model constraints that impose very low conductivity to bentonite barrier. Groundwater flow velocities in the fracture vary between 0.16 to 0.22 $m \cdot y^{-1}$ (Figure 5-2).

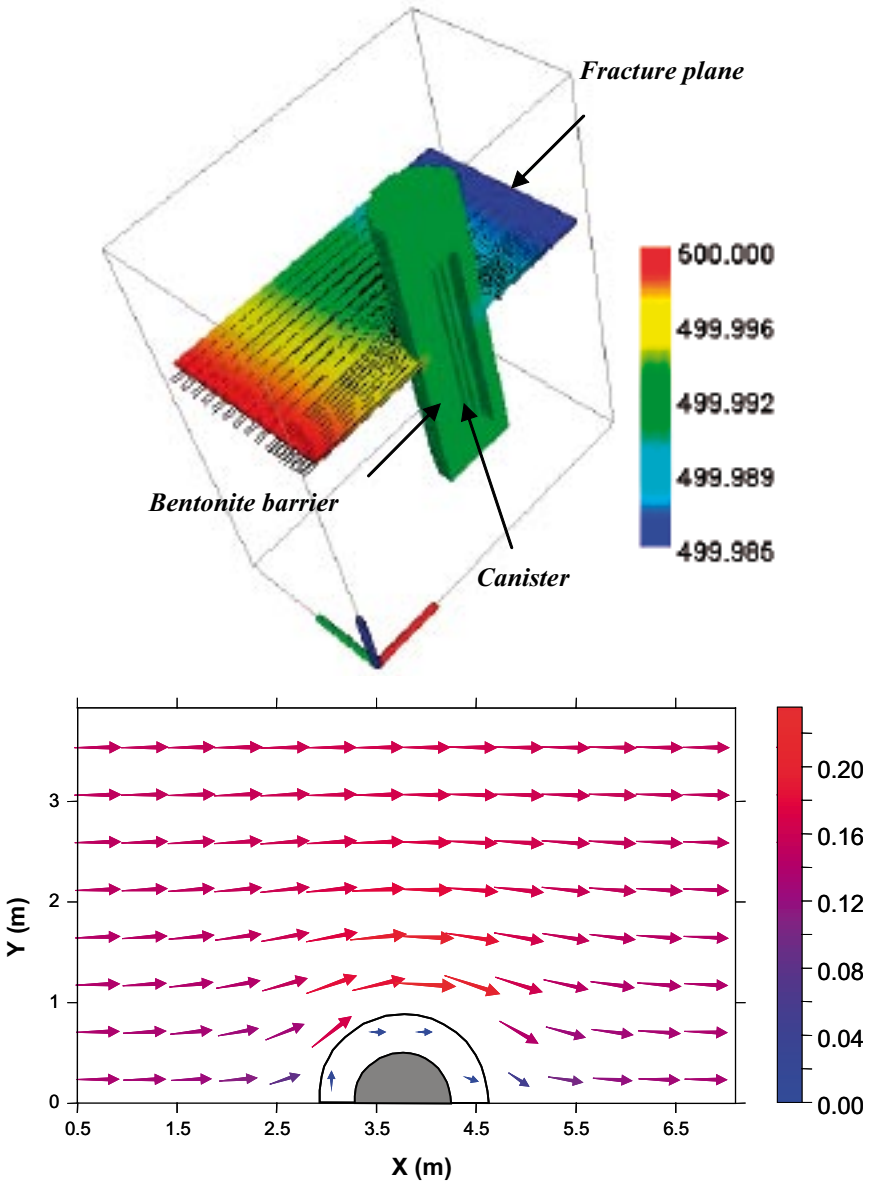

Figure 5-2. *(top) Fluid head (in colour) and flow vectors of the CASE-I model. Water flows from the left boundary to the right and flow vectors are diverted close to the bentonite barrier. Scale bar in metres. (bottom). Water flow velocities (in $m \cdot yr^{-1}$) in the fracture plane. Velocities are much lower (close to 0) in the bentonite (grey area).*

5.3.5 MX-80 bentonite

5.3.5.1 Reference case

The modelling results show that pH undergoes small changes due to the interaction between the Forsmark groundwater and the buffer (Figure 5-3). Initially, the pH in both the bentonite pore water and in the Forsmark groundwater is around 7.08, but as the simulation proceeds, a local plume of slightly higher pH, up to values of 7.43, is predicted to form at the fracture plane close to the buffer-fracture boundary (Figure 5-3). This pH plume reaches a maximum after 100 years and then decreases to disappear after 10,000 years of simulation. In the bentonite, a very small increase of pH is predicted, reaching a maximum pH value of 7.13 at the end of the simulation.

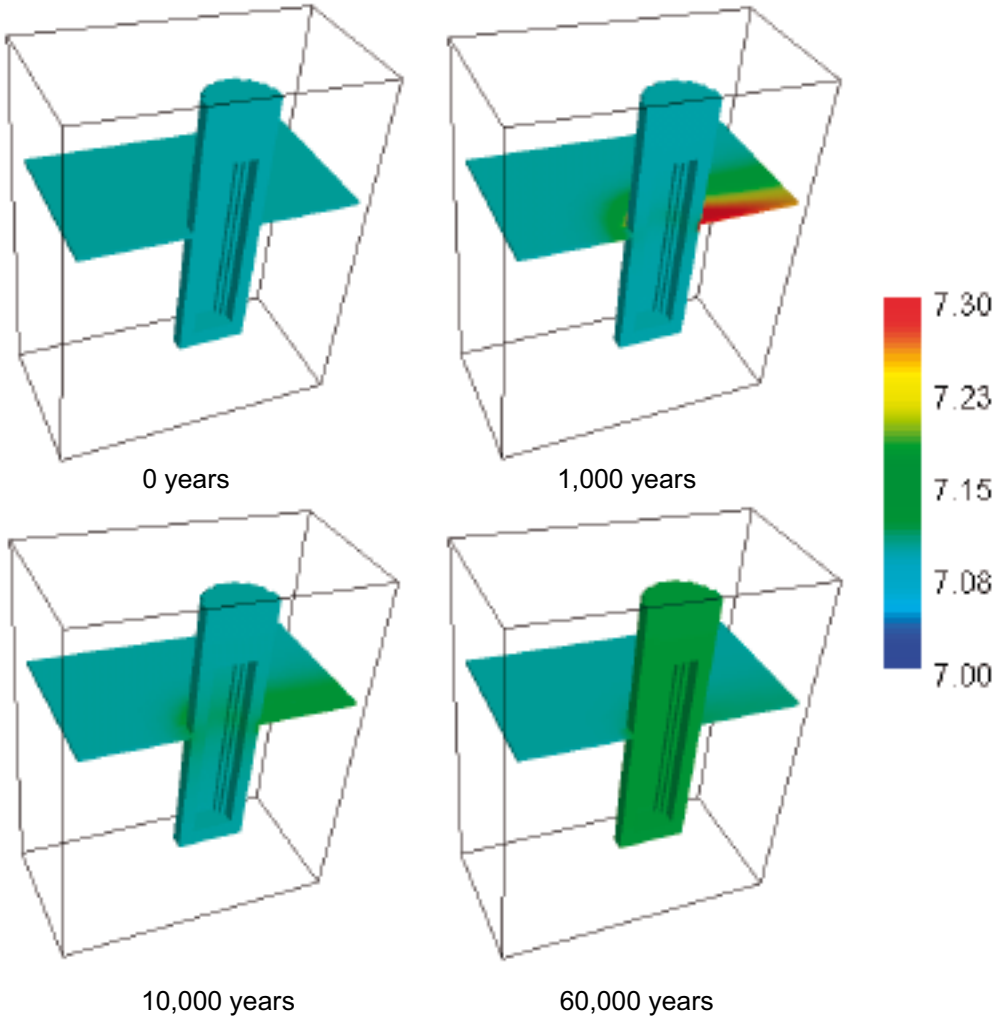

Figure 5-3. *pH evolution in the simulated domain (MX-80 bentonite). Note the plume of slightly higher pH in the fracture plane caused by local calcite buffering, especially in the initial 1,000 years. As the pH in the bentonite zone increases, this plume becomes less evident. Maximum pH in the buffer is reached at the end of the simulation at values of 7.2.*

The reason for the small changes in pH predicted by the model seems to be linked to changes in the calcium concentration of pore water in the bentonite and groundwater in the fracture around the buffer. As shown in Table 5-4 the calcium concentration in MX-80 bentonite pore water is two times lower than that in the Forsmark groundwater. This generates a calcium concentration gradient between the fracture and the bentonite producing a diffusion of calcium into the bentonite. This process results in a slight depletion of calcium in the fracture around the buffer (Figure 5-4), leading to the dissolution of small amounts of calcite (less than 0.002 moles per litre of groundwater during the first 100 years of simulation) and resulting in the previously described pH increase in the fracture around the bentonite. On the other hand, the increase of calcium concentration in the bentonite, due to diffusion from the fracture (Figure 5-4) and gypsum dissolution from the bentonite (Figure 5-5), results in the replacement of sodium by calcium in the cation exchanger, which is more pronounced in the bentonite zone close to the fracture zone (Figure 5-6). The absence of calcite in the bentonite lead to surface acidity reactions and Forsmark groundwater to control the pH of bentonite pore water.

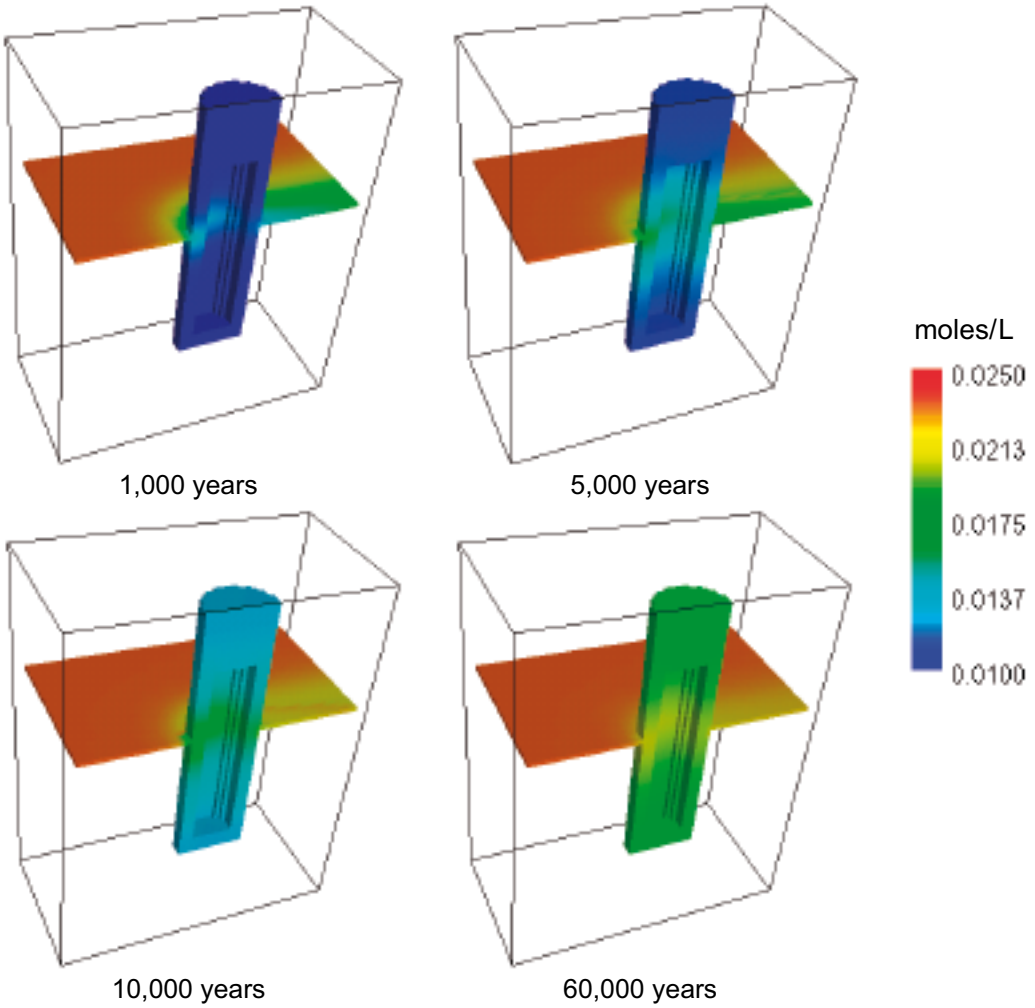

Figure 5-4. *Evolution of aqueous calcium concentration through time in the modelled domain. Calcium concentration in pore water increases in MX-80 bentonite buffer whereas in the fracture a plume of lower calcium concentration is observed.*

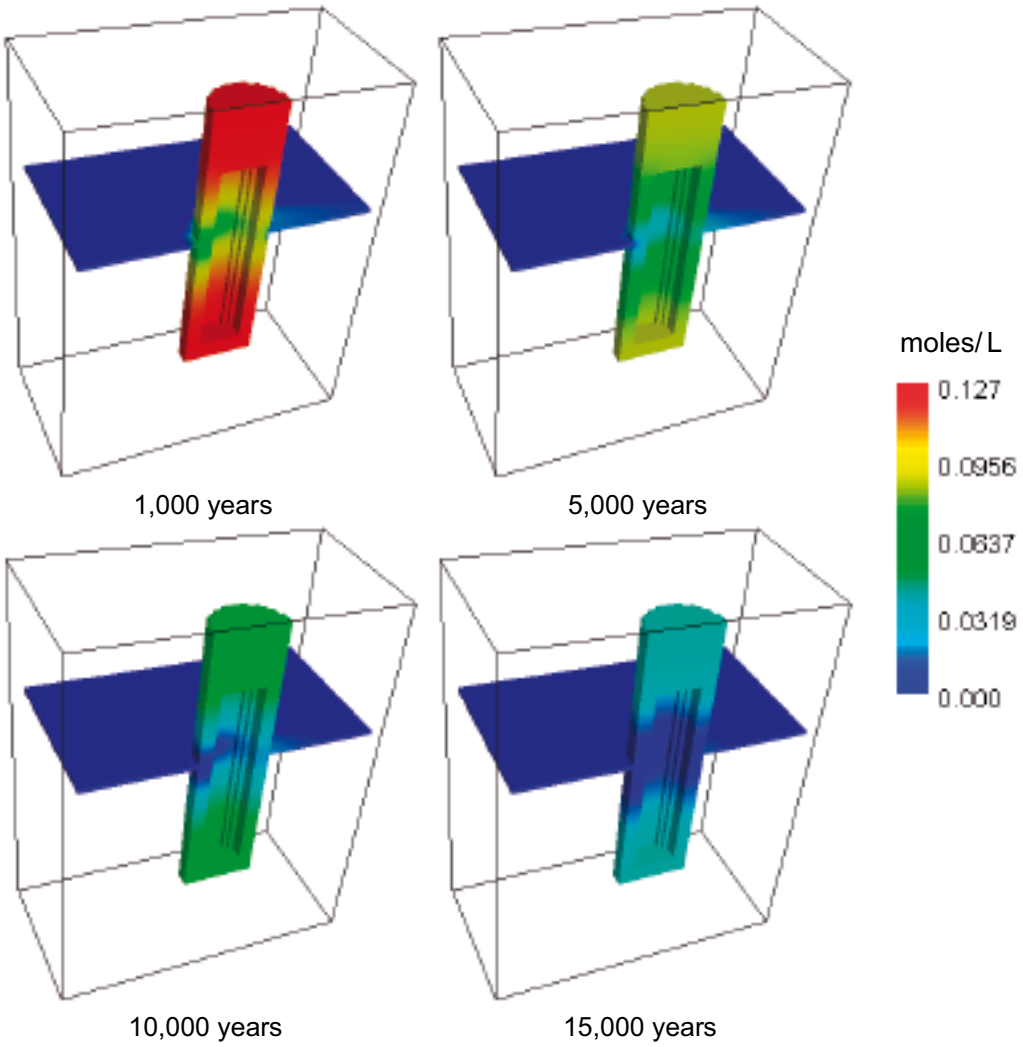

Figure 5-5. *Dissolution of gypsum during the simulation period. It is interesting to observe the fast dissolution at the fracture-bentonite interface: at 1,000 years gypsum concentration is a half of the initial inventory, and at 20,000 years it has almost been dissolved in the whole domain.*

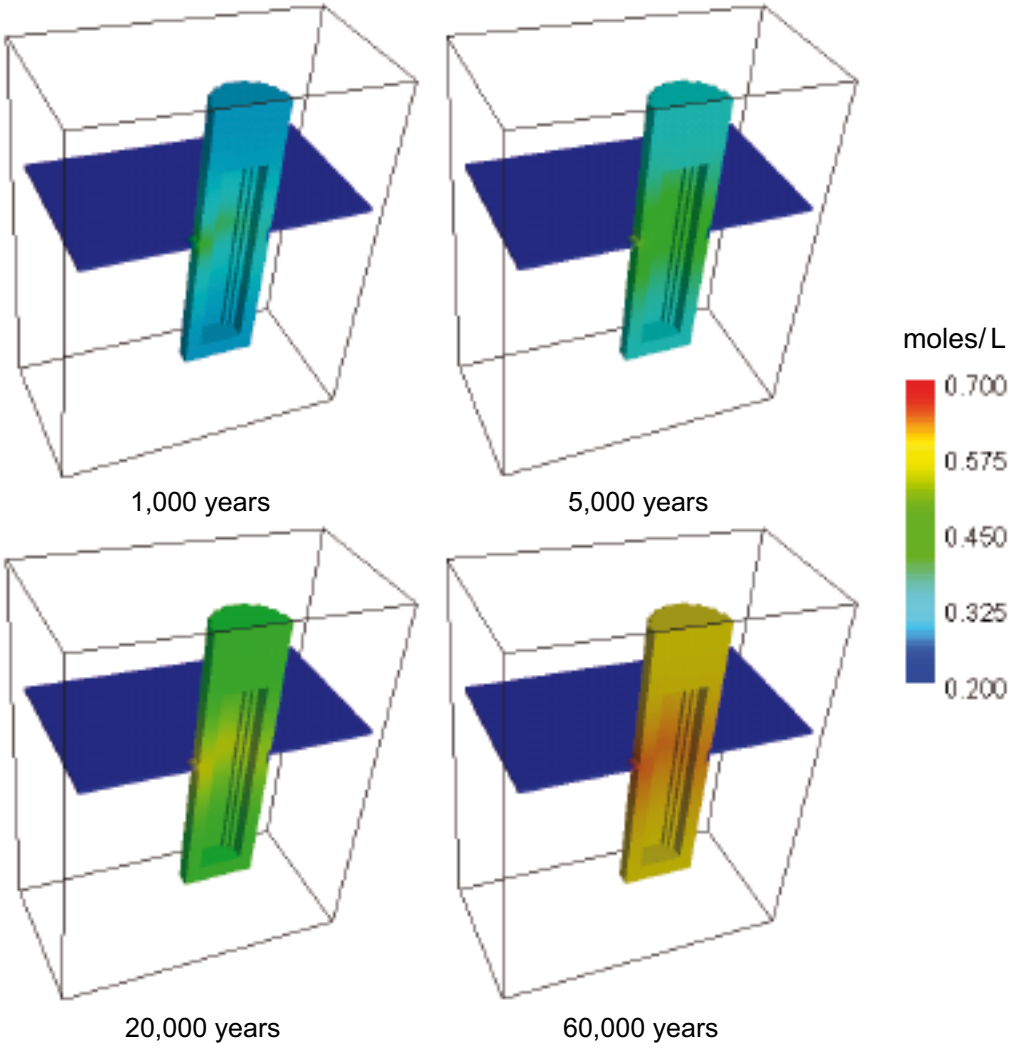

Figure 5-6. *Predicted evolution of Ca occupancy in the cation exchanger of the bentonite.*

Once gypsum from bentonite is completely dissolved, after 15,000 years of simulation (Figure 5-5), the increase of the calcium concentration in the bentonite pore water is slower, given that i) the only source for calcium is now Forsmark groundwater and that ii) the concentration gradient is lower than at the beginning of the simulation (Figure 5-7). For this reason, the replacement of Na by Ca in the exchanger also occurs at a lower rate, as shown in Figure 5-7. The continuous diffusion of calcium into the bentonite leads to the precipitation of very small amounts of calcite (less than 5×10^{-4} moles/L) close to the fracture (see Figure 5-8). Therefore, pH is still controlled by surface acidity reactions.

The redox state of the system does not change significantly through the simulation. In fact, the initial redox potential of the bentonite pore water is very similar to that of the Forsmark groundwater, which is very close to equilibrium with pyrite and siderite (Figure 5-9).

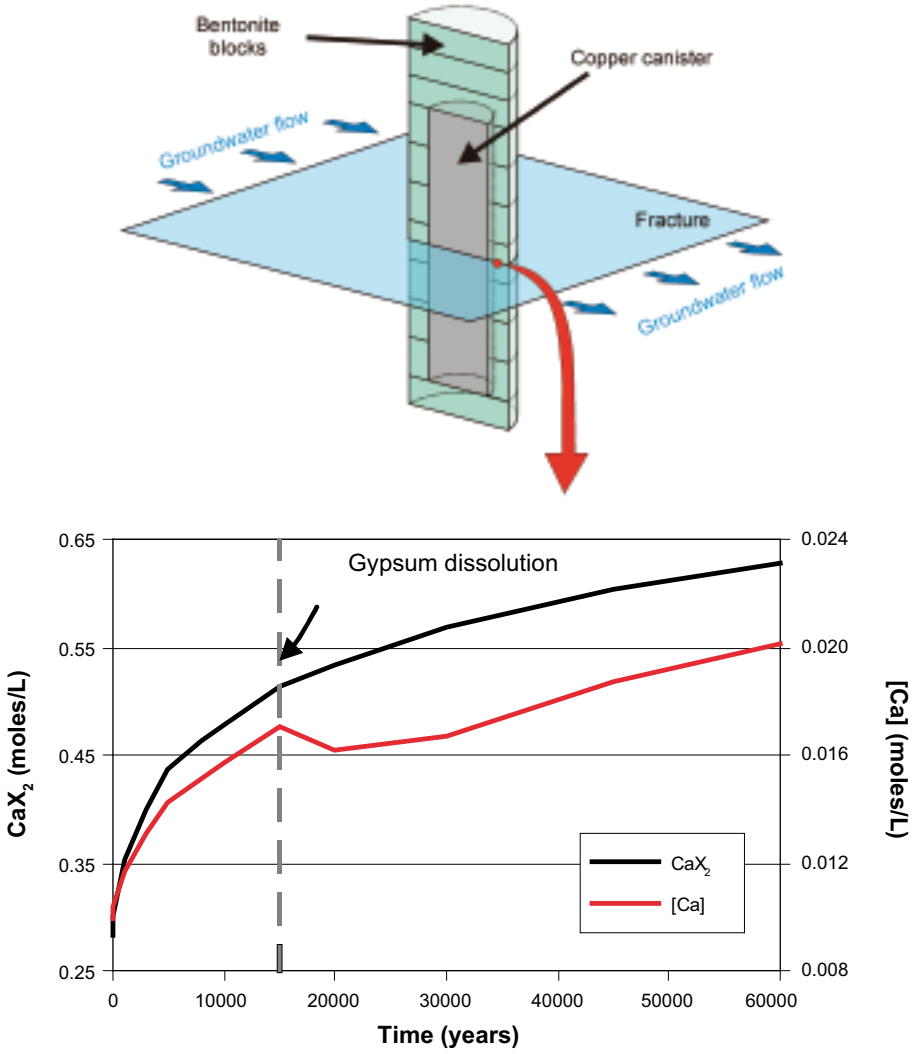

Figure 5-7. *Predicted evolution of calcium occupancy in the exchanger and calcium concentration of bentonite pore water in the bentonite close to the fracture as shown in upper graphic. The time at which gypsum is totally dissolved is also shown.*

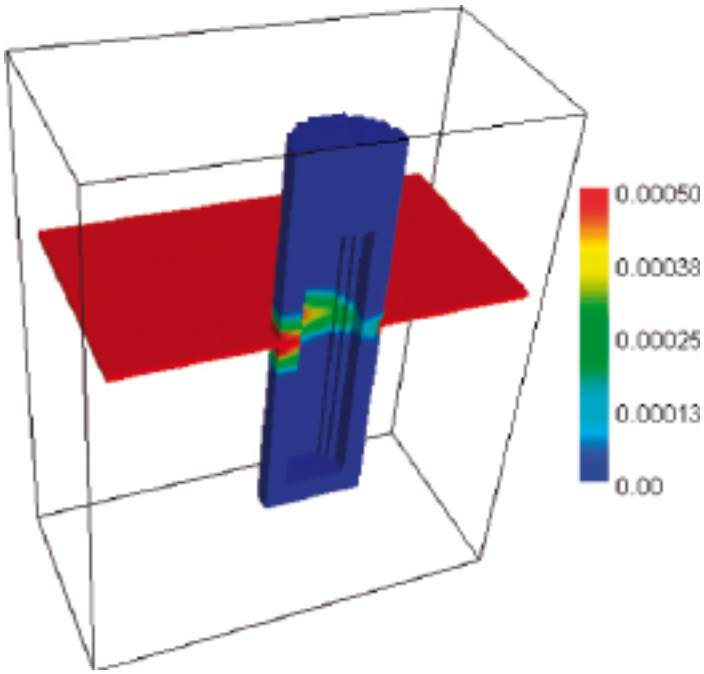

Figure 5-8. *Precipitation of secondary calcite at the end of the simulation (60,000 years). This precipitation is responsible for the decrease of pH observed in the latest stages. Calcite concentration in the fracture plane is much higher than indicated in the scale bar (11.5 mol/L). The scale bar (mol/L) has been limited to a very narrow range for a better observation in the bentonite.*

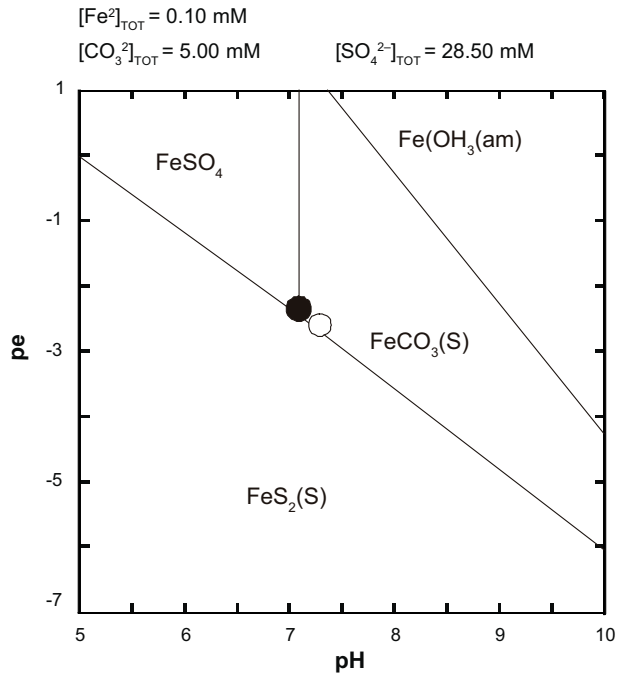

Figure 5-9. *pH-pe diagram showing the Fe system and the initial pH and pe for bentonite pore water (black dot) and Forsmark groundwater (white dot). In both cases pH-pe conditions are close to pyrite and siderite equilibrium.*

5.3.5.2 Reference case sensitivity analysis

One of the main uncertainties related to the near field geochemistry in the KBS-3 concept is the nature and heterogeneity in the distribution of the accessory minerals in the bentonite buffer. The reference mineralogical composition for the MX-80 bentonite assumes that carbonates (calcite and siderite) are not present as accessory minerals /SKB 2004b/. However, if present they will affect the geochemical evolution of the near field. For this reason, it is important to evaluate how the composition of pore waters changes when these solid phases are present.

The presence of carbonate minerals affects mainly the pH evolution of the system due to their buffering capacity. When assuming that both calcite and siderite (0.7 wt % each) are present in bentonite, the pH evolution in the system is different than that obtained in the reference case (Figure 5-10). The initial pH in the bentonite pore water is 7.16. Modelling results show that pH increases during the first 10,000 years of simulation, up to 7.3 far from the fracture and to 7.22 at the fracture level. During the rest of the simulation, the value of pH decreases again, and reaches values close to the initial ones at the end of the simulated period.

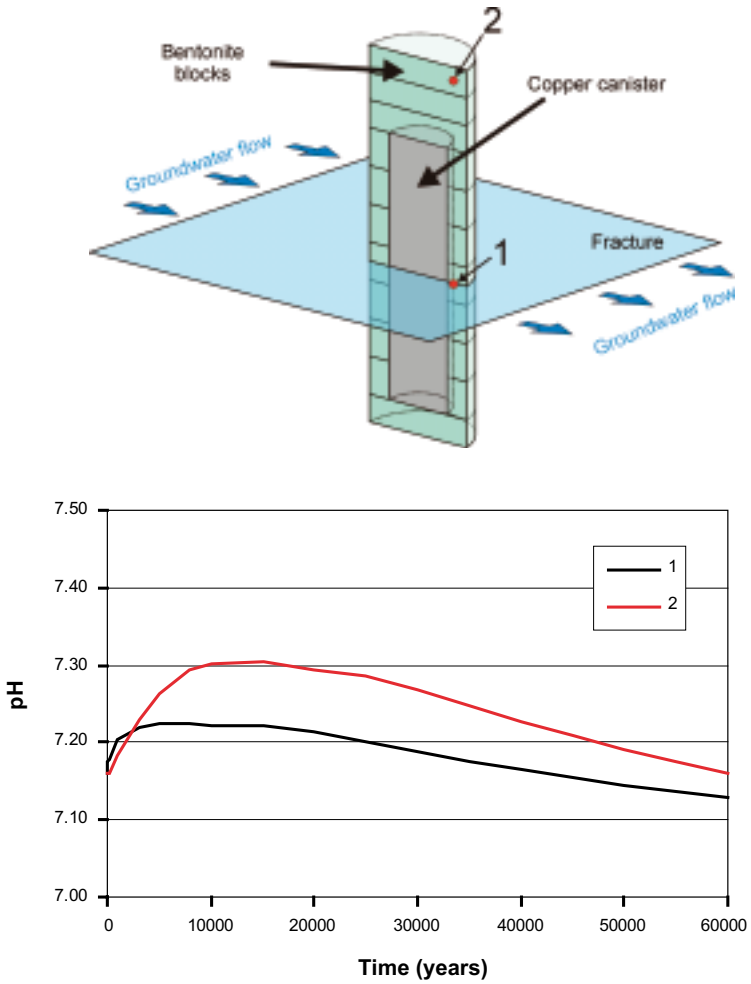

Figure 5-10. *Evolution of pH through time for MX-80 bentonite with calcite and siderite (0.7 wt % each) at two bentonite points as shown in the upper graphic (1) close to the fracture, and (2) far from the fracture. pH pore water in bentonite increases with time reaching a maximum of 7.30 at point 2 and 7.22 at point 1 after 10,000 years of simulation. At the end of the simulation, after 60,000 years, pH values are similar to the initial ones.*

Although the predicted variation in pH is still small when compared with the reference case, the difference is related to the presence of calcite in the bentonite, which dissolution-precipitation process has other more significant effects on the geochemical evolution of the near field. Calcite acts as an additional source of calcium for the Na by Ca exchange, but its behaviour is also affected by the out-diffusion of aqueous carbonate, due to the difference in concentration between bentonite pore water and Forsmark groundwater (4.98×10^{-3} and 2.20×10^{-3} moles/L, respectively). As aqueous carbonate diffuses out from bentonite during the first 10,000 years of simulation (Figure 5-11) and calcium is used for the Na by Ca exchange reaction, calcite becomes unsaturated and dissolves (Figure 5-12), leading to the increase of pH.

In fact, the dissolution of calcite is the result of two competing processes: 1) in-diffusion of calcium from Forsmark groundwater, and 2) out-diffusion of aqueous carbonate. The counter effect of these two diffusion processes results in a more pronounced dissolution of calcite in those parts far from the fracture, leading to a higher pH increase in these zones.

However, after 10,000 years of simulation, the carbonate concentration in bentonite pore water equals that of Forsmark groundwater (Figure 5-11). Whereas, calcium from Forsmark groundwater still diffuses into the bentonite (Figure 5-13), although at a lower rate due to the decrease in concentration gradients. For these reasons, calcite precipitates again in the bentonite until the end of the simulation decreasing again the pH (Figure 5-10).

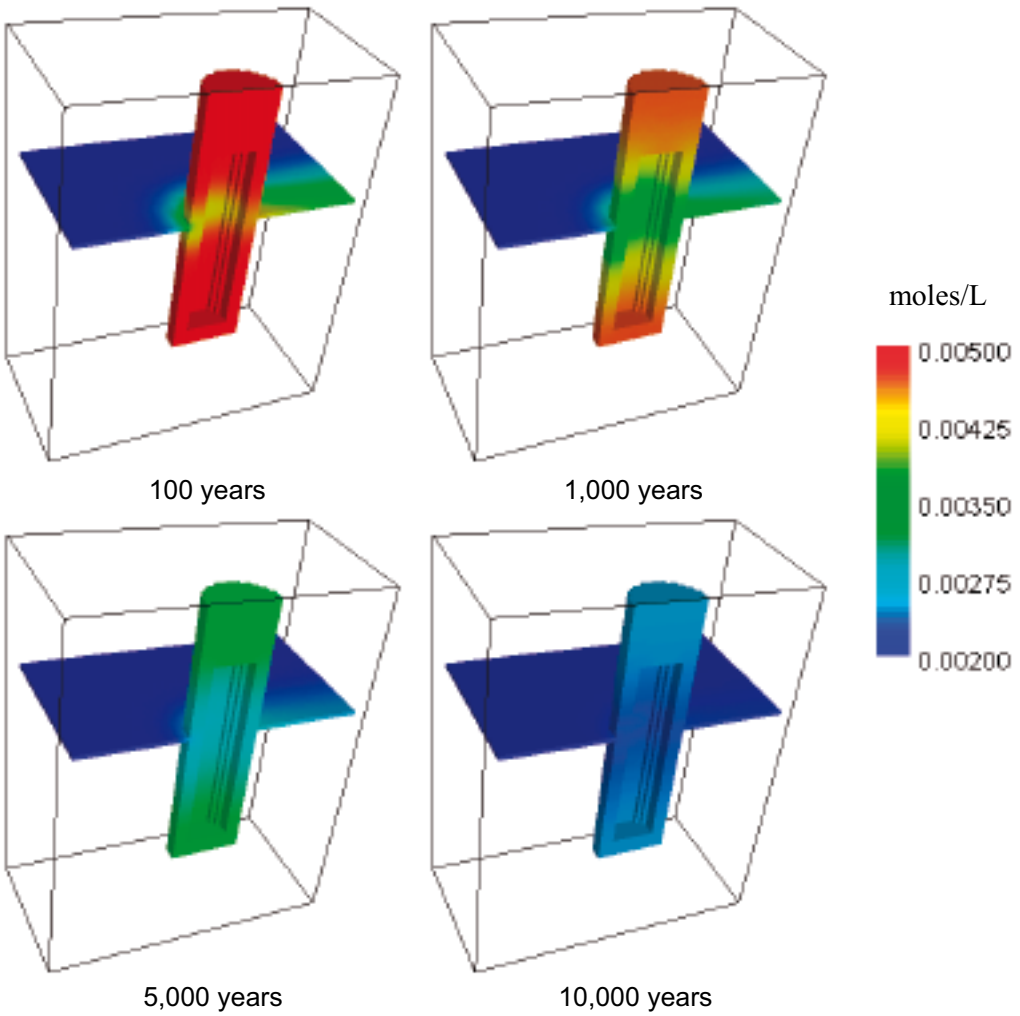

Figure 5-11. *Predicted time and spatial evolution of aqueous carbonate in the system. Note that aqueous carbonate diffuses out from bentonite until the same concentration as in Forsmark groundwater is reached after 10,000 years of simulation.*

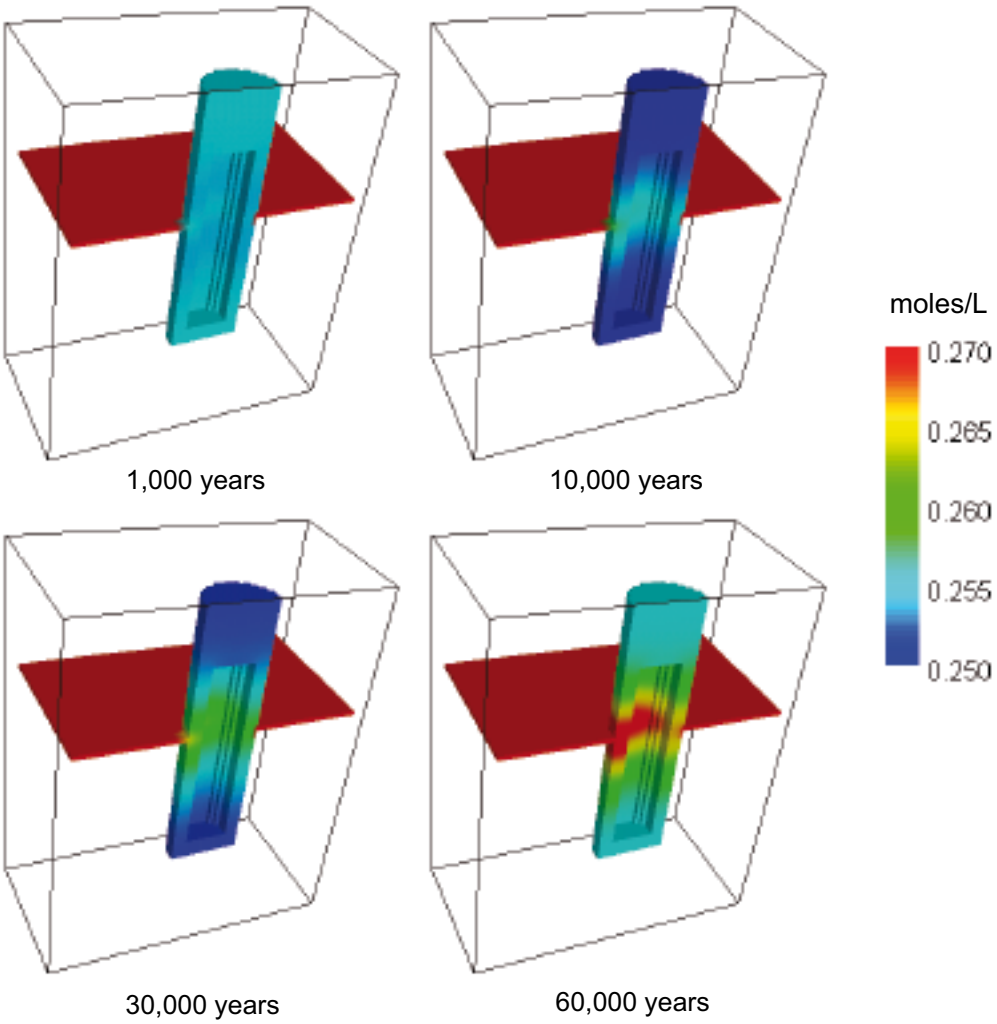

Figure 5-12. *Evolution of calcite content for MX-80 bentonite with calcite and siderite (0.7 wt % each). Note the dissolution of calcite during the first 10,000 years of simulation and its precipitation thereafter until the end of the simulation.*

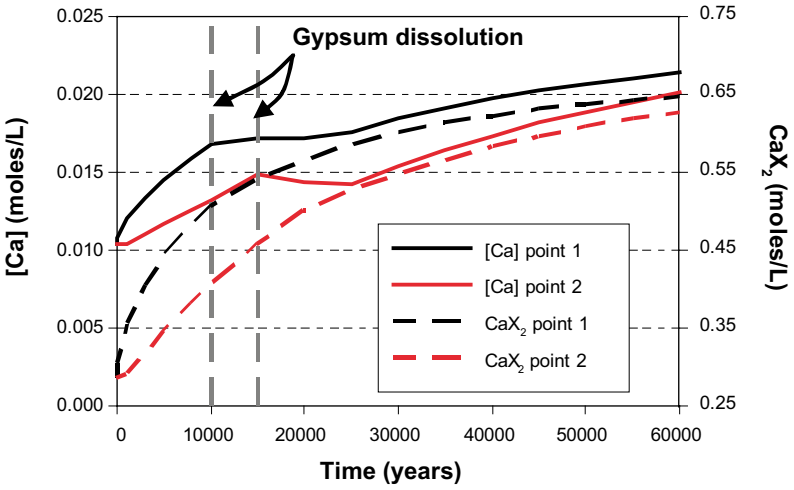

Figure 5-13. *Predicted evolution of calcium concentration in pore water and Ca occupancy in the exchanger at two points in the bentonite as shown in Figure 5-10, (1) at the fracture level, and (2) far from the fracture intersection. Gypsum complete dissolution in the two points is shown for comparison. Note that the concentration of calcium is always lower in point 2 respect to point 1, and consequently the Ca occupancy in the exchanger is also lower.*

Summarising, during the first 10,000 years of simulation calcite dissolves in the bentonite due to carbonate out-diffusion and replacement of Na by Ca in the exchanger. Whereas, after the first 10,000 years the Na by Ca replacement rate slows down due to three reasons: gypsum as a source of calcium is not acting anymore due to its complete dissolution (Figure 5-13); Ca diffusion into the bentonite decreases, as a consequence of a decrease in calcium concentration gradients; and part of the calcium diffusing into the bentonite precipitates as calcite.

5.3.5.3 Intrusion of ice-melting water

As already mentioned in Section 2.2, it is likely that waters different that present-day groundwater flowing at depth in the Forsmark site can reach the repository level. We evaluated two different possibilities: the intrusion of a water derived from ice melting, which is a plausible scenario at the end of a glacial period, and the up-rise of high-salinity water, which has been sampled at depth in a number of drill holes in the Fennoscandian shield. In both cases, it has been assumed that the intrusion could take place after 10,000 years of the construction of the repository (10,000 years after starting the simulation). The chemical features of the bentonite clay and hydrological parameters are the same as in the reference case.

Unlike the Forsmark groundwater, ice-melting waters are characterised by a very low salinity. As an example, in the present work we have selected the groundwater composition from the Grimsel site (Switzerland) corresponding to a glacial melt water slightly interacted with a granitic environment. This ice-melting groundwater is characterised by a high pH (pH = 9.6) and a composition dominated by Na and HCO_3^- (see complete composition in Table 2-1). Some bentonite accessory minerals, like gypsum, are undersaturated in contact with this water type (saturation index of –3.39), whereas others like calcite and quartz are close to saturation (saturation indexes of 0.21 and 0.34, respectively). In order to evaluate the effect of this groundwater on the near field, avoiding changes in the chemical composition due to the interaction with fracture filling minerals prior to reach the bentonite buffer, we assumed that this ice-melting water is in equilibrium with calcite and quartz. Then a slightly modified chemical composition will be used for modelling purposes instead of the raw chemical composition of Grimsel groundwater as shown in Table 5-5.

In the first 10,000 years of simulation, previous to the intrusion of ice-melting water, the evolution of the system is equal to that corresponding to the reference case (see Section 5.3.5.1). However, once ice-melting water reaches the near field system, the geochemical evolution of the system diverges from that of the reference case. The pH in the bentonite pore water tends to increase (Figure 5-14) until the end of the simulation, with a maximum pH of approximately 8.3 in the bentonite close to the fracture zone. This increase in pH is due to the high pH of the ice-melting water, which causes a modification of montmorillonite surface acidity, leading to the deprotonation of positively charged sites mainly increasing the concentration of neutral sites (Figure 5-15). Thus, acidity reactions on the clay surface buffer the pH of pore water to lower pH values than that of the ice-melting water. No other process, as dissolution or precipitation of accessory minerals, is responsible for this pH increase.

An additional effect relevant for the geochemical evolution of the system after the ice-melting water intrusion is the composition of the cation exchanger in the bentonite. Due to the low concentration of calcium in the ice-melting water, the diffusive transport of calcium in the system reverses and then calcium diffuses from the bentonite to the fracture zone and is flushed out of the near field system. Thus, the concentration of calcium in the bentonite pore water decreases very fast, so the Na by Ca exchange process is slowed down (Figure 5-16). This decrease in calcium concentration accelerates the complete dissolution of gypsum in the bentonite, predicting its complete dissolution before 13,000 years of simulation.

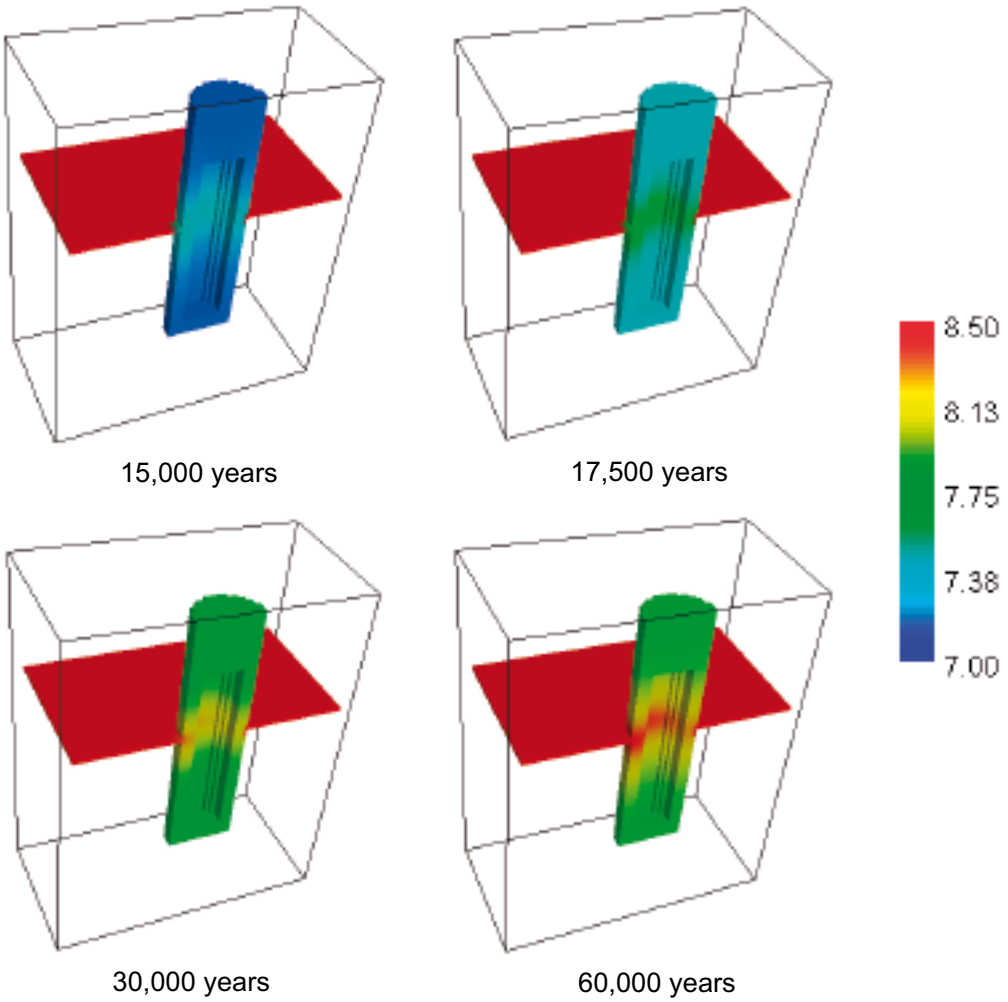

Figure 5-14. *Predicted pH evolution of the system after the intrusion of ice-melting water at 10,000 years of simulation.*

Table 5-5. Chemical composition of ice-melting waters as reported in /Hoehn et al. 1998/ and recalculated for modelling purposes.

Moles/L	Grimsel groundwater	Re-calculated
pH	9.6	9.58
pe	–3.38	–3.35
HCO_3^-	4.50×10^{-4}	4.08×10^{-4}
Ca	1.40×10^{-4}	9.75×10^{-5}
Cl	1.60×10^{-4}	1.60×10^{-4}
Fe tot	3.00×10^{-9}	3.00×10^{-9}
K	5.00×10^{-6}	5.00×10^{-6}
Mg	6.20×10^{-7}	6.20×10^{-7}
Na	6.90×10^{-4}	6.90×10^{-4}
SO_4^{2-}	6.10×10^{-5}	6.10×10^{-5}
SiO_2	2.05×10^{-4}	9.25×10^{-5}

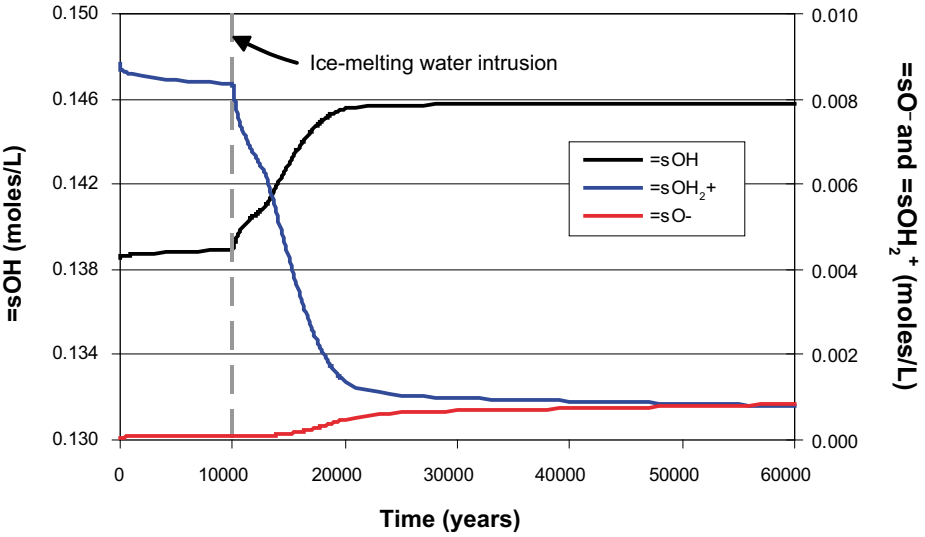

Figure 5-15. *Predicted evolution of the surface acidity (Z sites in Table 5-3) of the clay fraction in the bentonite at point 1 as indicated in Figure 5-10.*

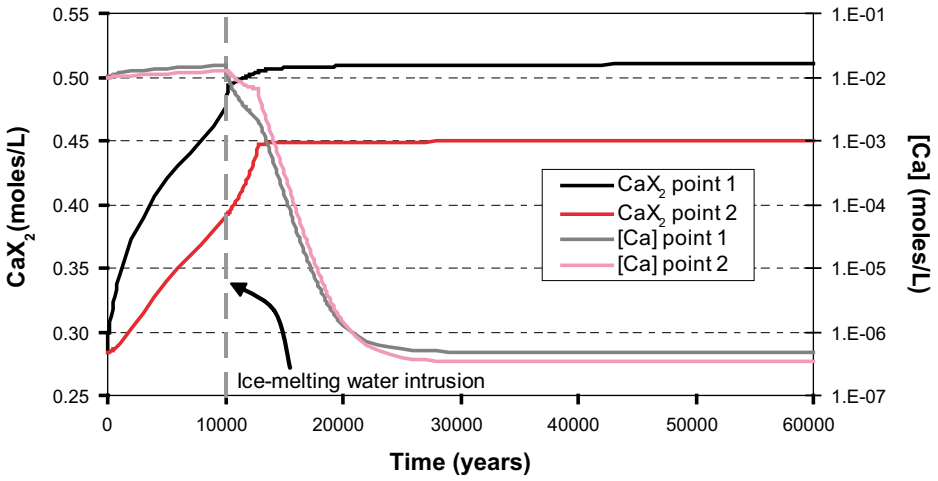

Figure 5-16. *Predicted evolution of Ca occupancy in the exchanger and aqueous calcium concentration at two points in the bentonite as shown in Figure 5-10, (1) at the fracture level, and (2) far from the fracture intersection. Note that approximately after ice-melting water intrusion (grey dashed line) the calcium occupancy in the exchanger is predicted to be constant.*

5.3.5.4 Intrusion of high-salinity groundwater

The high-salinity groundwater from Laxemar (Table 2-1) has a very low pe leading to the predominance of reduced sulphur and carbon aqueous species. Under these conditions, and assuming that it is likely that bacterial activity in the fractured granite allow sulphate to sulphide and carbonate to methane transformations, the aqueous sulphur and carbon dominant species are HS^- and CH_4, respectively (Figure 5-17), instead of S(VI) and carbonate aqueous species as in the reference case, where present-day Forsmark groundwater is considered.

Analytical data from Laxemar /Laaksoharju et al. 1995/ indicates that the dominant aqueous sulphur species are S(VI) species and no methane has been detected. Therefore, we modified the pe of the system by forcing equilibrium with pyrite. On the other hand, the carbonate concentration has been obtained by alkalinity titration, and considering the relatively high concentration of dissolved organic carbon (DOC), as reported in /Laaksoharju et al. 1995/ that can contribute

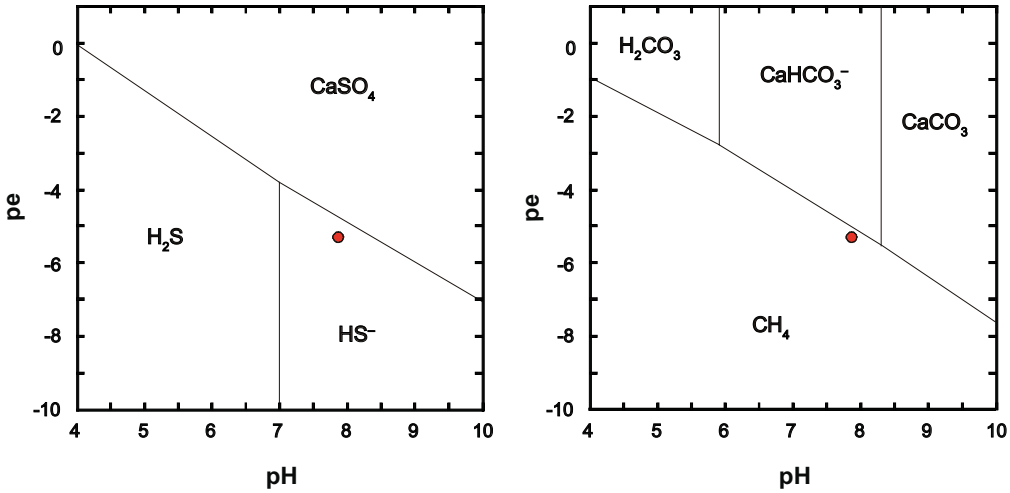

Figure 5-17. *Sulphur and carbon predominance diagrams for the Laxemar high-salinity groundwater according to chemical composition from Table 2-1. The red dot represents the high-salinity groundwater from Laxemar.*

effectively to the alkalinity, we can consider that the actual carbonate concentration must be below this alkalinity value. Thus, we forced carbonate concentration to be in equilibrium with calcite to obtain a lower aqueous carbonate concentration. Finally, gypsum is supersaturated in the system, owing the high sulphate and calcium concentrations. For this reason, we forced the equilibrium with gypsum. Thus, the resulting water composition differs from that reported in /Laaksoharju et al. 1995, SKB 2004b/, especially regarding the values of the redox potential and carbonate and sulphate concentrations (Table 5-6).

As in the previous case, the evolution of the system during the first 10,000 years of simulation will be the same as in the reference case. However, from this point to the end of the simulation a different evolution is predicted. During the first 10,000 years, pH increases to a maximum of 7.1 (Figure 5-3), beyond this point pH slightly decreases reaching a value of 7.0 and then increases again to a maximum value of 7.06 after 25,000 years of simulation (Figure 5-18).

Table 5-6. Chemical composition of saline waters as reported in /SKB 2004b/ and recalculated for modelling purposes.

Moles/L	/SKB 2004b/	Re-calculated
pH	7.9	7.9
pe	–5.08	–3.88
HCO_3^-	1.00×10^{-4}	3.24×10^{-5}
Ca	4.64×10^{-1}	4.58×10^{-1}
Cl	1.28	1.28
Fe tot	8.00×10^{-6}	8.00×10^{-6}
K	7.00×10^{-4}	7.00×10^{-4}
Mg	1.00×10^{-4}	1.00×10^{-4}
Na	3.49×10^{-1}	3.49×10^{-1}
SO_4^{2-}	9.00×10^{-3}	2.59×10^{-3}
SiO_2	8.00×10^{-5}	5.67×10^{-5}

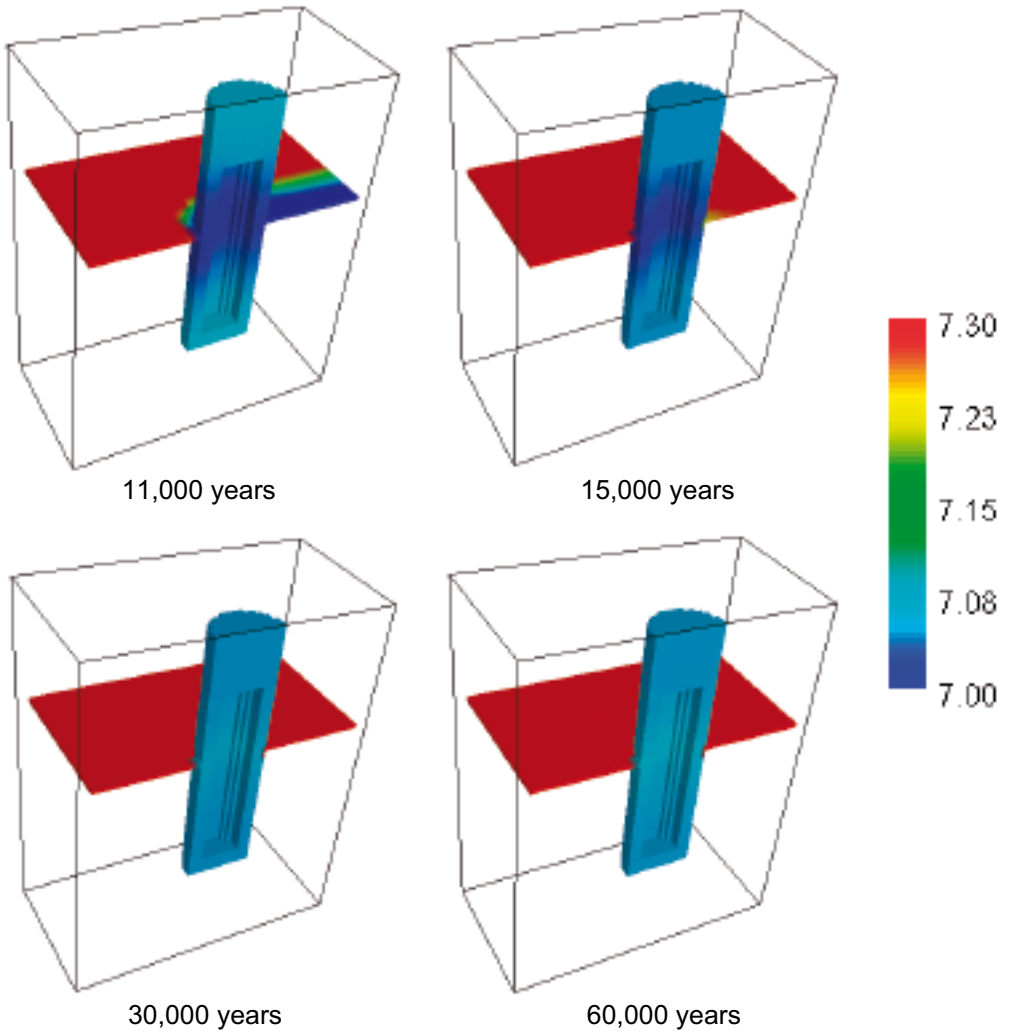

Figure 5-18. *Predicted pH evolution of the system after the intrusion of high-salinity water at 10,000 years of simulation.*

The decrease in pH coinciding with the intrusion of high-salinity water is related to the precipitation of calcite in the bentonite. The reason for the precipitation of calcite in the bentonite is the high concentration of calcium in the high-salinity water (20 times higher than Forsmark groundwater, see Table 5-4 and Table 5-6). Despite, the high-salinity water has a carbonate concentration two orders of magnitude lower than Forsmark groundwater, the high concentration in calcium lead to a large diffusion of calcium into the bentonite (Figure 5-19) allowing the precipitation of calcite. However, the diffusion of aqueous carbonate out of the bentonite, lead to the dissolution of the previously precipitated calcite (Figure 5-20), thus increasing again the pH of the bentonite pore water.

In addition, the diffusion of large amounts of calcium into the bentonite increases the Na by Ca replacement in the exchanger (Figure 5-21).

Finally, the diffusion of high amounts of calcium into the bentonite stops the dissolution of gypsum and even some precipitation occurs near the contact with the fracture. However, as aqueous sulphate is diffusing out of the bentonite, pore water approaches to equilibrium with gypsum (high-salinity water is assumed to be in equilibrium with gypsum), and only small amounts of this phase still precipitate at the end of the simulation (Figure 5-22).

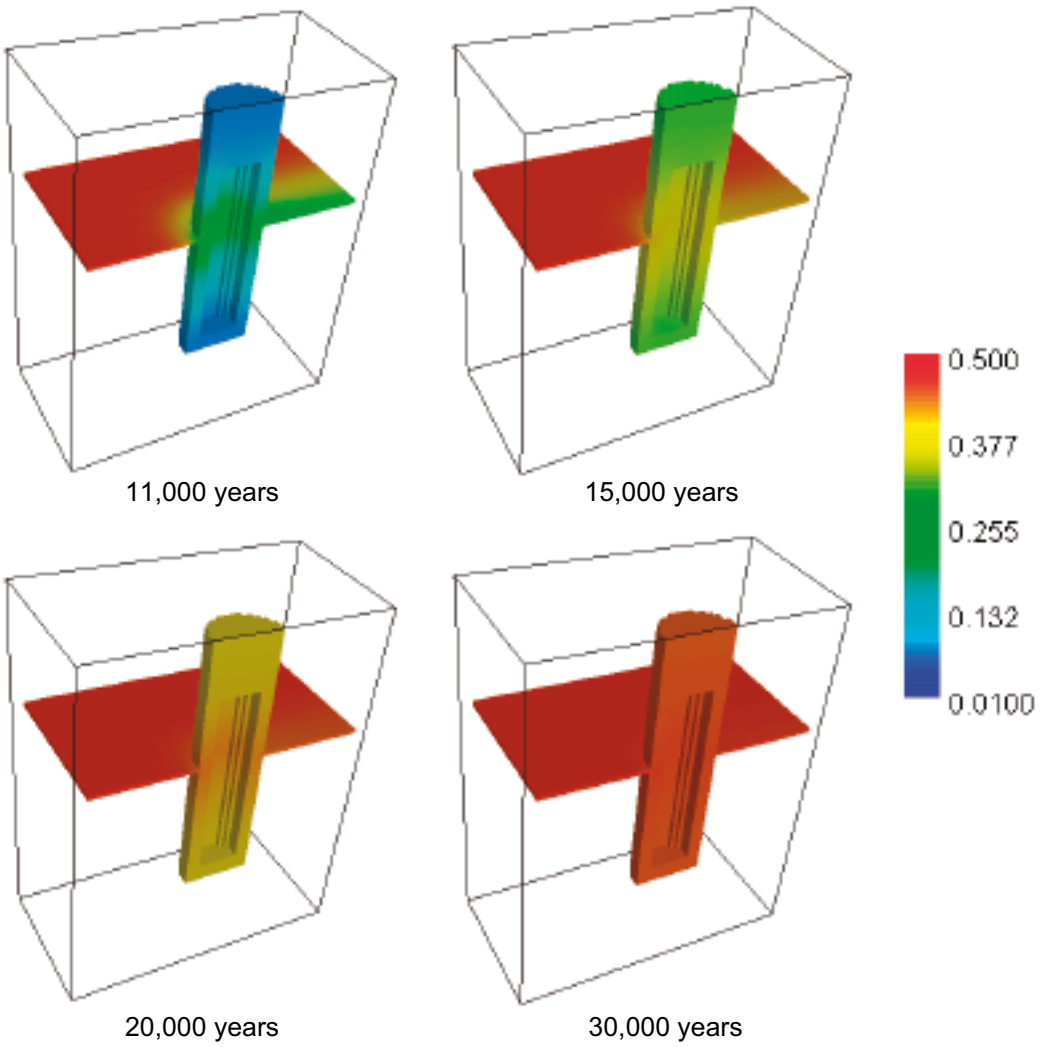

Figure 5-19. *Evolution of aqueous calcium concentration through time in the modelled domain after the intrusion of high-salinity water at 10,000 years of simulation. Note the different scale with respect to Figure 5-4.*

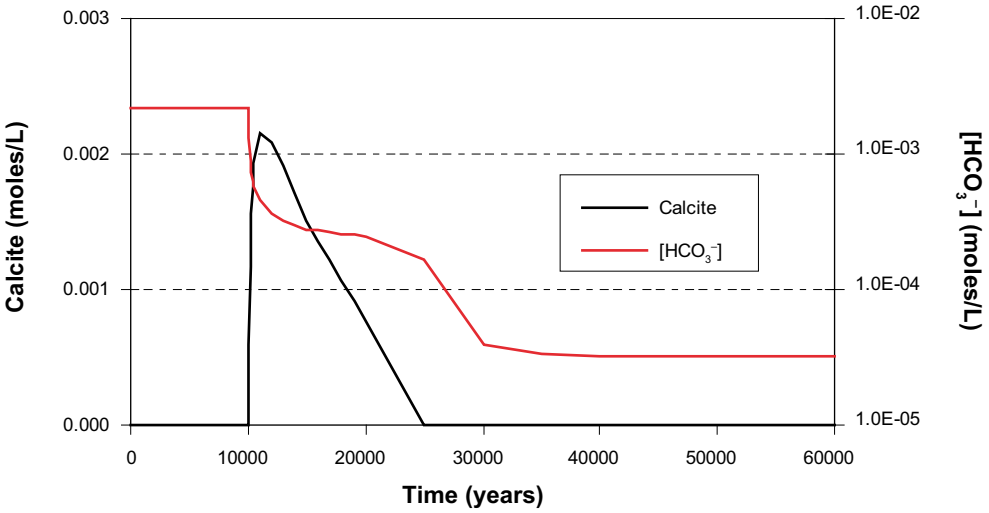

Figure 5-20. *Predicted evolution of the aqueous carbonate concentration and calcite content in the bentonite near the fracture zone (exact location as in Figure 5-7) due to the intrusion of a high-salinity groundwater after 10,000 years of simulation.*

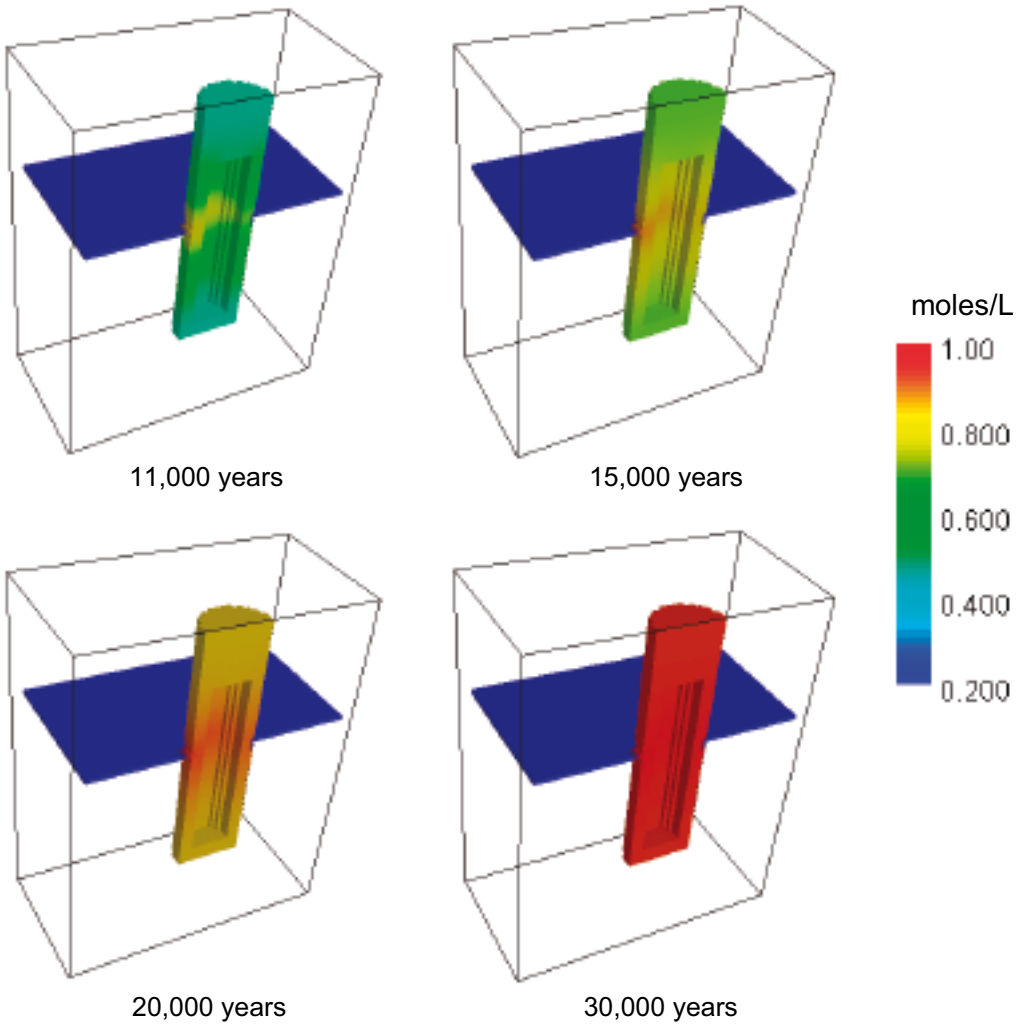

Figure 5-21. *Predicted evolution of Ca occupancy in the cation exchanger of the bentonite after the intrusion of high-salinity water.*

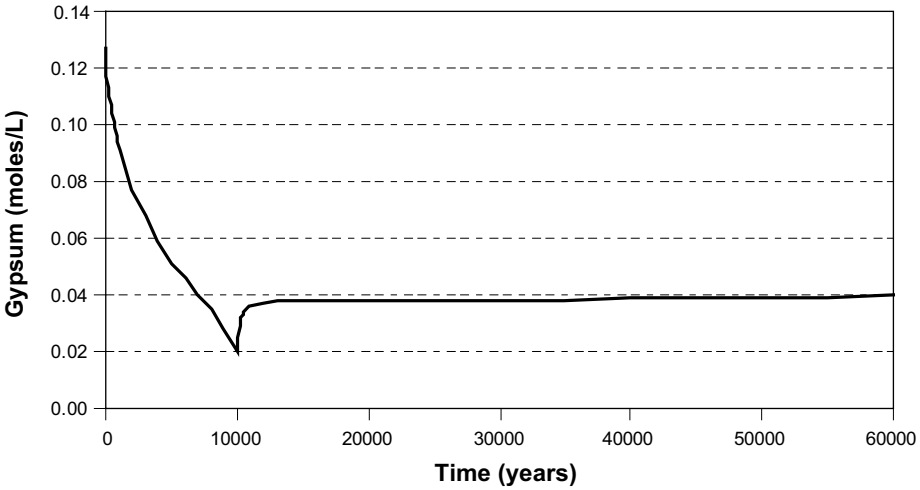

Figure 5-22. *Predicted evolution of the gypsum content in the bentonite close to the fracture (exact location as in Figure 5-7) after the intrusion of high-salinity water.*

5.3.5.5 Summary

The most relevant results of CASE-I simulations, considering MX-80 as the buffer material, are the following:

- Predicted changes in the bentonite buffer are more pronounced near the granite fracture than far from it.
- The predicted pH in the bentonite buffer does not change significantly when interacting with the Forsmark groundwater or with high-salinity water, even if calcite is considered initially present in the bentonite.
- If ice-melting water interacts with the bentonite buffer, the pH increases, especially close to the fracture zone, where a maximum pH of 8.3 is predicted.
- pH is buffered by the equilibrium with calcite, except when calcite is not initially present in the bentonite or ice-melting water enters into the system, as calcite is undersaturated and the increase of pH is partially buffered by protonation – deprotonation reactions on the montmorillonite surface.
- The precipitation – dissolution of calcite in the bentonite buffer is controlled by the evolution of calcium and carbonate aqueous concentration in pore water.
- Aqueous carbonate concentration in bentonite pore water is initially higher than all groundwater types considered in the model (Forsmark groundwater, ice-melting water and high-salinity water). Therefore, aqueous carbonate always diffuses out from the bentonite.
- Calcium concentration in pore water is controlled by gradient concentrations between groundwater and bentonite pore water and gypsum dissolution in the buffer.
  - When Forsmark groundwater is considered, calcium concentration in bentonite increases due to diffusion from the granitic fracture and gypsum dissolution. Leading to the replacement of Na by Ca in the exchanger and precipitation of calcite, restricted to the bentonite zone close to the fracture.
  - When ice-melting water contacts the buffer, calcium diffuses out from bentonite, accelerating the dissolution of gypsum and limiting the extent of the Na by Ca replacement in the exchanger.
  - When high-salinity water contacts the buffer, calcium diffusion into the bentonite increases, increasing the Na by Ca replacement in the exchanger, stopping the dissolution of gypsum, and allowing calcite precipitation, which re-dissolves when aqueous carbonate is depleted due to out-diffusion.
- The redox of the system seems to be controlled by the Eh of the groundwater contacting the bentonite buffer.

5.3.6 Deponit CA-N bentonite

5.3.6.1 Reference Case

When the Deponit CA-N bentonite is considered, the modelling results show that predicted changes in the chemical evolution of the system are less pronounced than in the case where MX-80 bentonite was considered. Thus, pH is predicted to continuously increase from 7.09 at the beginning of the simulation (Figure 5-23), reaching a maximum value of 7.16 at the end of the simulation.

The very small modification of pH is due to the equilibrium of bentonite pore water with calcite. The model predicts the precipitation of calcite from the beginning of the simulation. However, this precipitation is produced almost completely at expenses of the dissolution of dolomite (Figure 5-24). Thus, the precipitation of calcite in this case does not modify substantially the pH of the system.

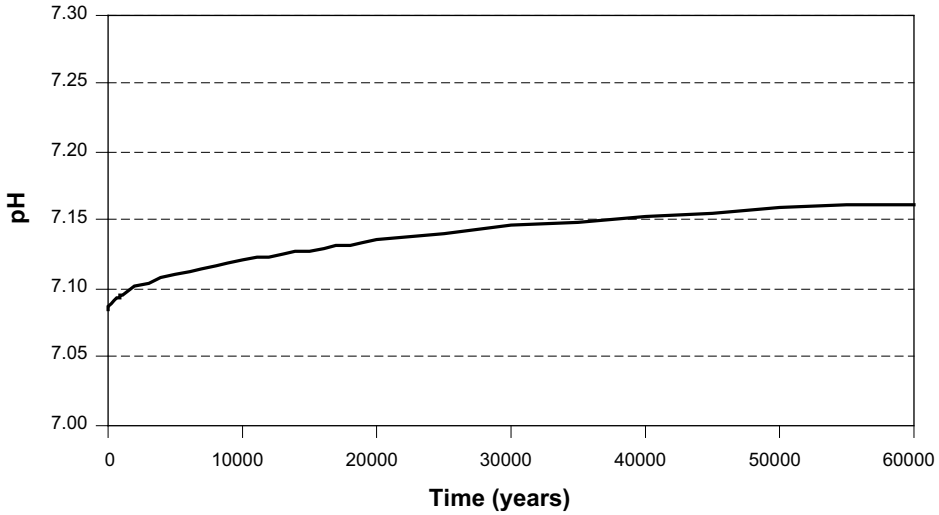

Figure 5-23. *Predicted pH evolution in the Deponit CA-N bentonite pore water near the fracture zone (exact location as in Figure 5-7).*

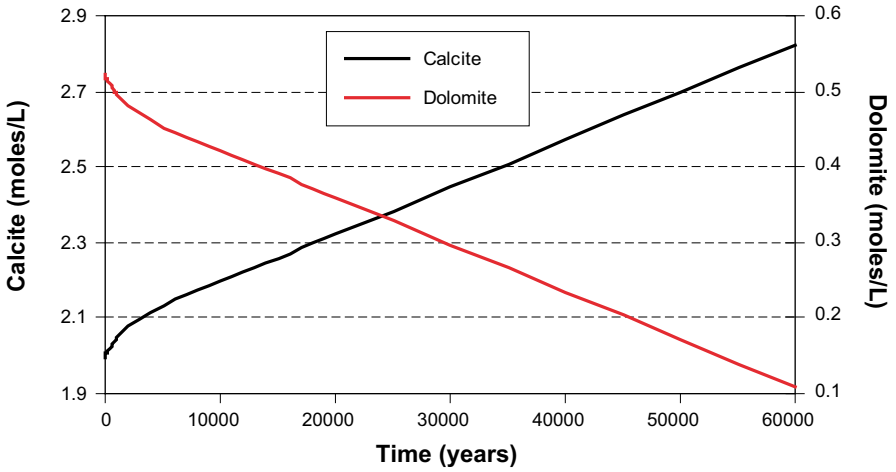

Figure 5-24. *Predicted evolution of the dolomite and calcite content in the Deponit CA-N bentonite near the fracture zone (exact location as in Figure 5-7).*

The reason for such a transformation is that the concentration gradient for magnesium, between the bentonite and the fracture, is larger than for calcium. Thus, magnesium diffuses out from the bentonite faster than calcium, producing the dissolution of dolomite, increasing the aqueous carbonate concentration in the bentonite and leading to the supersaturation with respect to calcite.

Despite this transformation of dolomite into calcite, both calcium and carbonate concentrations in bentonite pore water are slightly higher than in Forsmark groundwater. Thus, a slow but continuous diffusion of these two components out of bentonite is predicted during the simulation. To maintain equilibrium with calcite in the bentonite, calcium is supplied by two additional sources in the bentonite: i) cation exchange, and ii) gypsum dissolution, what slows down the impact that the diffusion of Ca out of bentonite may have. The slightly higher concentration of sodium in the Forsmark groundwater with respect to the bentonite pore water leads to the Ca by Na replacement in the exchanger (Figure 5-25).

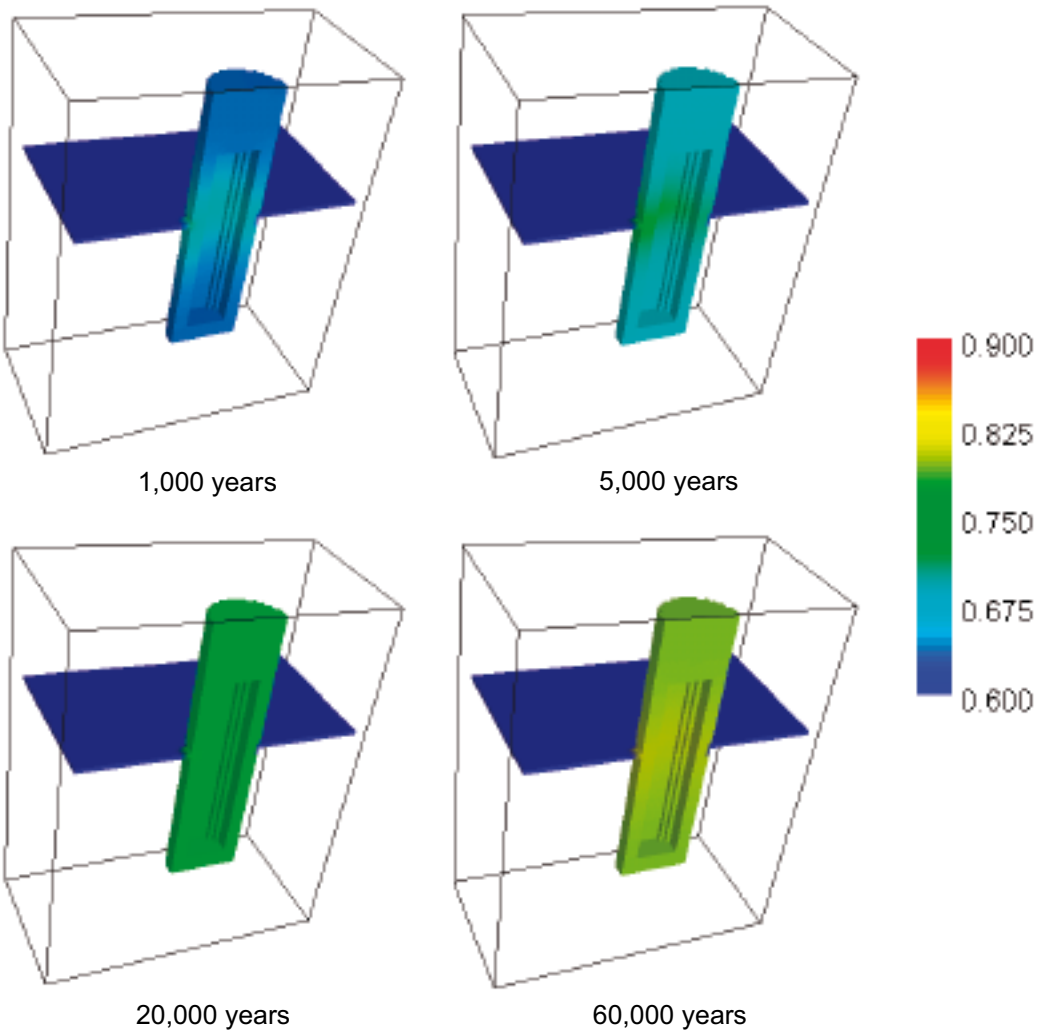

Figure 5-25. *Predicted evolution of Na occupancy in the cation exchanger of the bentonite.*

5.3.6.2 Intrusion of ice-melting water

The effect of the interaction of ice-melting waters with the Deponit CA-N bentonite is more complex than the case with the MX-80 bentonite, due to the presence of carbonate minerals (mainly calcite and dolomite). The behaviour of carbonate minerals during the interaction with diluted water of alkaline pH, could result in two opposite and competing processes: i) precipitation of carbonates to buffer the intrusion of high pH waters, and ii) dissolution of carbonates due to the out-diffusion of Ca and aqueous carbonate from the bentonite, imposed by the low concentration of these two components in the inflowing groundwater.

The results of the simulation indicate that pH in the bentonite pore water increases after the intrusion of ice-melting water (Figure 5-26), reaching a maximum pH of 9.3 near the fracture plane at the end of the simulation.

The reason for this increase in pH is related to the behaviour of aqueous calcium and carbonate in the system. Once ice-melting water contacts the near field, the strong calcium concentration gradient between this water and the pore water in the bentonite lead to a fast out-diffusion of calcium from the bentonite (Figure 5-27). This initial depletion in calcium concentration increases the amount of gypsum dissolved, supplying large amounts of calcium and sulphate to the pore water. In addition, as magnesium is also strongly depleted in the bentonite pore water due to out-diffusion, dolomite dissolution increases. Before ice-melting water intrusion,

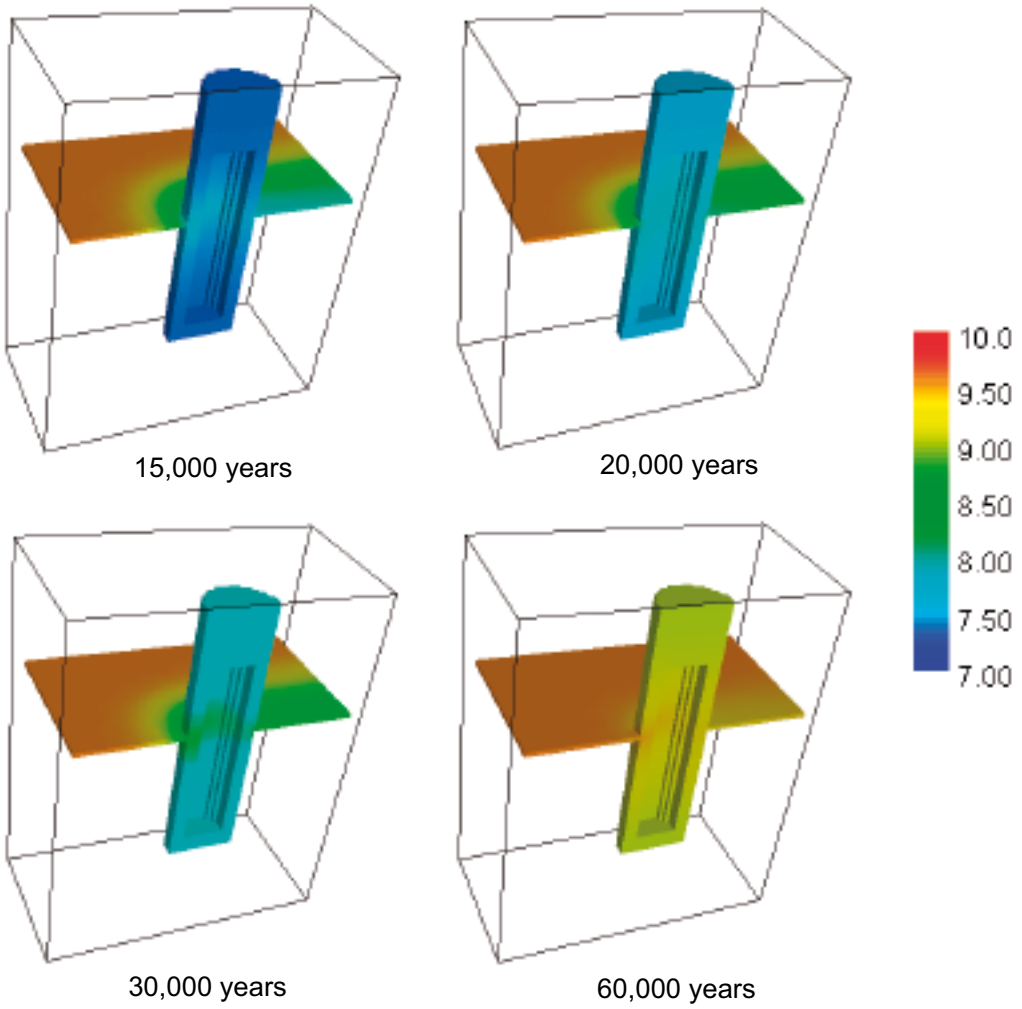

Figure 5-26. *Predicted pH evolution of the system after the intrusion of ice-melting water at 10,000 years of simulation.*

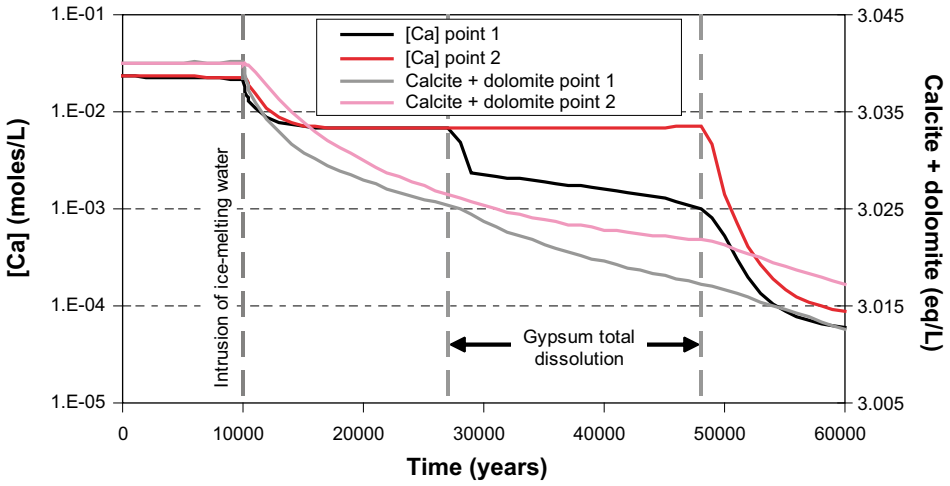

Figure 5-27. *Predicted evolution of calcium concentration in pore water and carbonate minerals at two points in the bentonite as shown in Figure 5-10, (1) at the fracture level, and (2) far from the fracture intersection. The time at which ice-melting water intrudes into the system has been indicated. Gypsum total dissolution indicates the time range from total dissolution in those bentonite cells at the fracture level and total dissolution in the whole bentonite.*

the amount of dissolved dolomite was almost equivalent to the amount of calcite precipitated. However, after the intrusion of ice-melting water the dissolution of dolomite is not fully compensated by the precipitation of calcite, resulting in a net dissolution of carbonates (Figure 5-28).

The net dissolution of carbonates has two effects: i) an initial increase in the aqueous carbonate concentration followed by a continuous decrease due to out-diffusion (Figure 5-28) and, ii) an increase in pH (Figure 5-29).

The system evolution explained above is maintained until gypsum starts to disappear from the bentonite. First, gypsum is totally dissolved in the bentonite close to the fracture (Figure 5-30) after 27,000 years of simulation, and is totally dissolved from the whole bentonite buffer after 48,000 years of simulation. At these two key points significant changes in the evolution of the system occur.

The first disappearance of gypsum accelerates the out-diffusion of calcium near the fracture plane (Figure 5-27), increasing the amount of carbonate minerals being dissolved (Figure 5-28); in fact, calcite dissolves for the first time from the start of the simulation. This behaviour of carbonate minerals near the fracture plane increased again momentarily the concentration of aqueous carbonate until it decreases again due to out-diffusion, and induce a jump in pH in the zone where gypsum disappeared (Figure 5-29).

Finally, when gypsum totally disappeared from the whole bentonite, calcium diffuses out from the bentonite reaching very fast the same concentration as in the ice-melting water (Figure 5-27). Again, this produces an additional increase in the amount of carbonates being dissolved (Figure 5-28), leading to a faster increase of the pH in the whole bentonite (Figure 5-29), reaching a maximum pH of 9.3 near the fracture plane at the end of the simulation.

This geochemical evolution has an effect on the cation occupancy in the exchanger of the bentonite. Initially, before ice-melting water intrusion, calcium and magnesium are replaced by sodium in the bentonite exchanger. However, after the intrusion of ice-melting water, as sodium

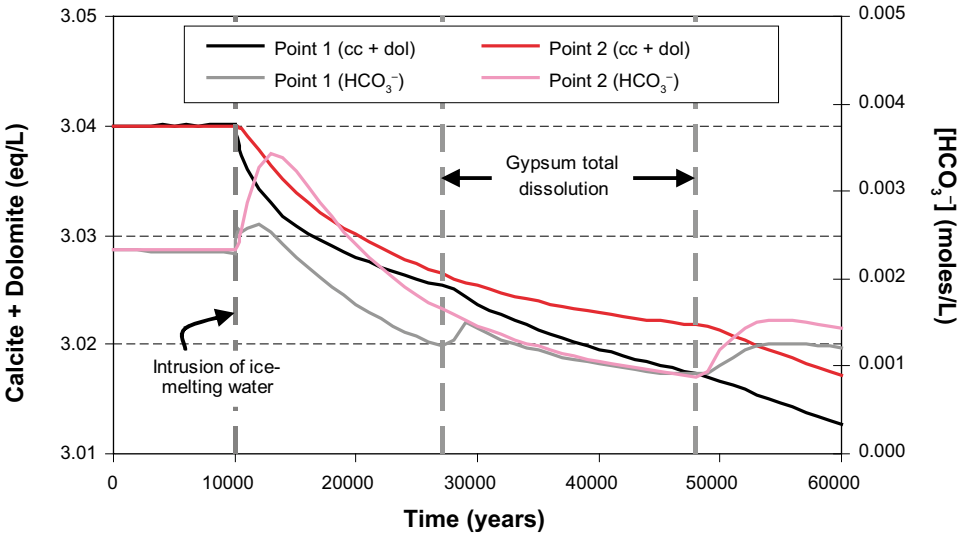

Figure 5-28. *Predicted evolution of total carbonate concentration and carbonate minerals (calcite + dolomite) at two points in the bentonite as shown in Figure 5-10, (1) at the fracture level, and (2) far from the fracture intersection. Note that before ice-melting water intrusion the net amount of carbonates is maintained nearly constant, whereas after the intrusion it is strongly depleted and accompanied by an increase in aqueous carbonate concentration.*

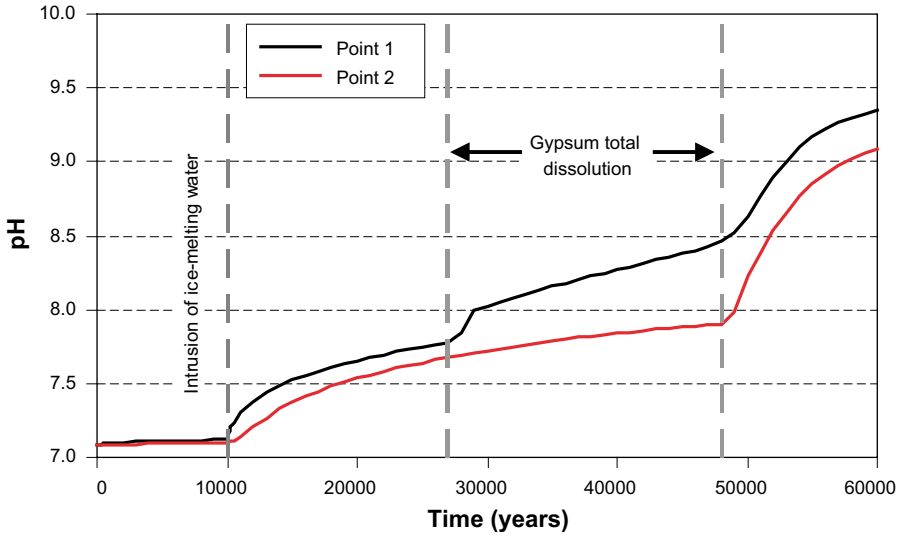

Figure 5-29. *Graphic showing the detailed evolution of pH at two points in the bentonite as shown in Figure 5-10, (1) at the fracture level, and (2) far from the fracture intersection. Note the three jumps in pH related to the intrusion of ice-melting water and gypsum dissolution.*

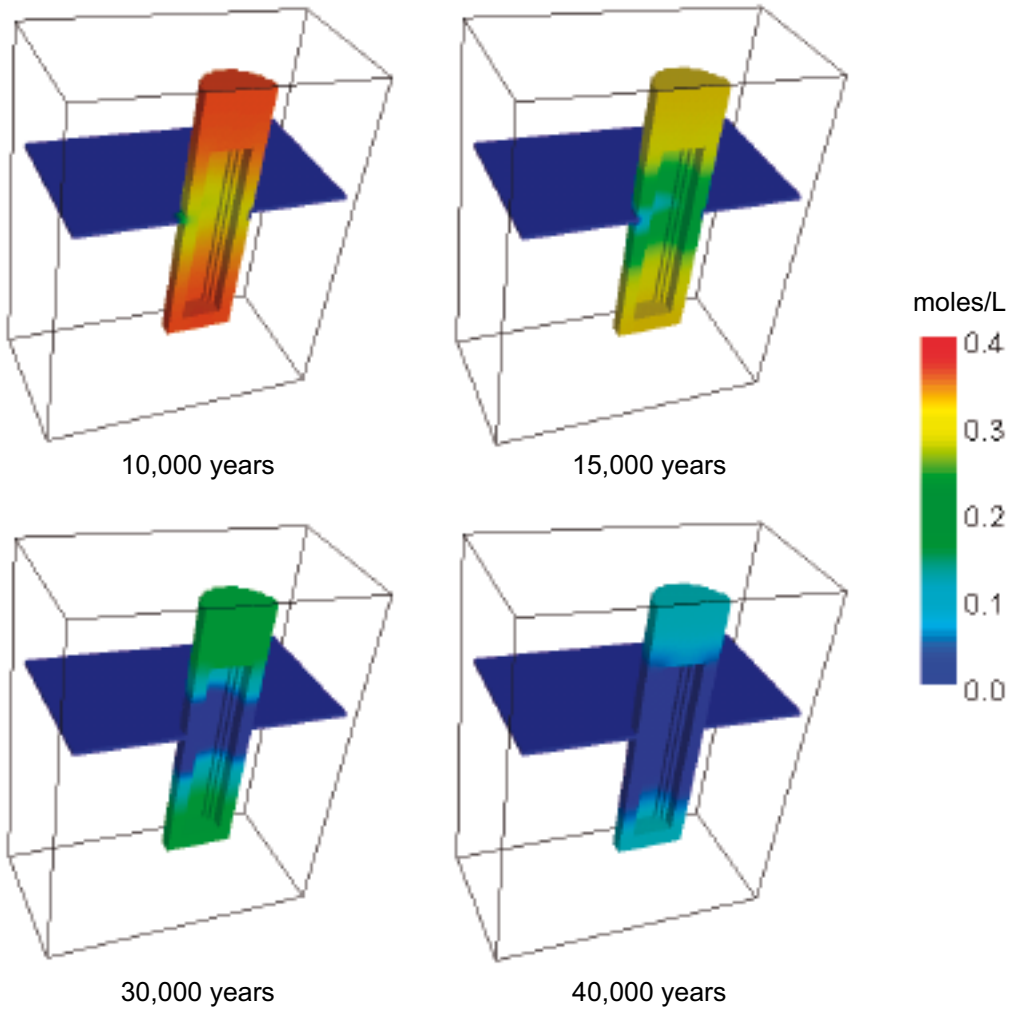

Figure 5-30. *Predicted evolution of the amount of gypsum present in the bentonite.*

diffuses out of the bentonite faster than calcium, the exchange process reverses, and calcium and magnesium replace sodium (Figure 5-31). The rate of the replacement depends on the evolution of calcium concentration, thus it is faster while gypsum is still present and slows down once gypsum is totally dissolved.

5.3.6.3 Intrusion of high-salinity groundwater

The predicted geochemical evolution of the system when considering the effect of high-salinity water intrusion is also related to the competition between the out-diffusion of aqueous carbonate and the in-diffusion of calcium, as in the simulation considering the MX-80 bentonite. However, in this case, the presence of carbonate minerals in the bentonite, prior to the intrusion of high-salinity water, will buffer the pH of the system. The pH in the bentonite follows the same evolution as in the reference case prior to the intrusion of high-salinity water. However, once the intrusion occurs, the model predicts a slight decrease in pH (from 7.12 to 7.05) in the whole bentonite (Figure 5-32). After this decrease, the pH tends to slowly increase again until the end of the simulation, when a maximum pH of 7.16 is reached.

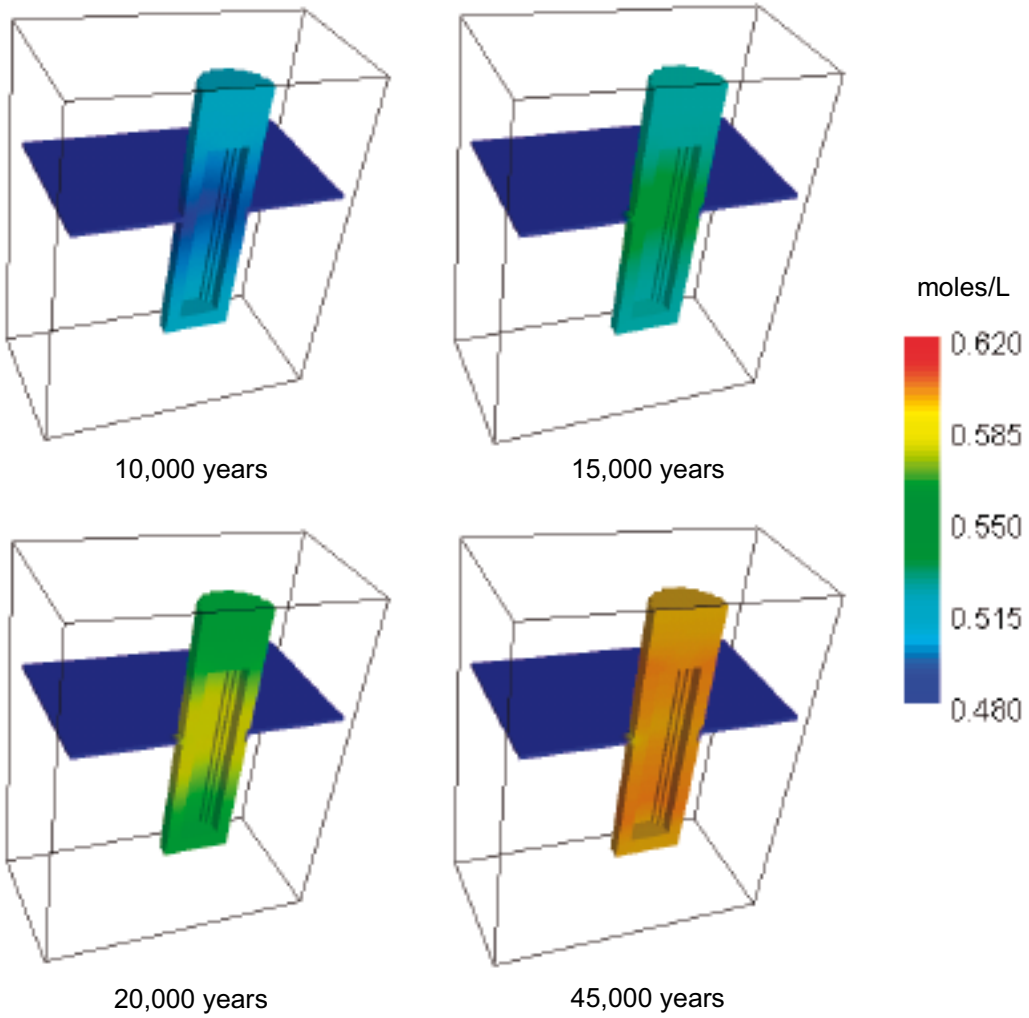

Figure 5-31. *Predicted evolution of Ca occupancy in the exchanger of the bentonite. Note that before ice-melting water intrusion the Ca occupancy decreases, whereas after the intrusion the processes reverses and Ca occupancy increases.*

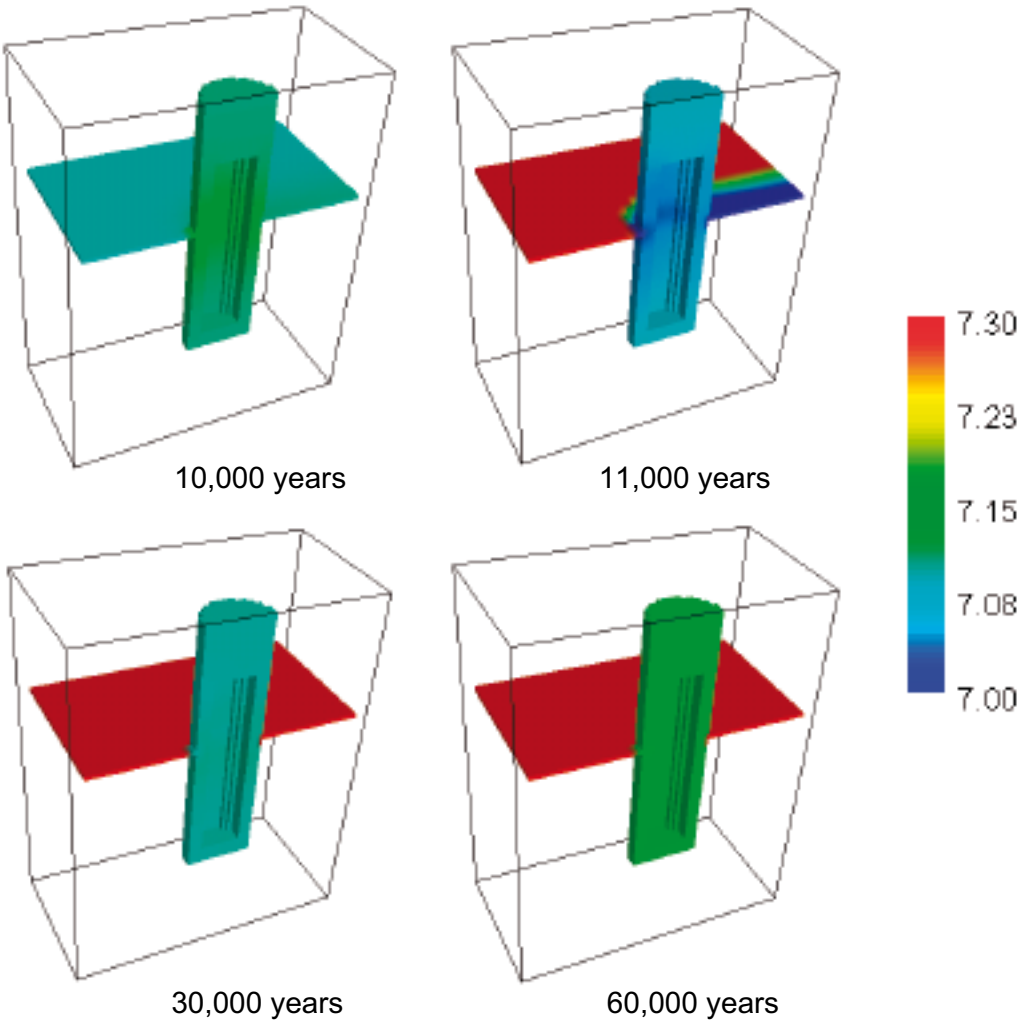

Figure 5-32. *Predicted pH evolution of the system after the intrusion of high-salinity water at 10,000 years of simulation.*

The reason for this increase in pH is the precipitation of carbonates, as dolomite dissolves and calcite precipitates during all the simulation, but the precipitation of calcite is always larger than the dissolution of dolomite, resulting in a net precipitation of carbonates. Moreover, after the intrusion of high-salinity water, the precipitation of calcite increases, due to the large amount of calcium diffused into the bentonite.

At the same time, the large diffusion of calcium into the bentonite increases the calcium occupancy in the exchanger and reverses the previous pattern of gypsum dissolution by leading a slight precipitation of gypsum.

5.3.6.4 Summary

The most relevant results of CASE-I simulations, considering Deponit CA-N as the buffer material, are the following:

- The predicted pH in the bentonite buffer does not change significantly, except when interacting with the ice-melting water, which lead to an increase of more than two pH-units.
- The equilibrium with carbonates (calcite and dolomite) buffers the pH in all the simulations.

- The concentration gradients of sodium, calcium, magnesium and carbonate between groundwater and pore water in the bentonite buffer control the precipitation – dissolution of carbonates.
  - When interacting with the Forsmark groundwater partial Ca by sodium exchange occurs in the bentonite due to sodium diffusion into the bentonite and dolomite in the buffer is partially transformed into calcite due to out-diffusion of magnesium.
  - When interacting with ice-melting water, sodium, calcium, magnesium and aqueous carbonate diffuse out from the bentonite, leading to the acceleration of gypsum dissolution, a net dissolution of carbonate minerals (calcite + dolomite) and reversing the replacement of calcium and magnesium by sodium in the exchanger.
  - When interacting with the high-salinity water the Na by Ca replacement reverses, increasing the Ca occupancy in the exchanger, gypsums precipitates instead of being dissolved, and calcite precipitation increases, surpassing the equivalent amount of dolomite dissolved.

5.3.7 Final remarks of CASE-I

The results from the different models in CASE-I show that most significant changes in the bentonite buffer occur near the fracture zone. Moreover, in some cases, changes near and far from the fracture are of opposite direction (i.e. dissolution of a given mineral near the fracture, whereas far from the fracture is precipitating). This is due to the different evolution of concentrations of major elements in solution, which depend on coupled transport processes (diffusion) and chemical processes.

In the simulated cases there are no major changes in pH, in general pH-values are within the range of 7.0 and 7.3, except when ice-melting waters reach the near field of a repository (Figure 5-33). In this scenario, if carbonate minerals are not initially present, the high pH of ice-melting waters controls the pH of the bentonite pore water and a minor buffering is exerted by surface acidity reactions in montmorillonite. Otherwise, when carbonate minerals are present, the low concentrations in aqueous carbonate and calcium lead to the dissolution of these carbonate minerals and pH can increase up to values close to 9.4.

In both reference cases, considering MX-80 and Deponit CA-N bentonites, most changes are due to the diffusion of aqueous species, until reaching the same concentrations as in the Forsmark groundwater. However, these changes do not affect in a substantial way the behaviour of bentonite and its capacity to buffer the most relevant parameters of the system (i.e. pH and Eh). Major changes predicted in reference cases are related to gypsum dissolution and changes on the cation occupancy in the exchanger of the bentonite.

Changes in the geochemical evolution of the system are predicted to be more pronounced when high-salinity water intrudes into the system. This is due to the higher concentration gradients created, although the simulations predict no significant changes in pH.

Finally, the effect of the intrusion of ice-melting waters leads to some important changes in the geochemical evolution of the system, especially in the presence of carbonate minerals in the bentonite, as they will dissolve leading to higher pH values. However, as other sources for calcium are present in the system, as gypsum, this increase in pH is not as strong as when gypsum disappears.

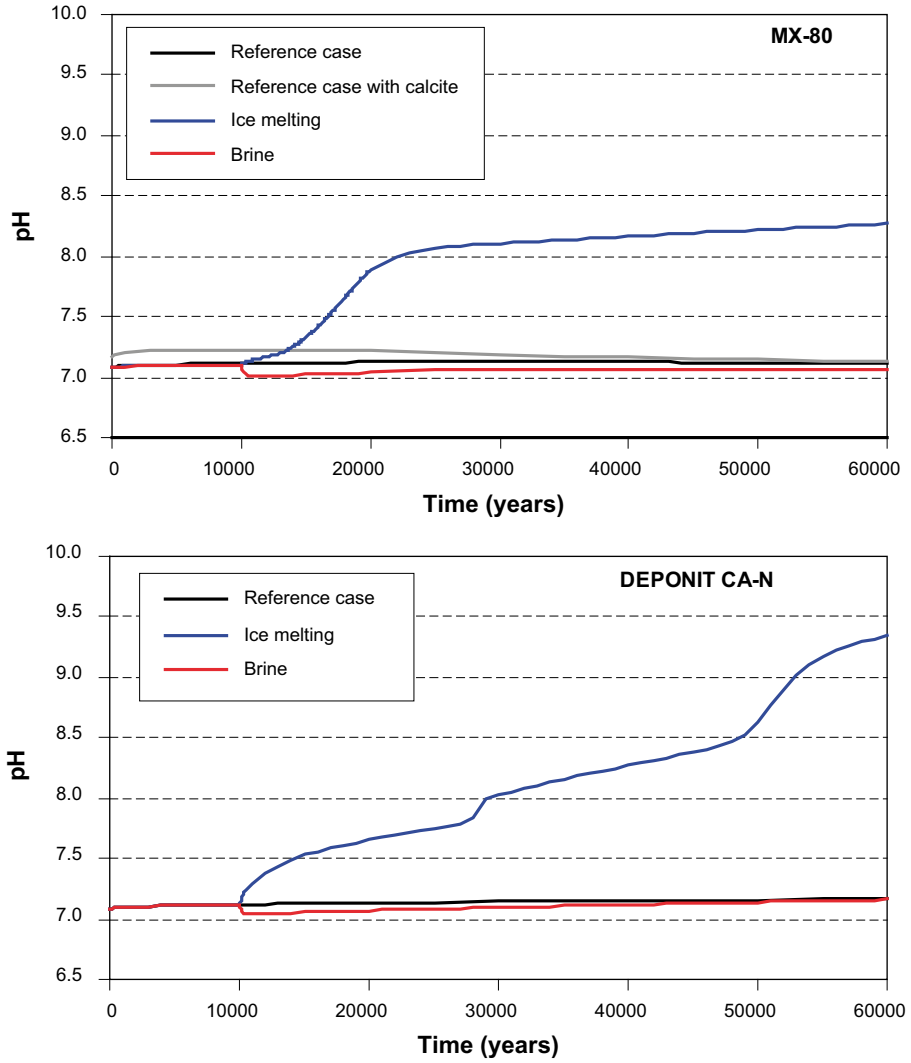

Figure 5-33. *Comparison of predicted pH evolution for the different scenarios considered in CASE-I at a point in the bentonite close to the fracture in granite, as shown in Figure 5-7.*

5.4 CASE-II: Groundwater-backfill-buffer interaction

5.4.1 The modelled domain and boundary conditions

The modelled domain in CASE-II is shown in Figure 5-34. It consists of a longitudinal section of the backfilled deposition tunnel and the deposition hole. Two sub-cases have been modelled, one considering a clay of Friedland type as backfill material, and the other considering the backfill as a mixture of 70% crushed granite and 30% bentonite clay (of the same type as used in the buffer). The domain has been discretised into 25,575 elements (51,984 nodes), with total X = 7,750 mm, Y = 16,730 mm. In the backfill zone, the element size ranges from 50×50 mm at the inner part of the zone in contact with the deposition hole, to 300×100 mm at the contact with the granite and at the margins. In the bentonite zone (deposition hole), element size is 50×50 mm.

Groundwater enters in the domain only through the left boundary of the deposition tunnel, and flows out through its right margin. Boundary conditions in the lateral margins corresponding to the granite zone are of no flow, as well as the upper and lower boundaries of the whole domain.

The time period of simulation is 60,000 years, with a time step varying from 1 to 250 years.

5.4.2 Hydraulic properties

As in CASE-I, granite surrounding both deposition tunnel and deposition hole is assumed to be inactive during calculations. Additionally, the inner part of the buffer domain, representing the canister, is also assumed to be inactive.

Between left and right boundaries of the modelled domain, it has been considered a prescribed hydraulic head gradient of 0.002 $m \cdot m^{-1}$. Hydraulic properties in bentonite surrounding the canister are the same as in CASE-I (see Section 3.1).

In CASE-I it was clear that transport through the fracture in granite was due to advection, whereas in the bentonite buffer diffusion was the dominant transport mechanism. In CASE-II, groundwater enters into the system through the backfill, where both advective and diffusive transport processes can be important.

The porosity of the backfill material has been selected as 0.36 (see Section 3.2), despite the backfill material considered, according to the data by /Ochs 2006/.

The effective diffusivities for the different backfill materials, as selected in Section 3.2, are 7×10^{-11} and 10^{-10} $m^2 \cdot s^{-1}$ for the Friedland Clay and 30/70 mixture, respectively. The water diffusivity (D), which is the value entered in the code for calculations, is calculated through the following expression:

$$D = D_e/\varepsilon$$

This results in water diffusivities of 1.93×10^{-10} and 2.79×10^{-10} $m^2 \cdot s^{-1}$, respectively for Friedland Clay and 30/70 mixture. However, the code only allows a single water diffusivity value for the entire modelling domain. Considering the D_e value from the bentonite buffer a value of 2.79×10^{-10} $m^2 \cdot s^{-1}$ for water diffusivity has been selected, leading to a D_e for the Friedland Clay backfill of 10^{-10} $m^2 \cdot s^{-1}$, which is slightly above the selected value.

As cited in Section 3.2.1, the hydraulic conductivity of the Friedland clay with a dry density of 1,780 $kg \cdot m^{-3}$ has been determined to be 10^{-12} m/s /Ochs 2006/, therefore, this is the value considered for the numerical simulations. On the other hand, the selected hydraulic conductivity of the 30/70 backfill is 5×10^{-11} $m \cdot s^{-1}$.

5.4.3 Numerical simulations and initial calculations

The same scenarios as in CASE-I have been considered in CASE-II (see Table 5-1). As in CASE-I, the reference simulations consider the MX-80 bentonite without carbonate minerals and Deponit CA-N, respectively. These bentonite types are present in both the buffer and the bentonite fraction in the backfill when the 30/70 backfill is considered, whereas when the Friedland Clay backfill is considered, Mx-80 and Deponit CA-N bentonites are only present in the buffer. The inflow water has the composition of the Forsmark deep groundwater (Table 2-1).

As variants, simulations consider two additional types of inflow waters, a dilute water, originated from ice melting (Grimsel type), and a high-salinity deep groundwater (Laxemar type). These water types have been simulated to enter into the system after 10,000 years of simulation through the left boundary in the backfill. The chemical composition of these waters is shown in Table 5-5 and Table 5-6. Initial pore water composition in the bentonite is as in CASE-I (Table 5-4). Initial pore water composition in the backfill has been calculated by equilibrating Forsmark groundwater with the minerals present in the backfill material and with the cation exchange capacity of bentonite fraction. The resulting water composition considered in the model is as indicated in Table 5-7. The cation exchange capacity and mineral composition of the backfill is as described in Section 3.2, but when the 30/70 backfill is considered, their initial amounts have been recalculated according to the bentonite/crushed rock ratio and the porosity in the backfill.

Table 5-7. Calculated chemical composition of backfill pore waters for the reference case.

moles/L	MX-80	Deponit CA-N	Friedland
pH	7.08	7.09	7.06
pe	–2.21	–2.31	–2.49
HCO_3^-	2.15×10^{-3}	2.33×10^{-3}	2.07×10^{-3}
Ca	1.15×10^{-2}	2.32×10^{-2}	2.54×10^{-2}
Cl	1.53×10^{-1}	1.53×10^{-1}	1.53×10^{-1}
Fe tot	3.31×10^{-5}	1.69×10^{-4}	3.31×10^{-5}
K	8.75×10^{-4}	1.37×10^{-3}	8.98×10^{-4}
Mg	9.30×10^{-3}	2.35×10^{-2}	1.00×10^{-2}
Na	8.88×10^{-2}	7.32×10^{-2}	9.06×10^{-2}
SO_4^{2-}	2.42×10^{-2}	1.34×10^{-2}	1.07×10^{-2}
Si	6.62×10^{-5}	6.64×10^{-5}	1.27×10^{-4}

Data from the simulations are analysed in two sections through the modelled domain (Figure 5-34), one following the deposition tunnel direction through the backfill (section 1), and the other perpendicular to section 1 and intersecting the backfill and the bentonite buffer (section 2).

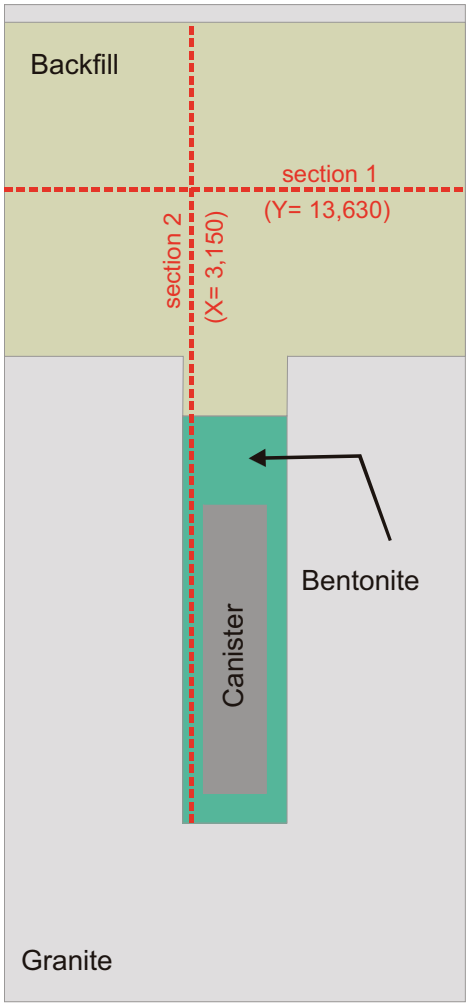

Figure 5-34. *Modelled domain of CASE-II, with selected sections, X and Y position in millimetres.*

5.4.4 Results

As constrained by boundary conditions and the relative hydraulic conductivities between the backfill and the bentonite buffer, advective flow is only significant in the backfill (Figure 5-35). Mean water flow velocities in the backfill are 2.0×10^{-7} and 8.7×10^{-6} m·y^{-1} for the Friedland Clay and 30/70 mixture backfills respectively. In the bentonite buffer, diffusion is the dominant transport mechanism. This migration pattern imply that major changes in pore water chemistry caused by the inflow groundwater will be mainly observed in the backfill rather than in the buffer, at least for the short- and mid-term.

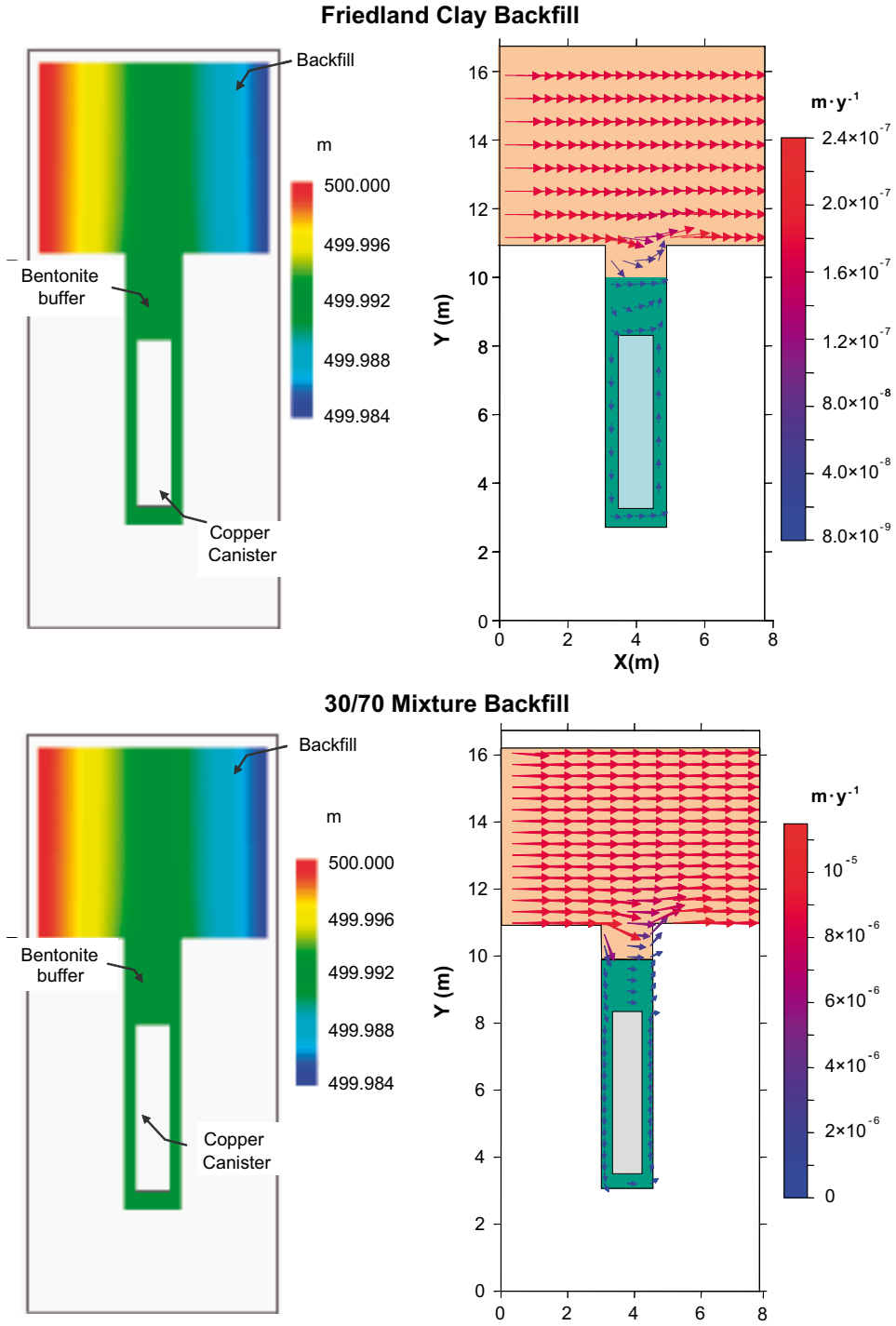

Figure 5-35. *Hydraulic gradient and interstitial velocity field for CASE-II, considering the two types of backfill materials. Note that water flow velocities are much higher in the backfill than in the deposition hole.*

5.4.5 Friedland Clay backfill

5.4.5.1 Reference case with MX-80 bentonite buffer

The results of the calculations in the reference case, where Friedland Clay is considered as the backfill material, MX-80 as the bentonite buffer and Forsmark groundwater as inflow water, indicate that no significant pH changes occur. pH in the bentonite buffer and in the backfill only ranges between 7.03 and 7.07.

These slight changes in pH are caused by precipitation-dissolution of calcite. The initial equilibrium of Forsmark groundwater with Friedland clay leads to the precipitation of tiny amounts of this mineral (6×10^{-5} moles/L) in the backfill. However, the diffusion of calcium from the backfill to the buffer implies a quick dissolution of this early calcite in almost all the backfill region between 15,000 and 20,000 years (Figure 5-36). On the other hand, calcite precipitates close to the boundary where the groundwater flows into the backfill.

Unlike calcium, sulphate is less concentrated in the backfill pore water so that it diffuses out from buffer. This sulphate migration leads to the precipitation of gypsum around the contact between the depositional tunnel and the depositional hole during the first 5,000 years (Figure 5-37). In the other parts of the modelled domain, gypsum dissolves, resulting in complete disappearance in the left margin from 20,000 years (Figure 5-38).

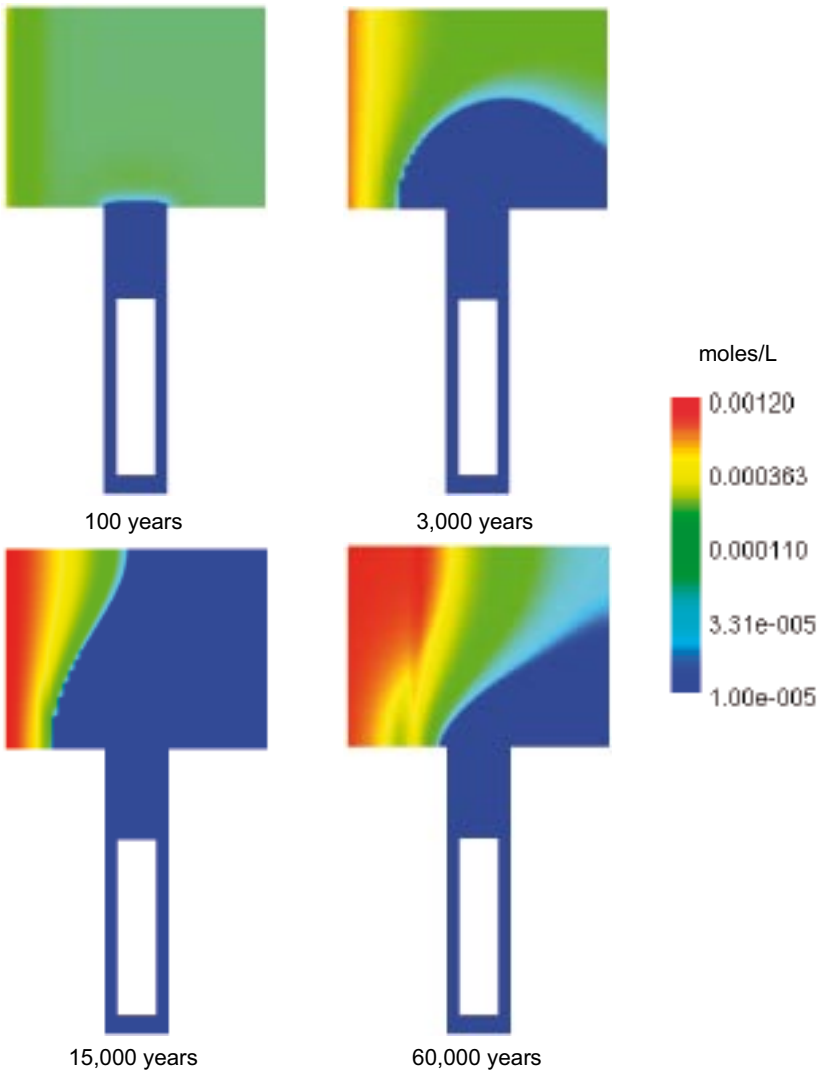

Figure 5-36. *Predicted evolution of calcite in the modelled domain of the reference case with Friedland backfill and MX-80 bentonite buffer. Note that the scale bar is logarithmic.*

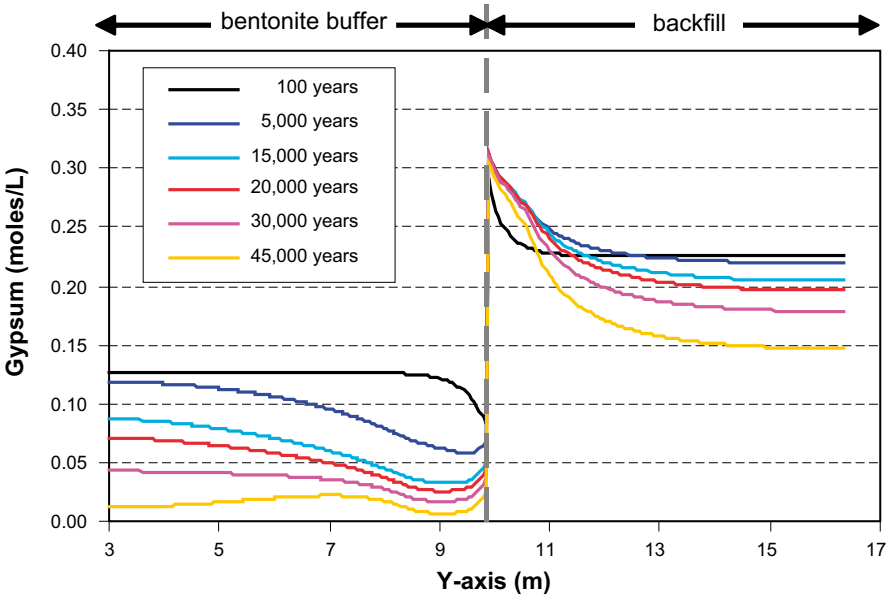

Figure 5-37. *Evolution of gypsum along the section 2. Gypsum continuously dissolves in the whole domain except in the contact between the backfill and the buffer where it precipitates during the initial 5,000 years.*

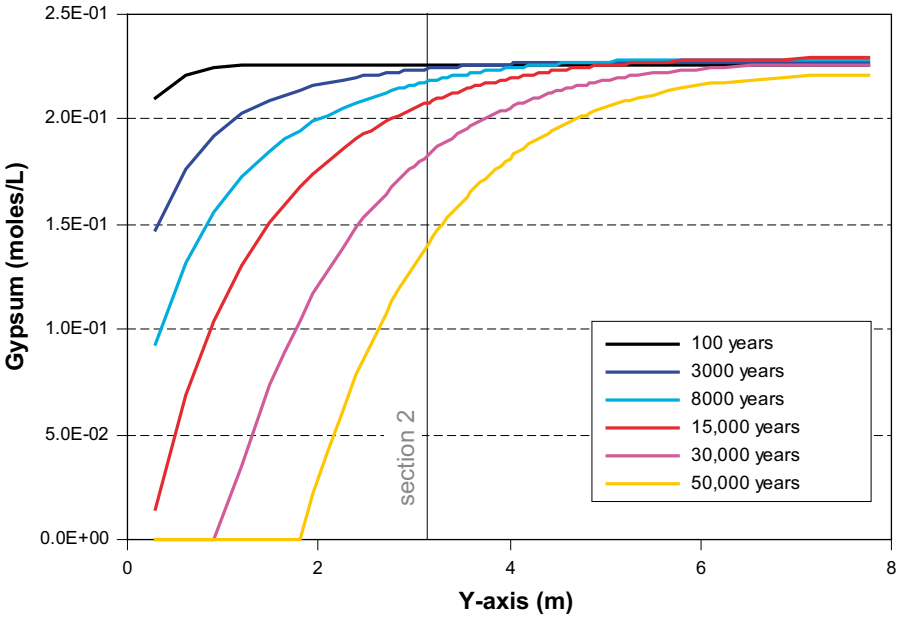

Figure 5-38. *Evolution of gypsum along the section 1 (backfill transect). Gypsum dissolution in the backfill is enhanced by the inflow of the Forsmark groundwater.*

5.4.5.2 Intrusion of ice-melting water (MX-80 bentonite buffer)

The intrusion of ice-melting water, which is more diluted than the Forsmark water (see Table 2-1), leads to significant changes in pore water chemistry. As in CASE-I the geochemical evolution of the system is the same as in the reference case until the ice-melting water enters into the system (set at 10,000 years after starting the simulation).

The ice-melting intrusion leads to an increase in the pH of the backfill pore water, reaching a maximum pH of 8.9 after 60,000 years near the boundary where ice-melting intrusion enters into the system (Figure 5-39). The absence of mineral buffers such as carbonates should lead to

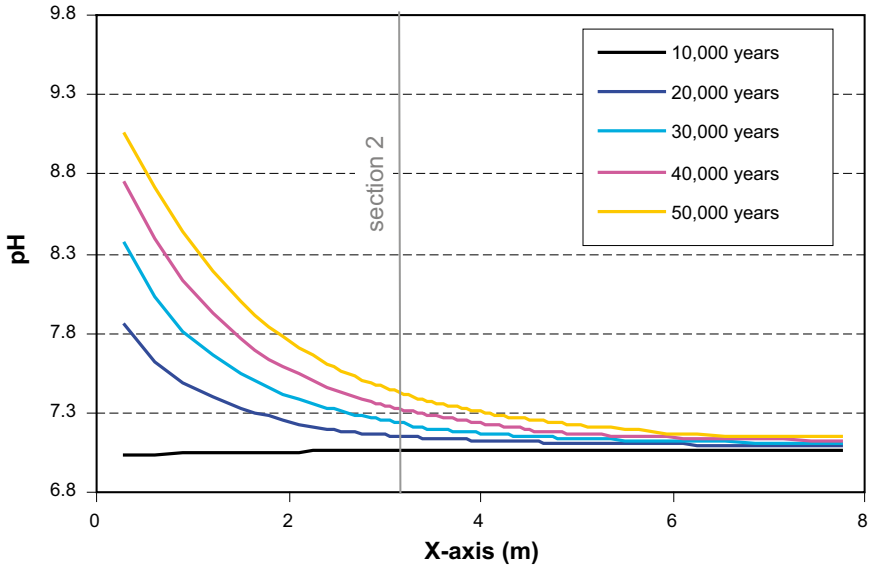

Figure 5-39. *Plot showing the predicted pH evolution after the ice-melting intrusion in section 1 (transect through the backfill, X=3.15 m). pH increases through time due to the alkaline character of the inflow groundwater after 10,000 years.*

a rapid increase of pH to values close to that of the Grimsel groundwater (pH = 9.6). However, pH increase is retarded due to the buffering effect exerted by the clay surface acidity reactions. As high-pH water enters into the system protonated surfaces ($\equiv sOH_2^+$) react to convert into neutral surfaces first ($\equiv sOH$) and to deprotonated surfaces ($\equiv sO^-$) later on (Figure 5-40). Thus, although there is an increase in pH in the backfill pore water, the buffering effect exerted by surface acidity reactions prevents that the relatively high-pH plume reaches the bentonite buffer in the deposition hole, where at the end of the simulation a maximum pH of 7.2 will be reached near the buffer-backfill boundary.

The intrusion of the diluted ice-melting water leads also to a faster dissolution of gypsum from both the backfill and the bentonite buffer. Total dissolution is predicted to occur in less than 15,000 years of simulation in the backfill and less than 30,000 years in the bentonite buffer.

Another process associated to the ice-melting intrusion is related to the diffusion of sodium out from the backfill, which is faster than out-diffusion of calcium. Thus the Na by Ca replacement in the exchanger is enhanced, especially in the backfill.

5.4.5.3 Intrusion of high-salinity groundwater (MX-80 bentonite buffer)

The effect of the intrusion of high-salinity groundwater into the system is very similar to that predicted in CASE-I. However, in the present case, the model predicts a slight decrease in pH, which is more pronounced in the contact between the backfill and the bentonite buffer (Figure 5-41). The decrease in pH is related to the precipitation of small amounts of calcite, especially in the backfill (Figure 5-42). The precipitation of calcite is, as in CASE-I, the result of the increase in calcium concentration in the pore water resulting from the higher concentration of calcium in high-salinity groundwater. On the other hand, the aqueous carbonate concentration in pore water decreases due to its lower concentration in the high-salinity groundwater. However, the decrease in aqueous carbonate concentration is slower than the calcium concentration increase due to the lower concentration gradient, implying a subsequent dissolution of previously precipitated calcite, and increasing the pH to nearly the initial values.

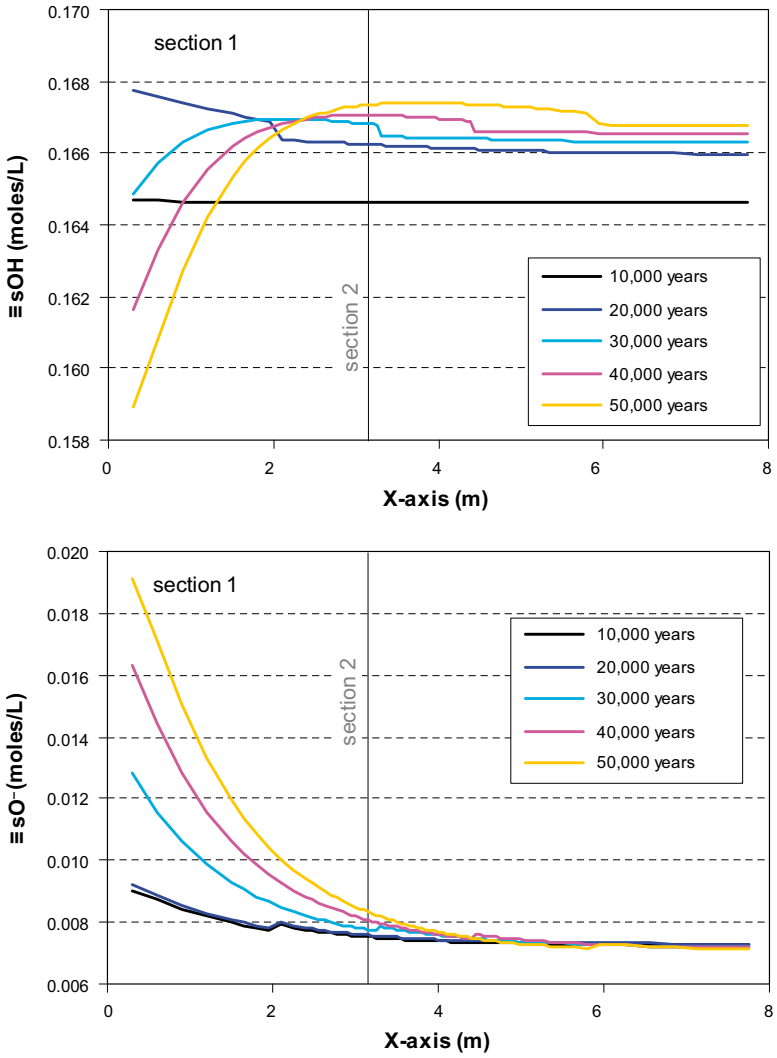

Figure 5-40. *Predicted evolution of neutral (upper plot) and deprotonated (lower plot) surfaces of clay fraction in the backfill and bentonite buffer. Clay surfaces are progressively deprotonated as a response to the intrusion of high pH water.*

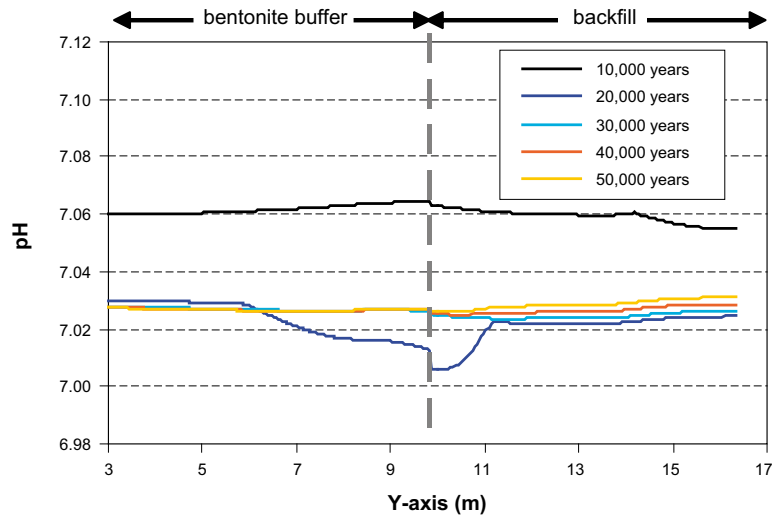

Figure 5-41. *Plot showing the predicted evolution of pH after the intrusion of high-salinity groundwater after 10,000 years of simulation in section 2.*

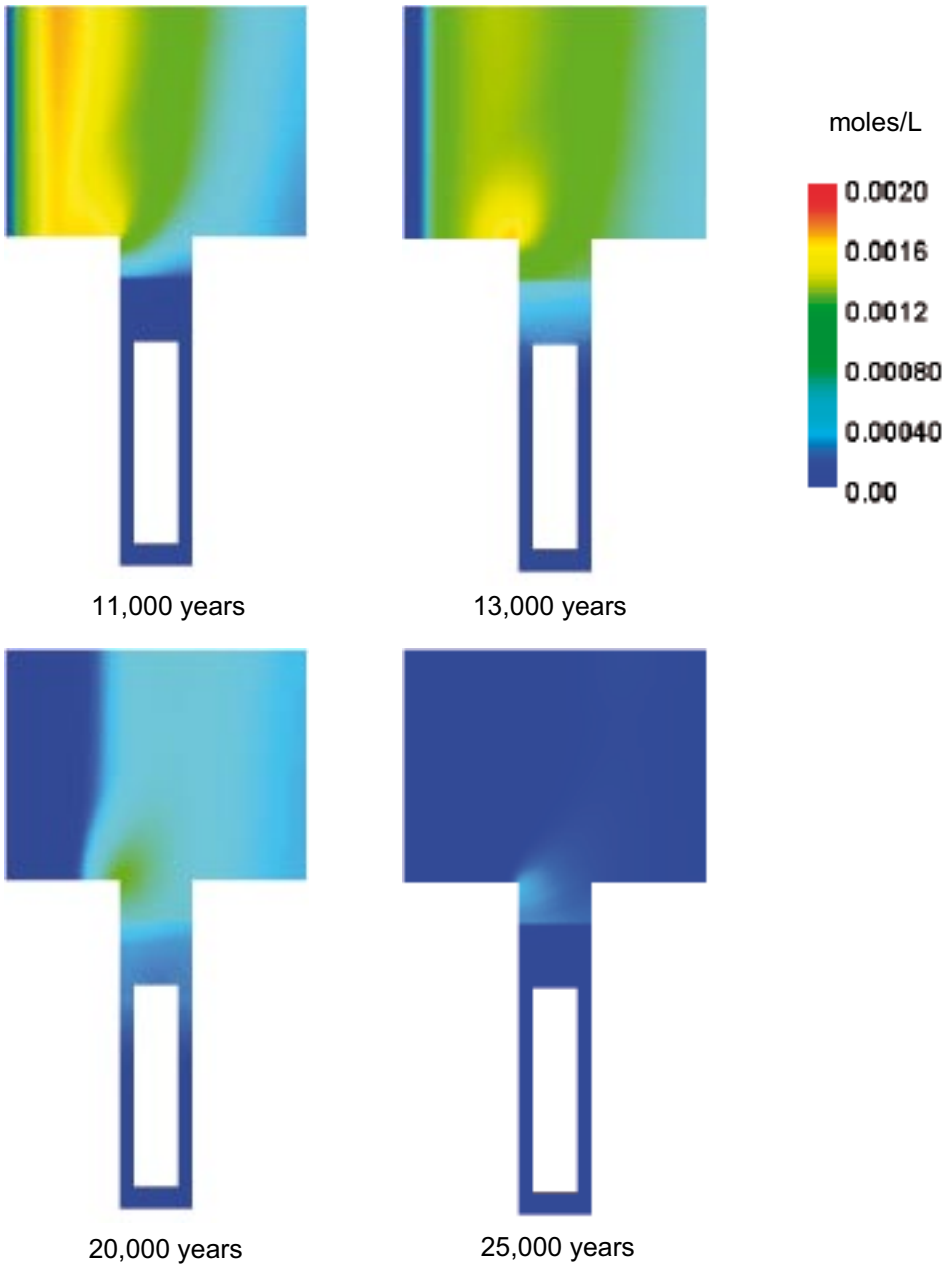

Figure 5-42. *Predicted precipitation and dissolution of calcite during the intrusion of high-salinity groundwater into the system.*

The increase in calcium concentration in the pore water of the backfill and bentonite has also an effect on other processes. It produces an increase on the Na by Ca replacement in the cation exchanger of the bentonite, resulting in higher calcium occupancy of the exchanger at the end of the simulation when compared with the reference case (Figure 5-43). On the other hand, this increase in calcium concentration results in reversing the behaviour of gypsum, which was predicted to dissolve prior to the high-salinity groundwater intrusion. Thus, once the intrusion started, the model predicts the precipitation of gypsum in both the backfill and the buffer.

5.4.5.4 Reference case with Deponit CA-N bentonite buffer

The results above shown indicate that backfill exerts an important control on the chemistry of the inflow groundwaters, and the buffer does not receive much influence of these waters. Consequently, the changes in composition of the buffer bentonite are not much significant. If

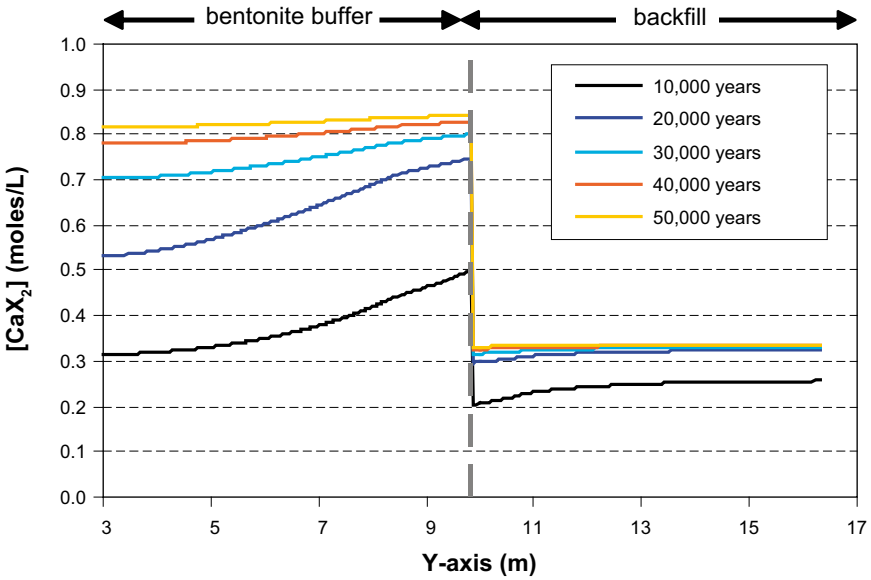

Figure 5-43. *Predicted calcium occupancy in the exchanger of the bentonite due to the intrusion of high-salinity groundwater in the section 2. The increase in the CaX_2 concentration in the exchanger is a consequence of the Ca-rich nature of the high-salinity groundwater.*

the Deponit CA-N bentonite is considered instead of MX-80, the results are very similar to those already presented, especially in the backfill pore water. Buffer pore water shows slight differences caused by the existence of carbonate minerals in the Deponit CA-N bentonite. The most notable changes are observed in the contact between the backfill and the buffer due to the ion transfer via diffusion. In Figure 5-44, it is observed the increase of pH through time in this contact as a result of the coupled dissolution of dolomite and precipitation of calcite (Figure 5-45). On the other hand, gypsum releases calcium to the pore water during all simulation time since it dissolves continuously (Figure 5-46).

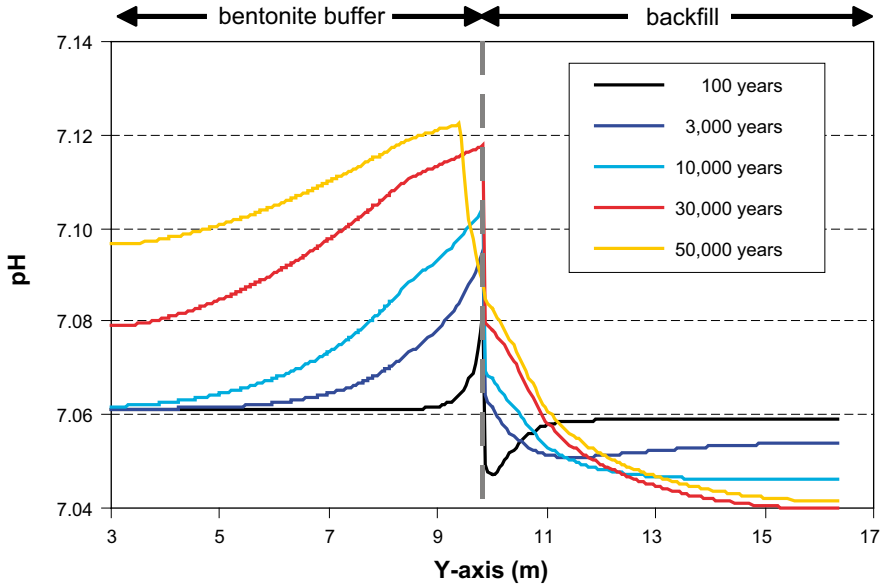

Figure 5-44. *Evolution of pH along the section 2 if Deponit CA-N bentonite is considered as buffer material. The increase in pH in the bentonite buffer close to the backfill is related to dolomite dissolution.*

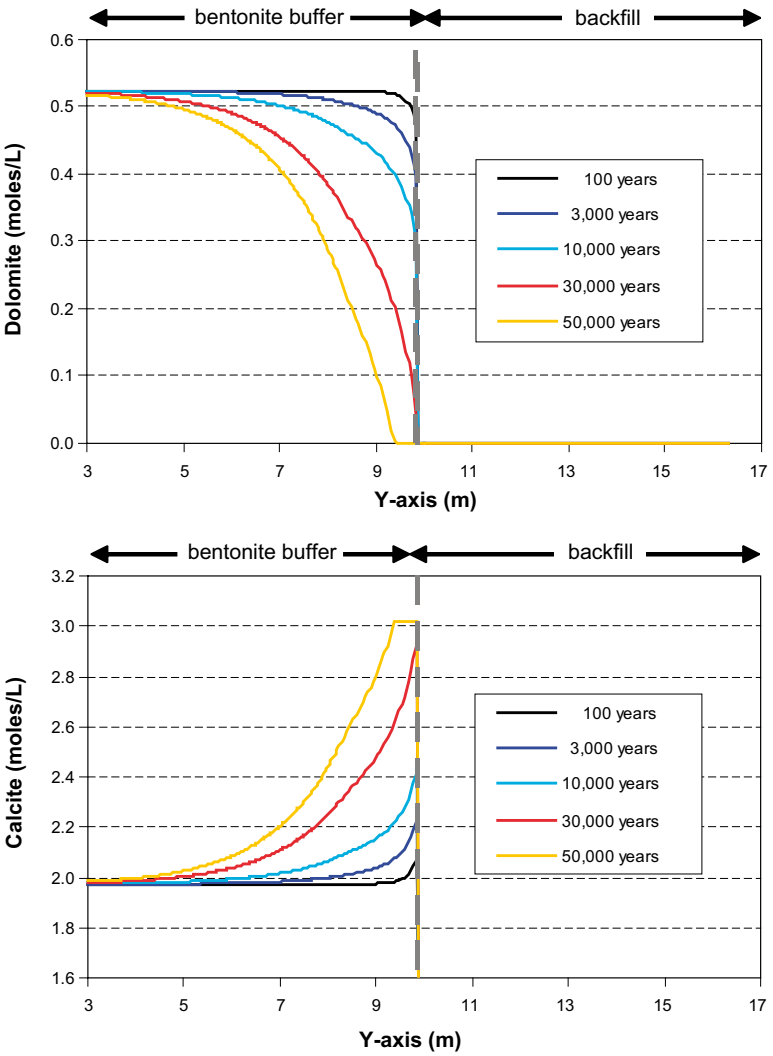

Figure 5-45. *Evolution of dolomite (upper plot) and calcite (lower plot) concentrations along the section 2 if Deponit CA-N bentonite is considered as buffer material. Because of this mineral evolution, pH undergoes a slight increase.*

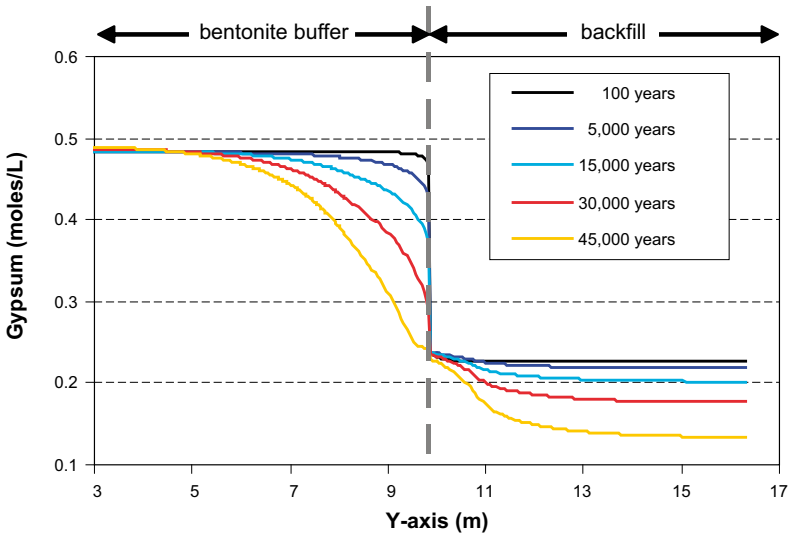

Figure 5-46. *Evolution of gypsum concentration along the section 2 if Deponit CA-N bentonite is considered as buffer material. This mineral is always undersaturated in pore water and, consequently, it dissolves.*

5.4.5.5 Intrusion of ice-melting water (Deponit CA-N bentonite buffer)

The intrusion of ice-melting water after 10,000 years of simulation causes also a similar response in pore waters as observed in the case with MX-80 bentonite. The most relevant changes are seen in pH in the buffer, which reaches values of 7.9 in the contact with the backfill (Figure 5-47) when considering the Deponit CA-N whereas a maximum value of 7.2 is reached with the MX-80. Another interesting difference is that in the entire simulation time, gypsum does not completely dissolve in the buffer. In addition, gypsum in the backfill dissolves more slowly than in the case with MX-80 because the concentration gradients of calcium between the buffer and the backfill are much less pronounced. Calcite and dolomite in the buffer show the same behaviour as seen in the previous case (intrusion of Forsmark groundwater and Deponit CA-N bentonite buffer).

5.4.5.6 Intrusion of high-salinity groundwater (Deponit CA-N bentonite buffer)

As in the intrusion of ice-melting water, the inflow of the saline waters does not change much the pore water chemistry of the buffer if the Deponit CA-N bentonite is used instead of the MX-80. In addition, the pore water chemistry in the backfill follows the same evolution.

5.4.5.7 Summary

The most relevant results of CASE-II simulations, considering Friedland clay as the backfill material, are the following:

- As water enters into the system through the deposition tunnel, it is predicted that most significant changes occur in the backfill material, minimising the effects on the bentonite buffer.
- Almost no changes in pH are expected in the system, in neither the backfill nor the buffer pore waters, except when ice-melting waters enters into the system, leading to increase pH to a maximum of 8.9 in the backfill near the boundary where enters into the system. However, pH increase in the buffer is less important.

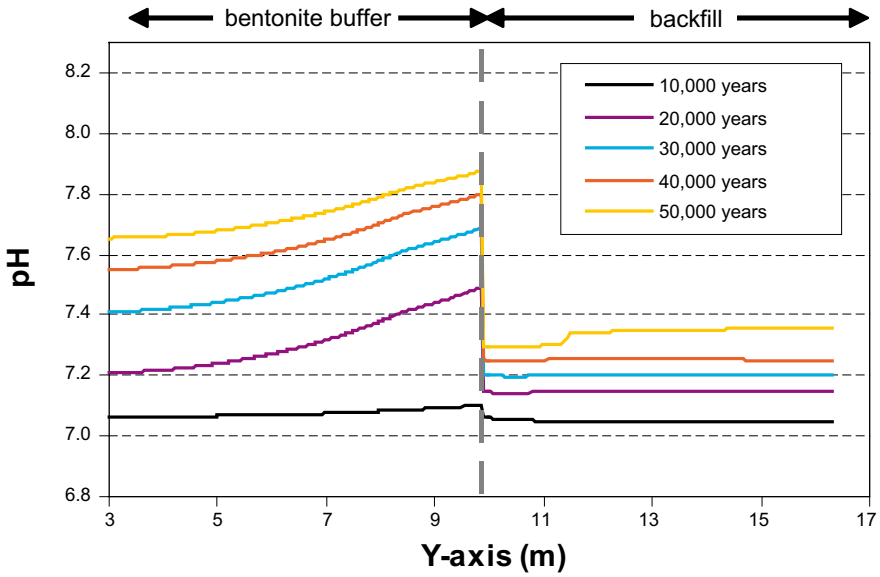

Figure 5-47. *Evolution of pH along the section 2 after the intrusion of ice-melting waters. Deponit CA-N bentonite is considered as buffer material. The increase in pH is significantly higher than the observed when using MX-80 as a buffer material.*

- When calcite is not being considered initially present in the system (MX-80 bentonite as buffer material), pH is partially buffered by surface acidity reactions. Whereas, if carbonate minerals are initially present (Deponit CA-N as buffer material), the equilibrium with these minerals buffers pH.
- Only when high-salinity water enters into the system, slight amounts of calcite are predicted to precipitate in the backfill, although the associated decrease of pH is not significant.
- The difference in aqueous sulphate concentration between pore waters in the backfill and the buffer, lead to the precipitation of gypsum in the backfill near the deposition hole and its dissolution in the rest of the system.
- The dissolution of gypsum in the bentonite buffer and the diffusion of calcium from the backfill into the bentonite lead to the Na by Ca replacement in the exchanger.
- When high-salinity water enters into the system, calcium diffuses to the backfill and the buffer, increasing the Na by Ca replacement in the exchanger, especially in the buffer, and enhancing the precipitation of gypsum in both the backfill and the buffer.
- As in CASE-I, the redox of the system is controlled by the Eh of groundwater.

5.4.6 30/70 backfill

5.4.6.1 Reference case with MX-80 bentonite buffer

The results of the calculations in the reference case where MX-80 bentonite is considered as the buffer material and the bentonite fraction in the 30/70 backfill, indicate that no changes of pH occur. The pH is maintained around 7.08, which is the initial pH in the bentonite and backfill pore water.

The only significant changes in the simulation are related to the out-diffusion of aqueous sulphate and the in-diffusion of calcium. The balance between these two opposite transport processes is the subsaturation of gypsum, which is predicted to dissolve during the simulation until it disappears, after 25,000 years in the backfill and after 45,000 years in the bentonite buffer (Figure 5-48). At the same time, the calcium occupancy in the bentonite exchanger increases at expenses of sodium in both the buffer and the backfill.

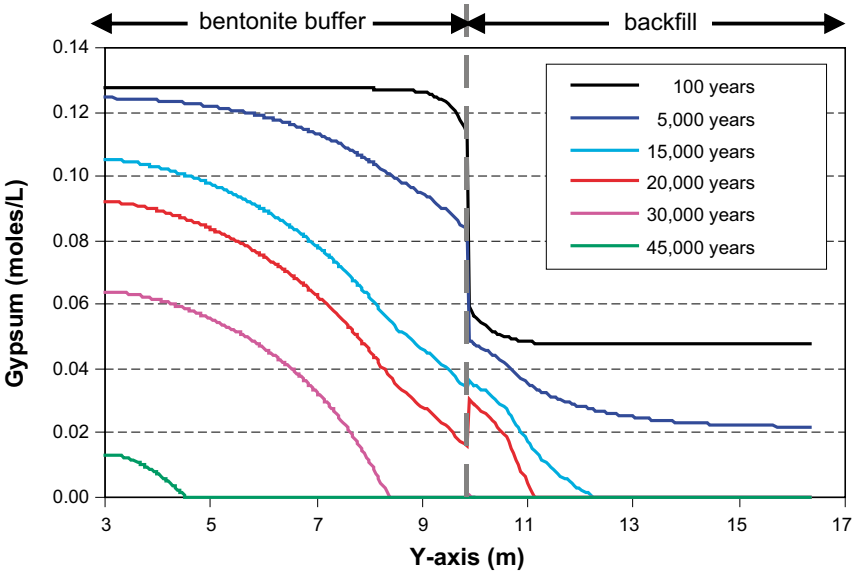

Figure 5-48. *Graphic showing the predicted evolution of the gypsum content in both the backfill and the buffer in section 2 as a function of simulation time (see Figure 5-34 for section location).*

5.4.6.2 Reference case with MX-80 bentonite buffer: Sensitivity analysis

As in CASE-I the sensitivity analysis consists in considering the presence of carbonate minerals (calcite and siderite) initially present in the bentonite from the buffer and backfill.

The modelling results show that the same processes as in the reference case are predicted to occur in the system without significant differences, this is in-diffusion of calcium, Na by Ca replacement in the exchanger of the bentonite, and gypsum dissolution. However, in this simulation some more significant changes in pH are predicted (Figure 5-49). It is noteworthy that initial pH in both the buffer and the backfill are higher than for the reference case, as pore waters have been forced to equilibrate with calcite. In the backfill pH increase from 7.2 to 7.24 (after 15,000 years of simulation), and then decreases again to 7.13. In the buffer pH increases from 7.16 to 7.34 far from the buffer – backfill boundary, whereas close to this boundary pH increases from 7.16 to 7.27 (after 15,000 years of simulation) and then decreases to 7.21 at the end of the simulation. This pH evolution is a consequence of the calcite dissolution, which is related to the in-diffusion of calcium and the out-diffusion of aqueous carbonate. In the backfill the advective transport is more relevant than in the buffer, thus the increase in the calcium concentration is faster than in the buffer, where transport is dominated by diffusion. Therefore, the dissolution of calcite is less important in the backfill and a lower pH increase is predicted. Once the concentration of aqueous carbonate in the backfill pore water is equivalent to that from the Forsmark groundwater, the predicted increase in calcium concentration reverses the calcite behaviour, starting the precipitation of this mineral and producing a decrease in pH. In the buffer, the initial dissolution of calcite due to the out-diffusion of aqueous carbonate during the first 15,000 years of simulation is then reversed due to the continuous diffusion of calcium, and calcite precipitation is predicted near the contact with the backfill leading to a decrease of pH. However, calcite dissolution still occurs far from the backfill, as the concentration of calcium is still low, resulting in a continuous increase in pH for the whole simulation period. Summarising, the inversion in the calcite behaviour occurs when the out-diffusion of aqueous carbonate becomes less important as concentration gradients are minimised, but calcium concentration still increases due to diffusive transport.

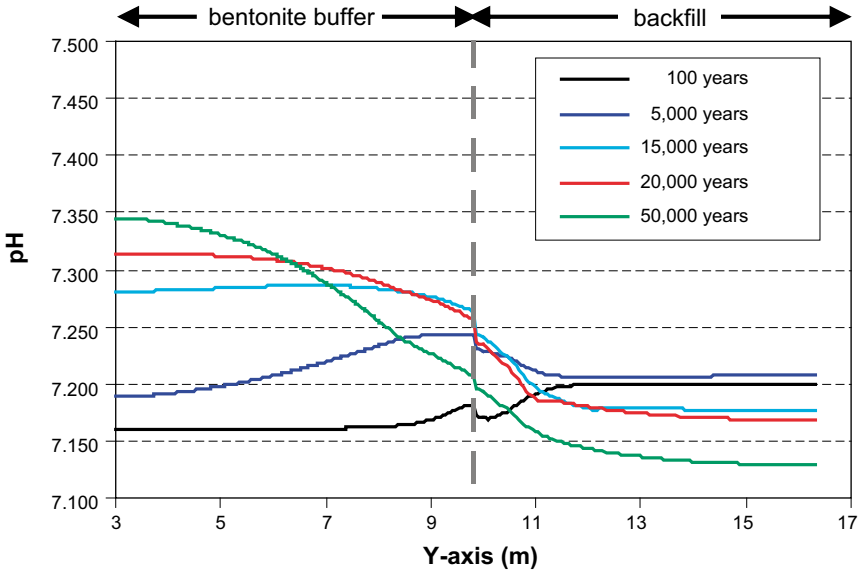

Figure 5-49. *Graphic showing the predicted pH evolution as a function of time in section 2 (see Figure 5-34 for section location in the modelled domain).*

5.4.6.3 Intrusion of ice-melting water (MX-80 bentonite buffer)

The intrusion of ice-melting water, which is more diluted than the Forsmark water (Table 5-5), leads to significant changes in pore water chemistry. As in CASE-I the geochemical evolution of the system is the same as in the reference case until the ice-melting water enters into the system (set at 10,000 years after starting the simulation).

The ice-melting intrusion leads to an increase in the pH of the backfill pore water, reaching a maximum pH of 8.9 near the boundary where ice-melting intrusion enters into the system (Figure 5-50). However, pH decreases along the flow direction within the backfill. The reason for this behaviour is related to the pH buffering effect exerted by the clay surface acidity reactions. As high-pH water enters into the system protonated surfaces ($\equiv sOH_2^+$) react to convert into neutral surfaces first ($\equiv sOH$) and to deprotonated surfaces ($\equiv sO^-$) later on (Figure 5-51). Thus, although there is an increase in pH in the backfill pore water, the buffering effect exerted by surface acidity reactions prevents that the relatively high-pH plume reaches the bentonite buffer in the deposition hole, where at the end of the simulation a maximum pH of 7.8 will be reached near the buffer-backfill boundary (Figure 5-50).

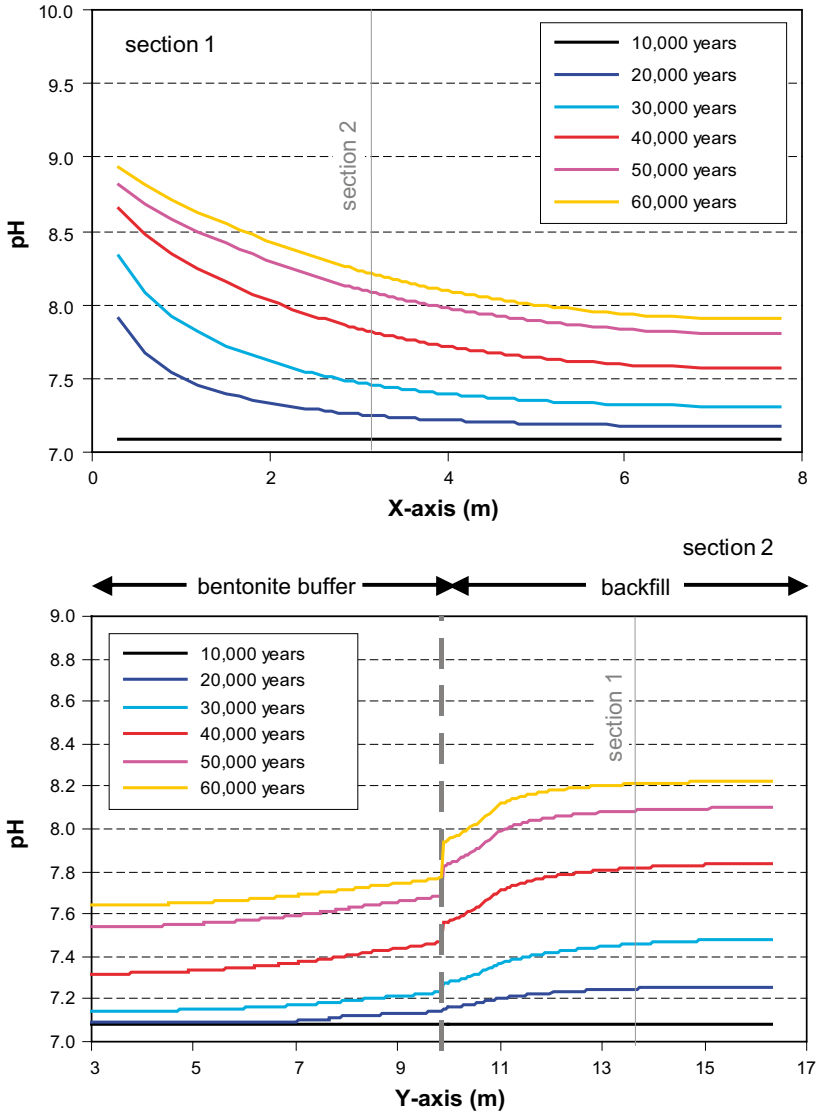

Figure 5-50. *Graphics showing the predicted pH evolution after the ice-melting intrusion in two perpendicular sections (see location in Figure 5-34), one parallel to the deposition tunnel (upper graphic) and the other parallel to the deposition hole and including the backfill above it (lower diagram).*

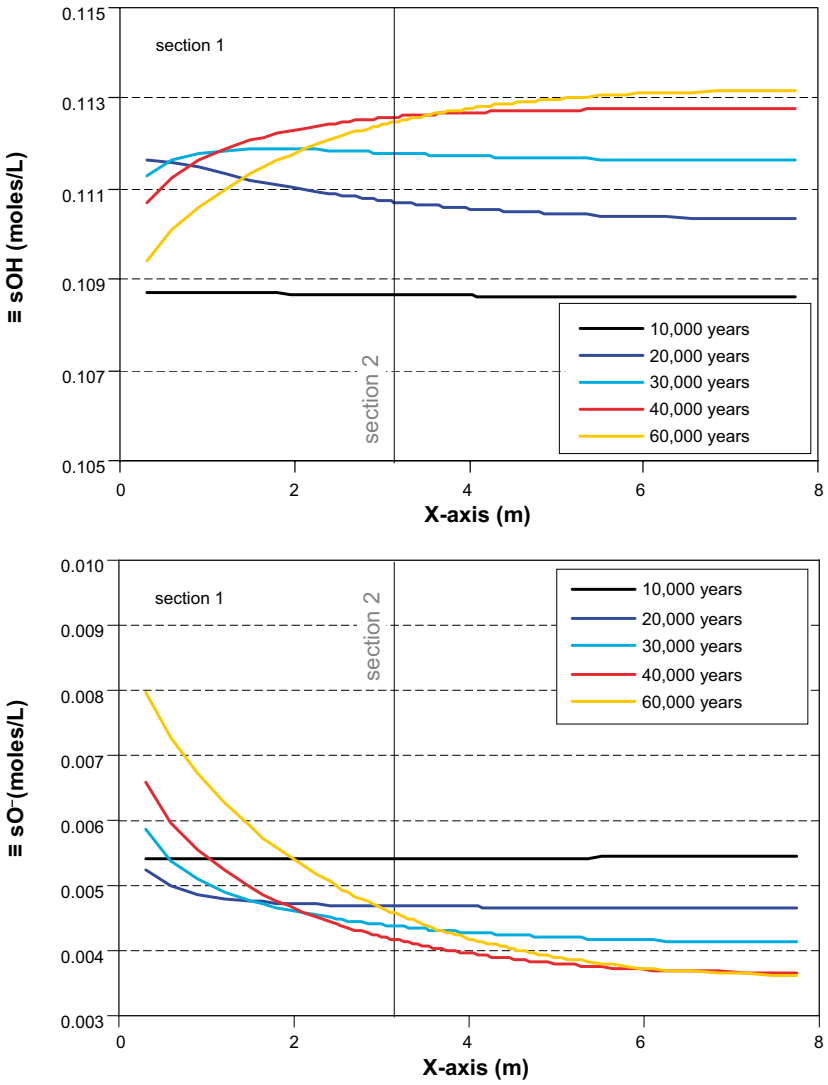

Figure 5-51. *Graphics showing the predicted evolution of neutral (upper graphic) and deprotonated (lower graphic) surfaces of clay fraction in the backfill.*

Finally, the intrusion of the diluted ice-melting water leads to the faster dissolution of gypsum from both the backfill and the bentonite buffer, total dissolution is predicted to occur in less than 15,000 years of simulation in the backfill and less than 30,000 years in the bentonite buffer.

5.4.6.4 Intrusion of high-salinity groundwater (MX-80 bentonite buffer)

The effect of the intrusion of high-salinity groundwater into the system is very similar to that predicted in CASE-I. However, in the present case, the model predicts a slight decrease in pH, which is more pronounced in the backfill (Figure 5-52). The decrease in pH is related to the precipitation of small amounts of calcite, especially in the backfill (Figure 5-53). The precipitation of calcite is, as in CASE-I, the result of the increase in calcium concentration in the pore water resulting from the higher concentration of calcium in high-salinity groundwater. On the other hand, the aqueous carbonate concentration in pore water decreases due to its lower concentration in high-salinity groundwater. However, the decrease in aqueous carbonate concentration is slower than the calcium concentration increase due to the lower concentration gradient, resulting in the subsequent dissolution of previously precipitated calcite, increasing the pH, to nearly the initial values.

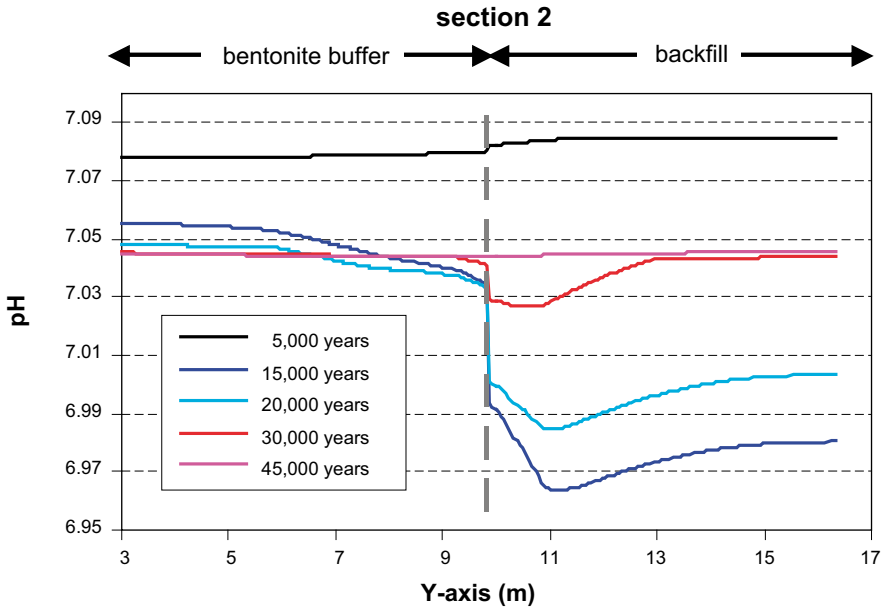

Figure 5-52. *Graphic showing the predicted evolution of pH after the intrusion of high-salinity groundwater in section 2.*

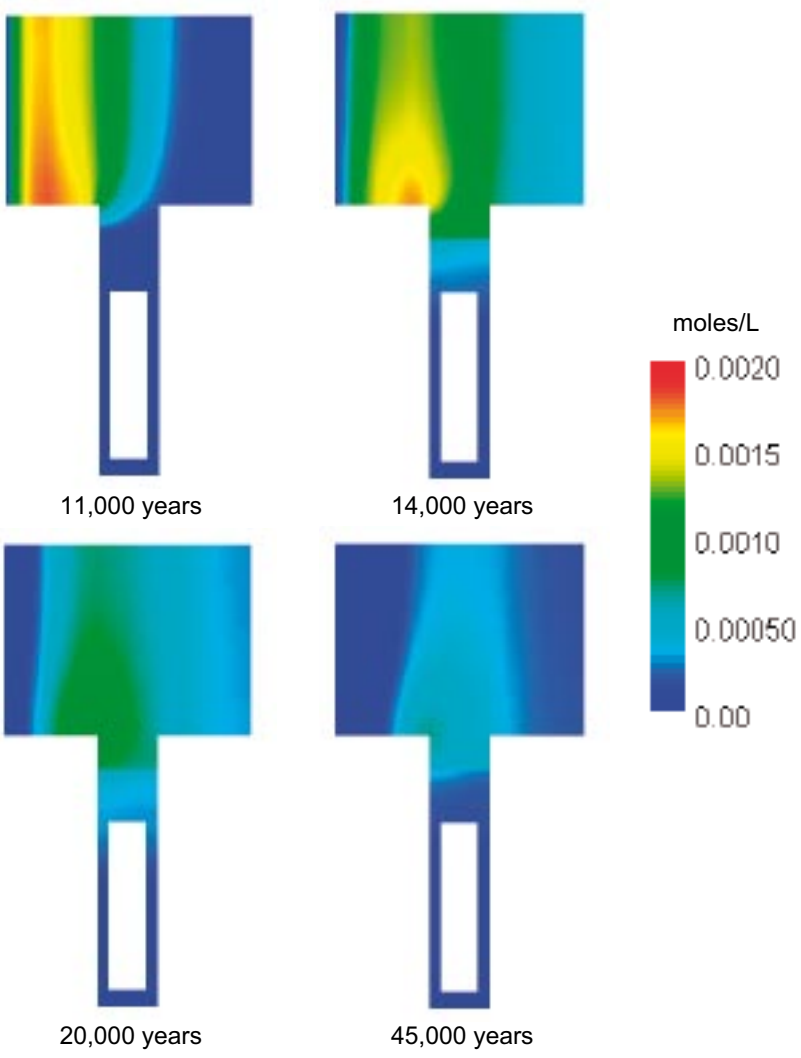

Figure 5-53. *Predicted precipitation and dissolution of calcite during the intrusion of high-salinity groundwater into the system.*

The increase in calcium concentration in the pore water of the backfill and bentonite has also an effect on other processes. On the one hand, it produces an increase on the Na by Ca replacement in the cation exchanger of the bentonite, resulting in higher calcium occupancy of the exchanger at the end of the simulation when compared with the reference case (Figure 5-54). On the other hand, this increase in calcium concentration results in reversing the behaviour of gypsum, which was predicted to dissolve prior to the high-salinity groundwater intrusion. Thus, once the intrusion started, the model predicts the precipitation of gypsum in both the backfill and the buffer (Figure 5-55).

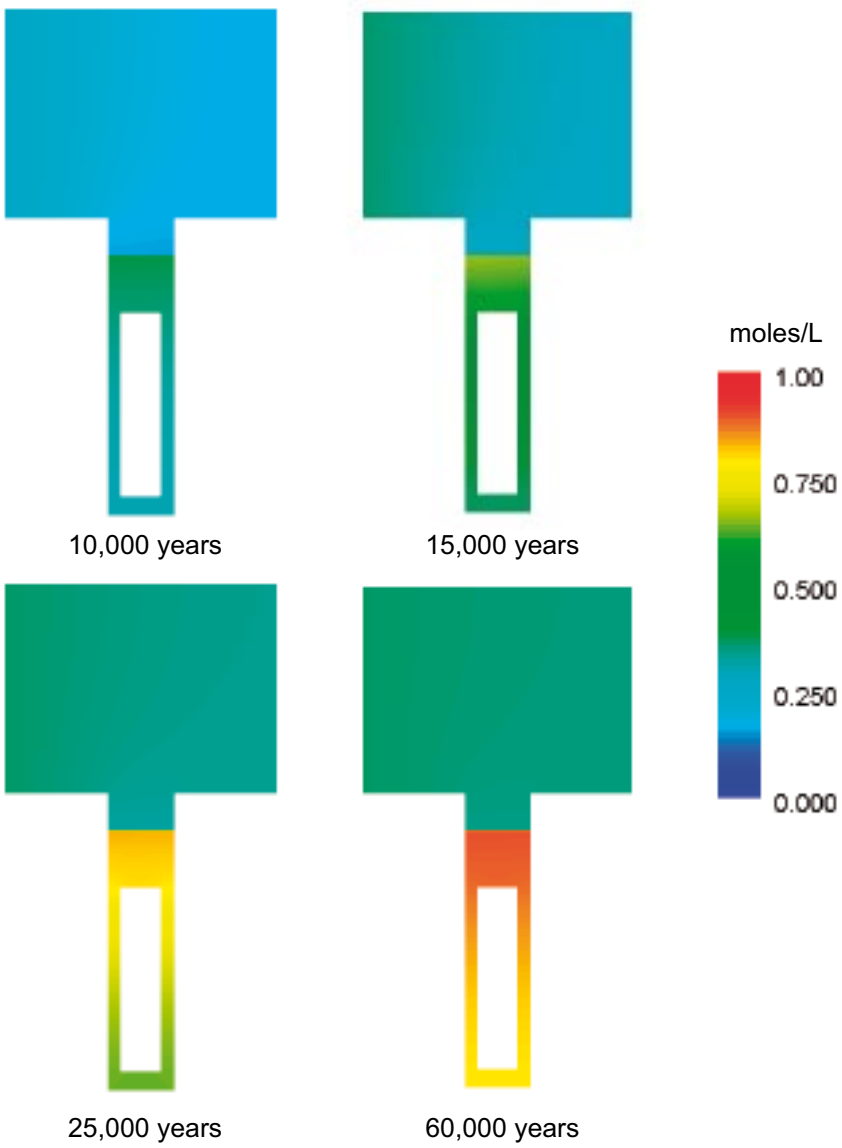

Figure 5-54. *Predicted calcium occupancy in the exchanger of the bentonite due to the intrusion of high-salinity groundwater.*

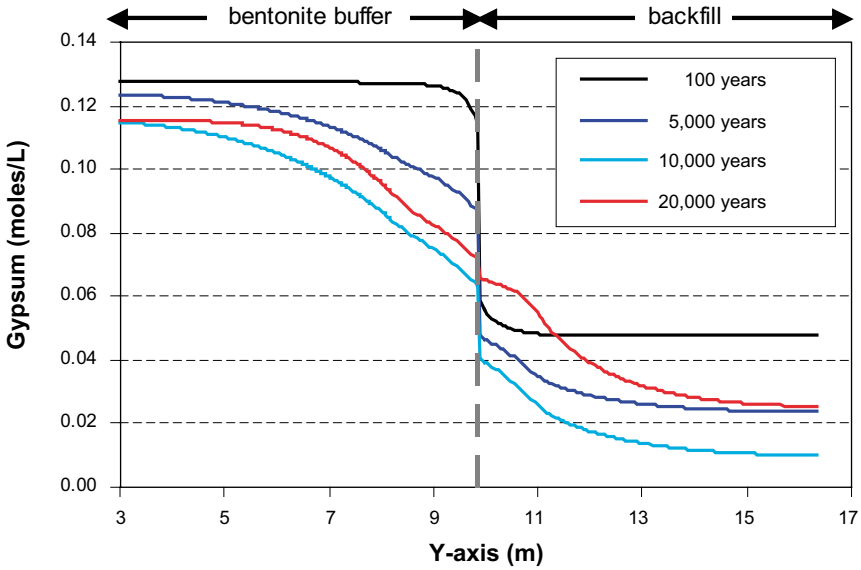

Figure 5-55. *Predicted behaviour of gypsum in the system due to the intrusion of high-salinity groundwater. Note that after the high-salinity intrusion (10,000 years) gypsum precipitates again in both the backfill and the buffer.*

5.4.6.5 Reference case with Deponit CA-N bentonite buffer

In the present reference case, where Deponit CA-N bentonite is considered as the buffer material and the bentonite fraction in the 30/70 backfill, the pH is predicted to increase from an initial value of 7.09 to 7.15 in the buffer and to 7.17 in the backfill (Figure 5-56). However, the pH evolution shows that this increase is followed by a decrease in pH. As in CASE-I, this evolution is related to the precipitation-dissolution of carbonate minerals. Although there is a general increase in the amount of calcite, the predicted net amount of carbonate minerals decreases with time, as more dolomite dissolves than the equivalent calcite precipitates. This is related to the decrease in magnesium concentration (the concentration in Forsmark groundwater is lower than in the pore water from both the buffer and the backfill), which leads to the dissolution of dolomite, thus increasing the concentration in calcium and aqueous carbonate, so calcite is supersaturated and precipitates. As both calcium and carbonate concentrations are very similar in both the Forsmark groundwater and the pore water in the buffer and backfill, there is not a significant variation of the concentration of these components due to the groundwater-bentonite interaction.

In contrast, the lower sulphate concentration in the Forsmark groundwater with respect to the bentonite pore water, leads to the decrease in sulphate concentration in both the backfill and the buffer, producing the dissolution of gypsum, and thus increasing the concentration in calcium in the pore water. This increase in calcium concentration enhances the precipitation of calcite and minimise the net dissolution of carbonate minerals (the difference between dissolved dolomite and precipitated calcite in equivalents per litre). The total dissolution of dolomite in the backfill results in a sharp decrease in the precipitation of calcite (Figure 5-57). However, as calcite still precipitates and no more dolomite is dissolving the net amount of carbonate minerals increase, thus leading to the decrease in pH as shown in Figure 5-56 and Figure 5-57. On the other hand, the pH in the buffer increases continuously during the simulation. This is because dolomite in the buffer is not exhausted during the simulation period, and thus the net amount of carbonate minerals is always decreasing (more dolomite is predicted to dissolve than calcite precipitates).

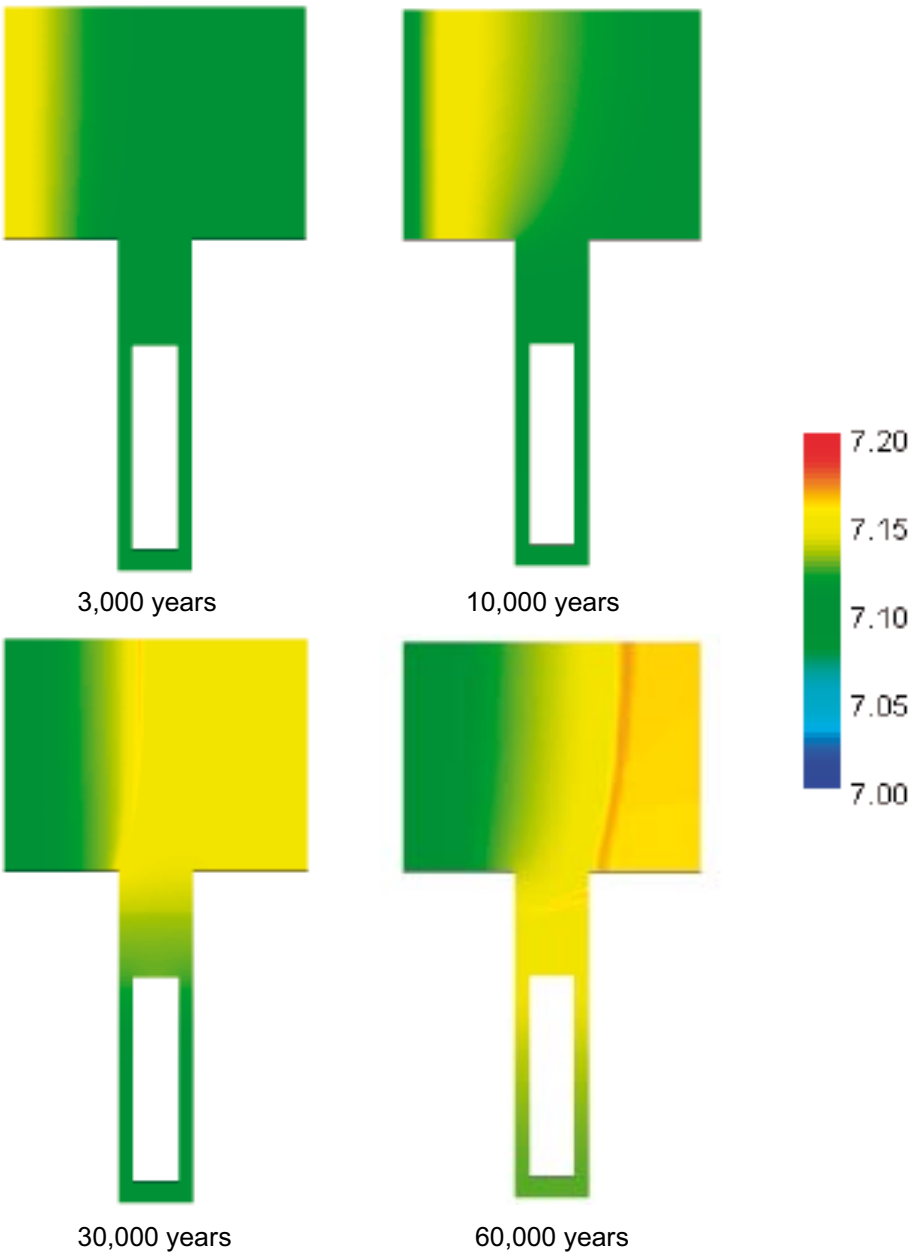

Figure 5-56. *Predicted pH evolution due to the interaction of Forsmark groundwater with Deponit CA-N bentonite in the buffer and in the 30/70 backfill.*

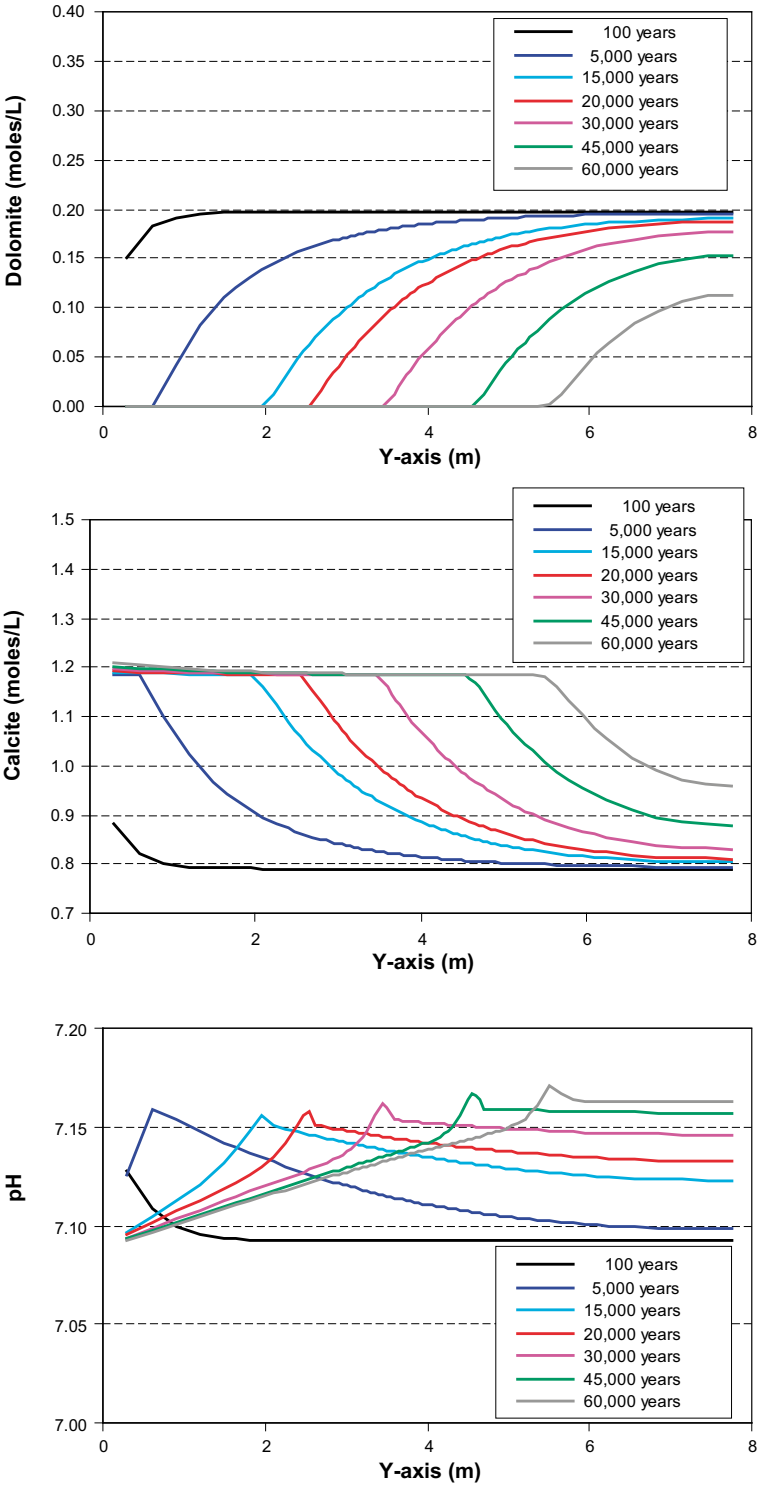

Figure 5-57. *Graphics showing the predicted evolution of the amount of dolomite, calcite and pH in section 1, through the backfill.*

The evolution of the calcium concentration affects the calcium occupancy of the exchanger (Figure 5-58). While gypsum and dolomite are present, the calcium occupancy in the exchanger of the bentonite fraction does not change significantly, the calcium concentration is buffered by the dissolution of these minerals and the precipitation of calcite. However, once gypsum and dolomite disappear (only predicted to occur in the backfill during the simulation), less calcite precipitates due to the exhaustion of dolomite as a source for aqueous carbonate. Moreover, calcium occupancy in the exchanger increases by replacing magnesium, whose concentration sharply decreases due to the lack of any magnesium source from this moment on.

5.4.6.6 Intrusion of ice-melting water (Deponit CA-N bentonite buffer)

The evolution of the system during the first 10,000 years (prior to the ice-melting water intrusion) is identical to that of the reference case. However, once the ice-melting water enters into the system, its higher pH, as well as its diluted composition, enhances the increase of pH of the system. Once the high pH water contacts the backfill calcite starts to dissolve (dolomite in the first cells of backfill has been totally dissolved prior to the intrusion), thus increasing the pH of the system and reaching higher pH values than in ice-melting water at the end of the simulation (Figure 5-59).

However, in those parts of the backfill where intruding water has a pH buffered by previous calcite dissolution and by clay surface acidity reactions, the behaviour is similar to that illustrated in the reference case. The only difference is that dolomite, as it is more subsaturated, dissolves faster than in the reference case, and calcite precipitation is more limited, thus leading to an increase of pH, although not as high as near the boundary where ice-melting water intrudes into the system. Therefore, the higher carbonate dissolution occurs near the boundary where intrusion takes place (Figure 5-60), thus leading to a higher pH increase.

As in previous cases, the intrusion of ice-melting water also increases the dissolution of gypsum, which is predicted to be totally depleted from the backfill after some 36,000 years of simulation. In the buffer, the increase in pH is less than in the backfill, with maximum values of around 7.8. The reason for such a limited effect on pH is that pore water in the backfill, near the bentonite in the deposition hole, is already buffered by carbonate dissolution. Thus, carbonate dissolution in the upper part of the buffer is very limited, leading to a relatively small increase in pH when compared with pH increase in the backfill (Figure 5-61). Gypsum dissolution in the buffer is also limited, and complete dissolution of gypsum in the upper part of the bentonite buffer only occurs after 55,000 years. When this occurs, the net dissolution of carbonate minerals decrease, leading to a pH increase of up to 8.03, the maximum value in the buffer during the simulation (Figure 5-61).

The geochemical evolution of pore water in the system does not reflect major changes in cation exchange composition in the bentonite and the backfill, where minor increases of calcium and magnesium occupancy occur by replacing sodium.

5.4.6.7 Intrusion of high-salinity groundwater (Deponit CA-N bentonite buffer)

The geochemical evolution of the system due to the intrusion of high-salinity groundwater is similar to the one shown in previous calculations by using this type of water composition. No major changes in pH are expected to occur in the system: in the bentonite buffer, pH values range between 7.04 and 7.10 (Figure 5-62), whereas in the backfill a higher pH increase is predicted (between 7.0 and 7.4).

The pH evolution predicts a slight increase prior to the high-salinity groundwater intrusion. Once the intrusion starts, the pH of the system decreases to the lowest values and then gradually increases again until reaching the higher pH values in the backfill and near to initial values in the bentonite buffer.

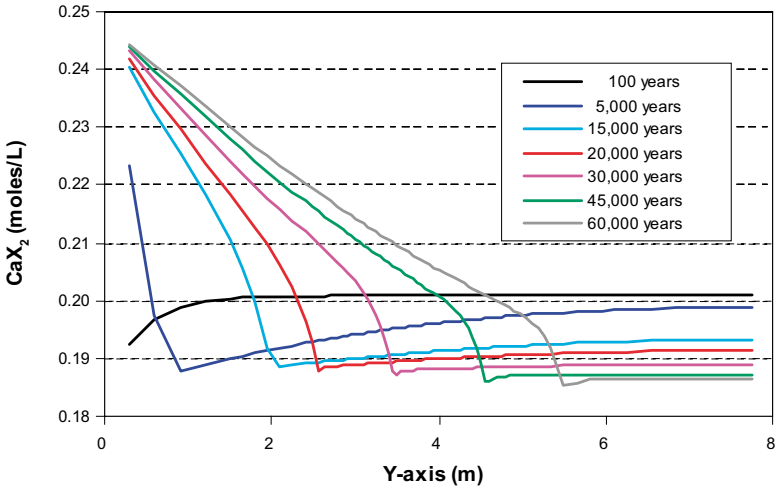

Figure 5-58. *Graphic showing the predicted calcium occupancy in the exchanger of the bentonite in section 1 through the backfill. Note the reverse behaviour calcium once dolomite and gypsum have been dissolved, thus increasing the calcium occupancy in the exchanger.*

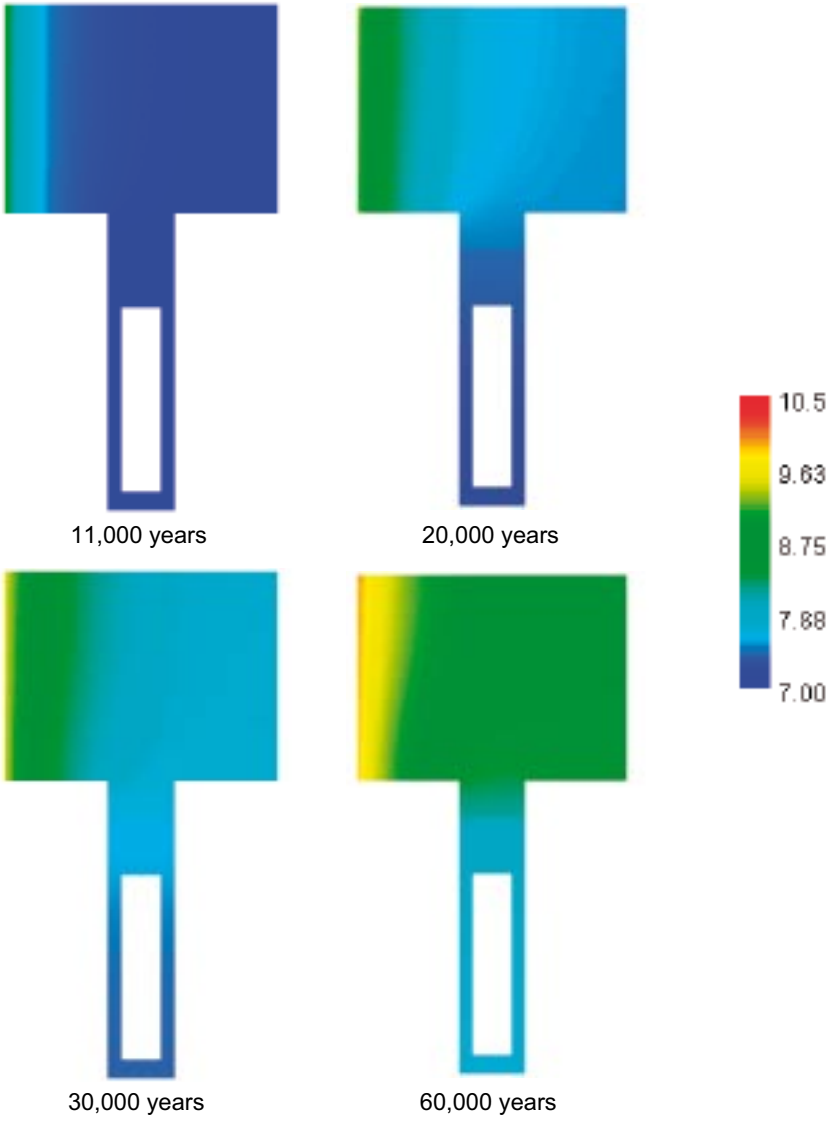

Figure 5-59. *Predicted pH evolution after the intrusion of ice-melting water, which interacts with the backfill and the buffer.*

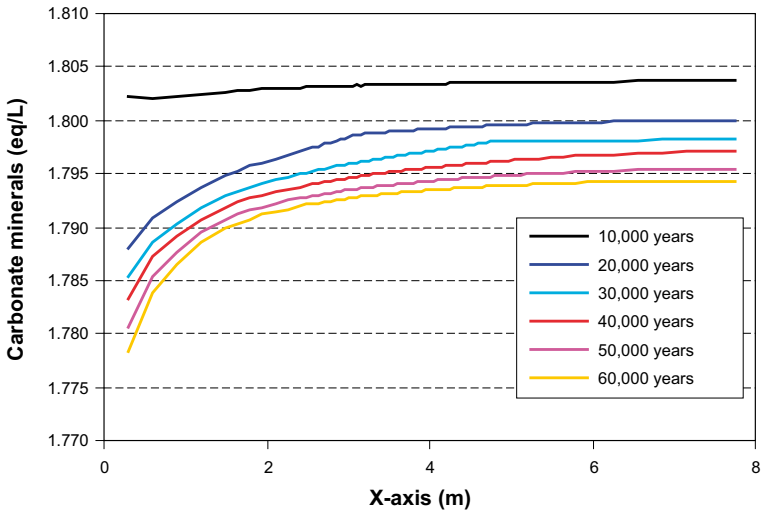

Figure 5-60. *Predicted evolution of the net amount of carbonate minerals in the backfill in section 1.*

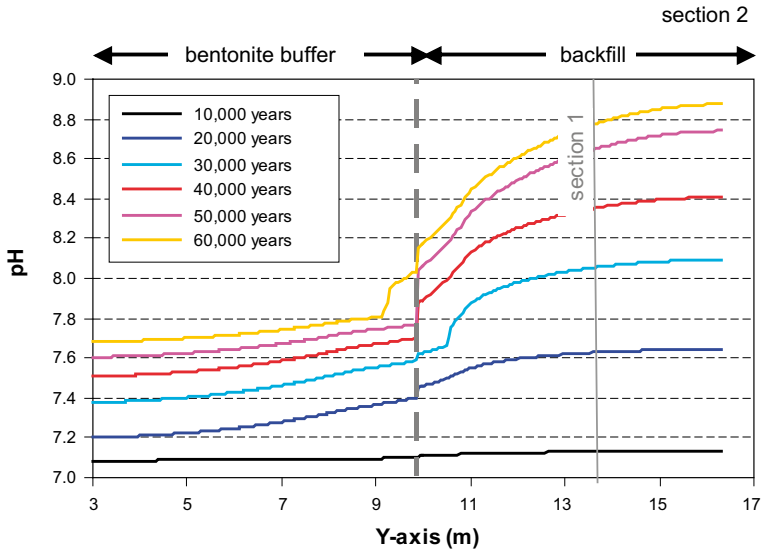

Figure 5-61. *Predicted pH evolution due to the intrusion of ice-melting water in section 2.*

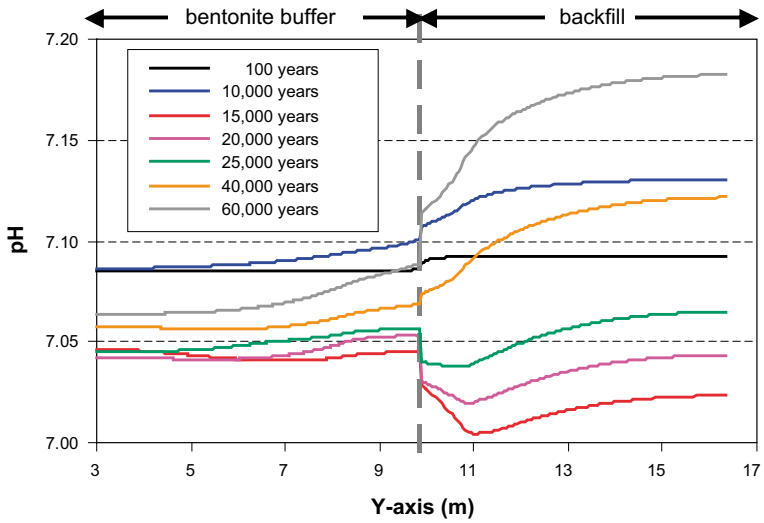

Figure 5-62. *Predicted evolution of pH in the backfill and the buffer during high-salinity groundwater intrusion in section 2.*

The pH evolution in the system is once again a consequence of the precipitation-dissolution processes of carbonate minerals. Dolomite, which is being dissolved prior to the high-salinity water intrusion, dissolves faster once the intrusion starts. This behaviour is related to the lower magnesium concentration of the intruding water with respect to the pore water from the backfill and the buffer. Thus, dolomite is totally exhausted in the backfill after 15,000 years and after less than 35,000 years in the bentonite buffer. The behaviour of calcite is the reverse than that of dolomite, it always precipitates, although in very low amounts when no dolomite is present to supply carbonate for the calcite precipitation. The process of calcite precipitation is responsible for the slight decrease in pH, which is lower while dolomite is still dissolving.

The dissolution of gypsum occurring prior to the high-salinity groundwater intrusion is reversed once the intrusion starts. The reason for this change is the higher calcium and sulphate concentration of the high-salinity groundwater.

The increase in calcium concentration in pore water leads to a significant increase in the calcium occupancy of the exchanger, which doubles the initial occupancy after 60,000 years of simulation in both the backfill and the buffer.

5.4.6.8 Summary

The most relevant results of CASE-II simulations, considering the 30/70 mixture as the backfill material, are the following:

- Almost no changes in pH are predicted in the simulations, except when ice-melting water is considered to contact the near field, where pH is predicted to reach a value above 9 in the backfill close to the boundary of ice-melting water penetration.
- pH buffering is exerted by carbonate minerals if present, otherwise pH is partially controlled by surface acidity reactions.
- Gypsum dissolution is predicted to occur, except when high-salinity water enters into the system. In this case, gypsum is predicted to precipitate, especially in the backfill, where the increase in aqueous calcium due to diffusion is higher.
- In all cases, calcium replaces sodium in the exchanger, although the extent of such replacement depends on the calcium availability and the decrease in sodium concentration associated to the intrusion of ice-melting water.

5.4.7 Final remarks of CASE-II

The geochemical evolution of the system when groundwater enters into the modelled domain through the backfill and then reaches the buffer is controlled by the diffusive transport of calcium and aqueous carbonate, as in CASE-I. This process is responsible for the behaviour of calcite and thus the pH evolution in the system, although in the reference case, where MX-80 bentonite is considered, the absence of carbonate minerals lead to the surface acidity of the clay fraction in the bentonite to buffer the pH.

When considering the Deponit CA-N bentonite, the diffusion of magnesium has an additional effect on the dissolution-precipitation of dolomite, and consequently on the behaviour of calcite. Then the net dissolution-precipitation of carbonate minerals exerts the control on the pH evolution of the system.

In the reference case, both considering the MX-80 and Deponit CA-N bentonite, as well as when high-salinity water intrusion is considered, the effect on pH is minimal, and very small changes on the pH are predicted (Figure 5-63). Furthermore, in the present case, the buffering effect exerted by the backfill minimises the changes in the bentonite buffer. This is especially true when considering the intrusion of ice-melting water, where the increase of pH due to the high-pH of ice-melting water and the dissolution, when present, of carbonate minerals is buffered by the presence of the backfill. The reason for such a buffering effect exerted by the

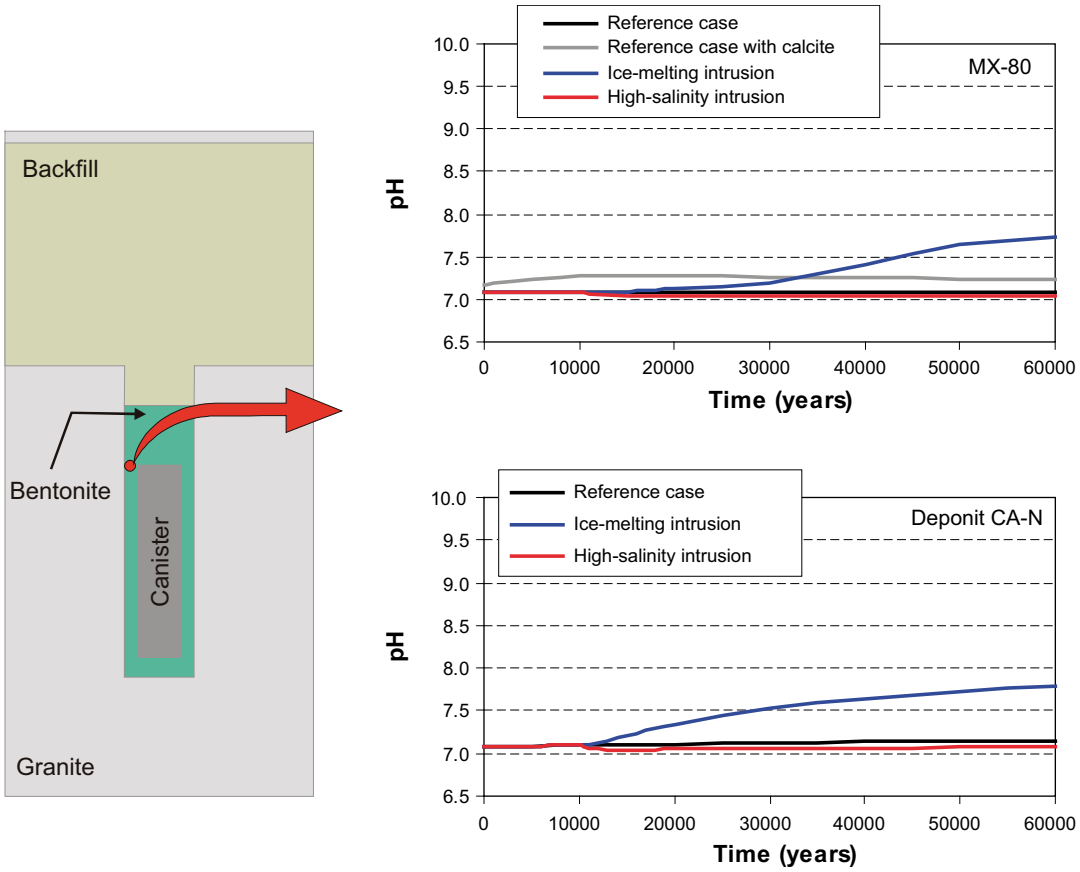

Figure 5-63. *Predicted pH evolution in the bentonite buffer close to the upper part of the canister.*

backfill is double; first slow transport processes in the backfill slow down the diffusion of solutes in the bentonite buffer, and second the reactions in the backfill buffer the pH of the pore water in contact with the bentonite buffer.

5.5 CASE-III: Thermal effect

5.5.1 The modelled domain, thermal field and boundary conditions

Heat production from radioactive decay in the spent fuel affects the near field by increasing the temperature of the materials used in the engineered barrier system and in the nearest host rock. Thermal models of the near field show that maximum temperatures reached by the buffer in the deposition hole are around 80°C after around 10 years (Figure 5-64; SKB 2004a). Temperatures at the contact with the host rock are expected to be around 50°C. After 10,000 years, temperature in the near field has decreased down to 25°C.

Numerical simulations presented in CASE-I and CASE-II assume reactive transport at constant temperature (15°C). According to the thermal data above exposed, low temperatures are typically found in the host rock, and also in the buffer 10,000 years after the spent fuel storage. The reactions between inflow groundwaters and accessory minerals may be largely influenced by the thermal field. For this reason, the model CASE-III is focused on the assessment of the effect of the thermal field on the pore water and the accessory minerals of the bentonite buffer.

The CASE-III simulates the thermal effect at two distinct levels of the bentonite buffer. The first section is located in contact with a fracture plane (section 1 in Figure 5-65), and consequently, it will be expected a significant alteration of the bentonite pore water chemistry and accessory minerals by the advective migration of regional groundwater. The second section is located at

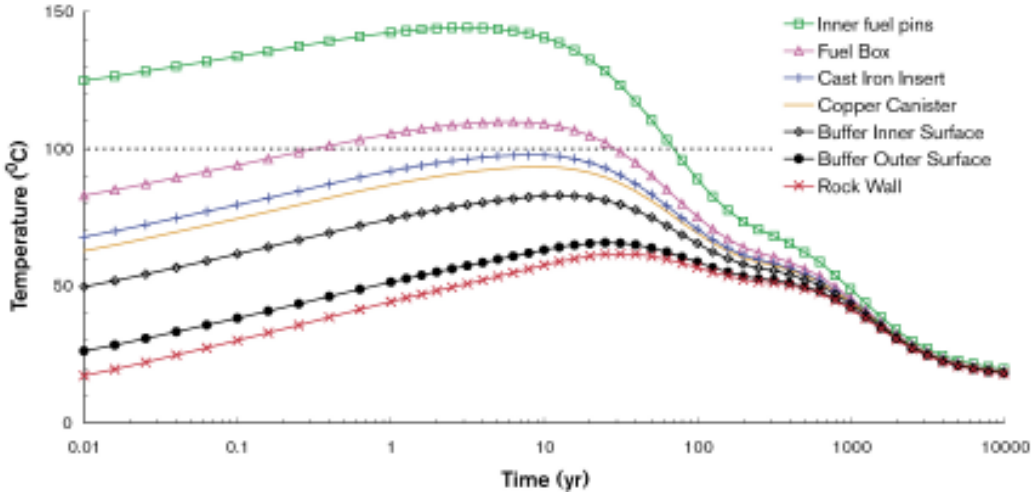

Figure 5-64. *Calculated thermal evolution of the near field. Note that temperatures in the buffer reach up to 80°C in the initial times of spent fuel storage. Adapted from /SKB 2004b/.*

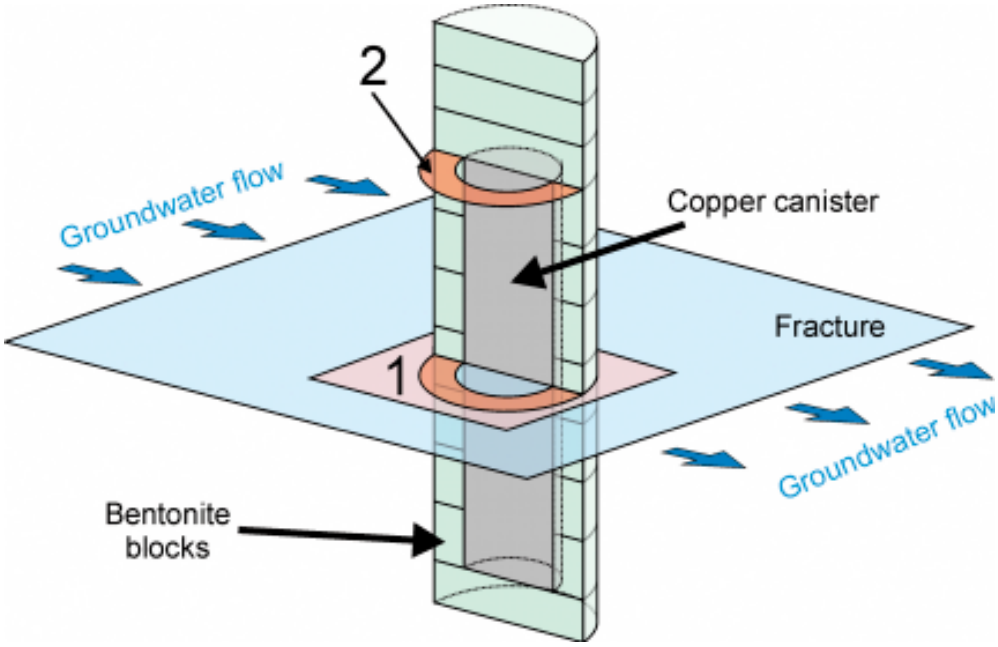

Figure 5-65. *Location of the two sections considered in CASE-III. Section 1 is corresponds to the fracture level and granitic groundwater effect is expected, whereas section 2 is far from the fracture level, and therefore geochemical changes are only expected as a consequence of the thermal gradient.*

some distance from the fracture level (section 2 in Figure 5-65), where the influence of regional groundwater flowing through the fracture plain can be considered negligible, at least in the first 1,000 years. In addition, the mass transfer between granite host and bentonite has not been permitted in order to enhance the effect induced by the thermal gradient within the bentonite.

Following the data showed in Figure 5-64, the temperature difference in the simulations between the canister-bentonite and the granite-bentonite boundaries is 30°C (from 50 to 80°C; Figure 5-66). Temperature in the granite domain ranges from 50 to 15°C, this latter value is the temperature expected to be found at repository depths at Forsmark /SKB 2004a/. Since the PHAST code is not capable of simulating heat transport, no initial transitory stage of warm up and subsequent cooling down of the domain is considered, so that a stationary thermal field is

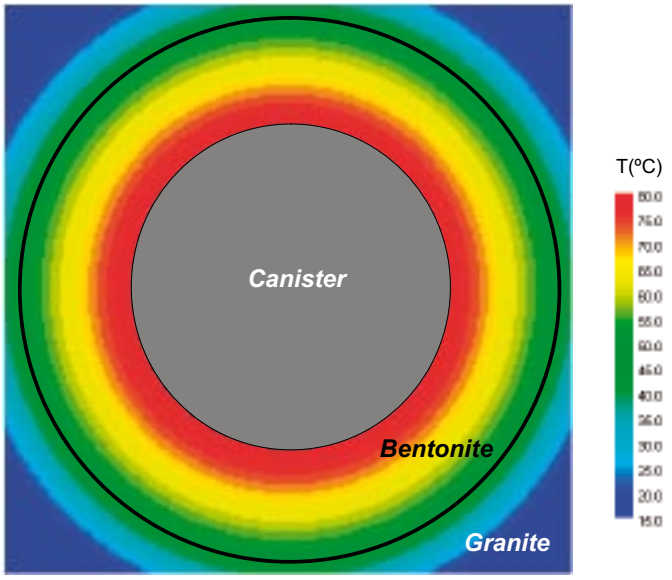

Figure 5-66. *Modelled section in the CASE-III showing the temperature field considered in the model. Scale bar indicates the temperature range in °C.*

assumed during the entire period of simulation. To model the thermal gradient, 18 concentric groundwater zones have been assumed. In the bentonite domain, the temperature gradient is regularly spaced resulting in $\Delta T = 3°C$ between zones. Whereas, in the granite the step is 5°C between zones. As initial conditions, pore water chemistry in both bentonite and granite has been re-equilibrated according the temperature of each zone (see Section 5.3.3).

In the first case (section at fracture level), the modelled domain is a two-dimension square section with X = Y = 1,810 mm, discretised into 32,761 elements (33,124 nodes). In fact, this section is comparable to the fracture plane studied in the CASE-I, although the spatial discretisation is much finer, since $\Delta X = \Delta Y = 10$ mm. In the second case, the active domain is slightly smaller, with X = Y = 1,700 mm (31,329 elements and 31,684 nodes).

Boundary conditions are the same as those imposed in CASE-I: a prescribed hydraulic head in left and right boundaries; upper and lower margins are no flow boundaries. Groundwater flows from the left to right boundary with a head gradient of 0.002 $m \cdot m^{-1}$. Solute composition is only fixed in the left boundary, whereas it is allowed to change in the right boundary.

The time step ranges from 0.5 to 5 years, in a total period of simulation of 1,000 years, as this is the time at which temperature gradients are minimal (Figure 5-64).

5.5.2 Hydraulic properties

The hydraulic properties of the actives zones defined in the CASE-III (fracture and bentonite) are the same as considered in the CASE-I (see Table 5-2). For further details of the properties, see Section 5.3.1. As in CASE-I, the canister zone is assumed to be inactive (i.e., neither water flow nor solute transport takes place).

5.5.3 Initial calculations

The initial chemistry of pore water in each of the thermal zones defined in Section 5.5.1 has been determined by using the PHREEQC code /Parkhurst and Appelo 1999/. As in the reference simulation of CASE-I, calculations have been done by equilibrating Forsmark groundwater at the specific temperature with a set of reactive minerals. In the fracture, quartz and calcite are considered to react until reaching thermodynamic equilibrium, whereas pyrite is allowed to

kinetically dissolve (see Section 4.2). Secondary carbonate minerals such as siderite, gypsum, FeS and $Fe(OH)_3$ are allowed to precipitate if they become oversaturated. In the MX-80 bentonite, groundwater reacts in thermodynamic equilibrium with gypsum, quartz, and oxidative dissolution of pyrite is allowed. In addition of these minerals, dolomite, siderite, and calcite are also included when using the Deponit CA-N bentonite in the simulation. Secondary minerals that are able to precipitate as a result of reactions include calcite, dolomite, siderite, FeS, $Fe(OH)_3$ and anhydrite. The latter mineral is included because at high temperatures is the stable form of calcium sulphate instead of gypsum. Moreover, in thermal zones with temperatures higher than 65°C, hematite is preferred to precipitate as Fe(III) oxide instead of $Fe(OH)_3$. In addition to reactions with accessory minerals, Na-Ca-Mg-K exchange and protonation/deprotonation reactions are considered in the bentonite.

The initial equilibrium results in a complete replacement of gypsum by anhydrite in the bentonite zone. In addition, tiny amounts of secondary calcite and hematite precipitate.

5.5.4 Results

5.5.4.1 MX-80 bentonite buffer at fracture level

The predicted geochemical evolution of the system indicates an increase in pH in the fracture domain surrounding the bentonite buffer, reaching a maximum value of 7.6 after 100 years, but only close to the outflow part of the buffer (Figure 5-67). Such an increase is caused by dissolution of calcite. After this increase in pH in the fracture pore water, the model predicts a decrease in pH in the entire buffer, with a minimum pH of 6.35 after 1,000 years. This pH evolution in the bentonite is in part a consequence of the precipitation of carbonate minerals, mainly dolomite (Figure 5-68), which in turn, is controlled by the $[Ca^{2+}]$ of pore water.

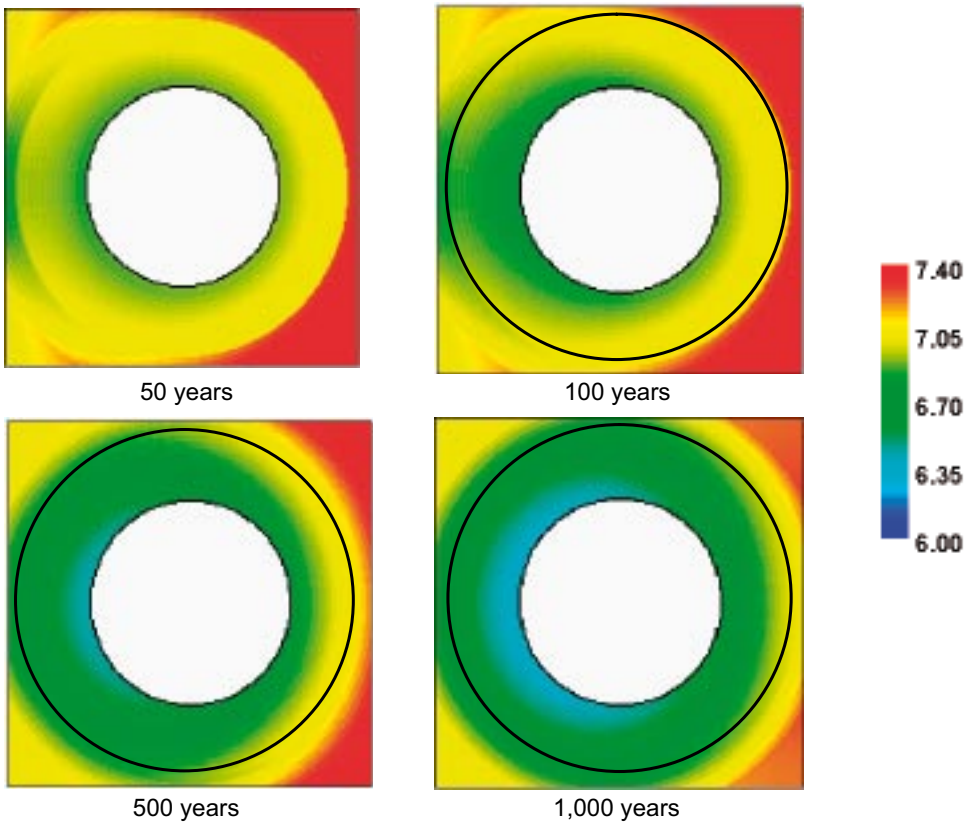

Figure 5-67. *Predicted pH evolution of the system during the thermal stage at the fracture level where MX-80 is used as a bentonite buffer.*

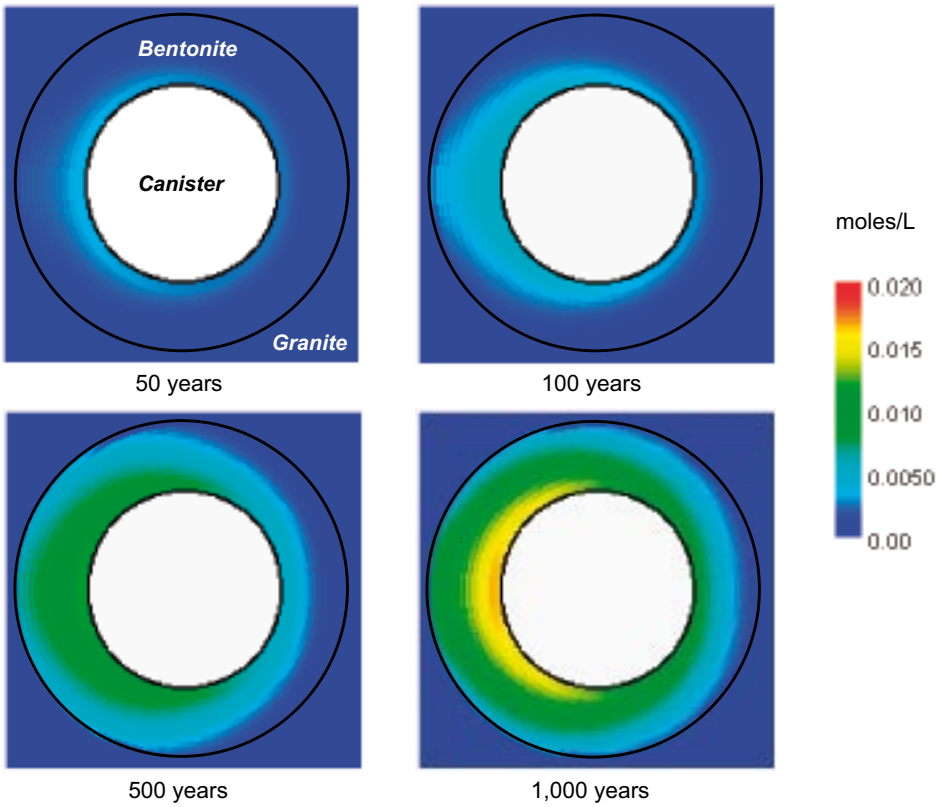

Figure 5-68. *Evolution of dolomite concentration in the buffer section at fracture level. Note the progressive precipitation of this mineral through time. The smaller precipitation of dolomite in the right hand side part of the bentonite domain, especially during the initial times, is caused by the opposite behaviour of anhydrite, which dissolves in the left hand side part and precipitates in the right hand side part (see Figure 5-69).*

It is worth mentioning that the decrease in pH associated to the thermal effect and the diffusive transport through the bentonite is not necessarily associated with an acidification of the system. This is because neutral pH decreases with increasing temperature, thus for the temperature range in the bentonite (45–80°C) the neutral pH decreases to 6.7 and 6.3 respectively. Then, the resulting pH predicted during the simulation is still neutral or even slightly alkaline, as it is maintained within the described range.

Anhydrite quickly dissolves when the inflow water access to bentonite, since Forsmark groundwater is undersaturated in this phase. Part of the released calcium is precipitated again as anhydrite in other parts of the bentonite, although as long as the groundwater flows, this mineral completely dissolves (Figure 5-69). Calcium availability determines the saturation state of calcite and dolomite, and, therefore, the pH.

Part of calcium and sulphate released from anhydrite re-precipitates as gypsum in those zones with temperatures lower than 30°C (outside the bentonite buffer), reaching its highest concentration after 250 years. In the next 300 years, gypsum dissolves to total disappearance.

In addition, the increase in calcium concentration in the bentonite pore water leads to an increase in calcium occupancy in the exchanger (from 0.27 to 0.65 moles/L; Figure 5-70). In a similar way to precipitation dolomite, such an increase is less pronounced in the right hand side part of the bentonite in the first 100 years, since the precipitation of anhydrite fixes the *excess* calcium.

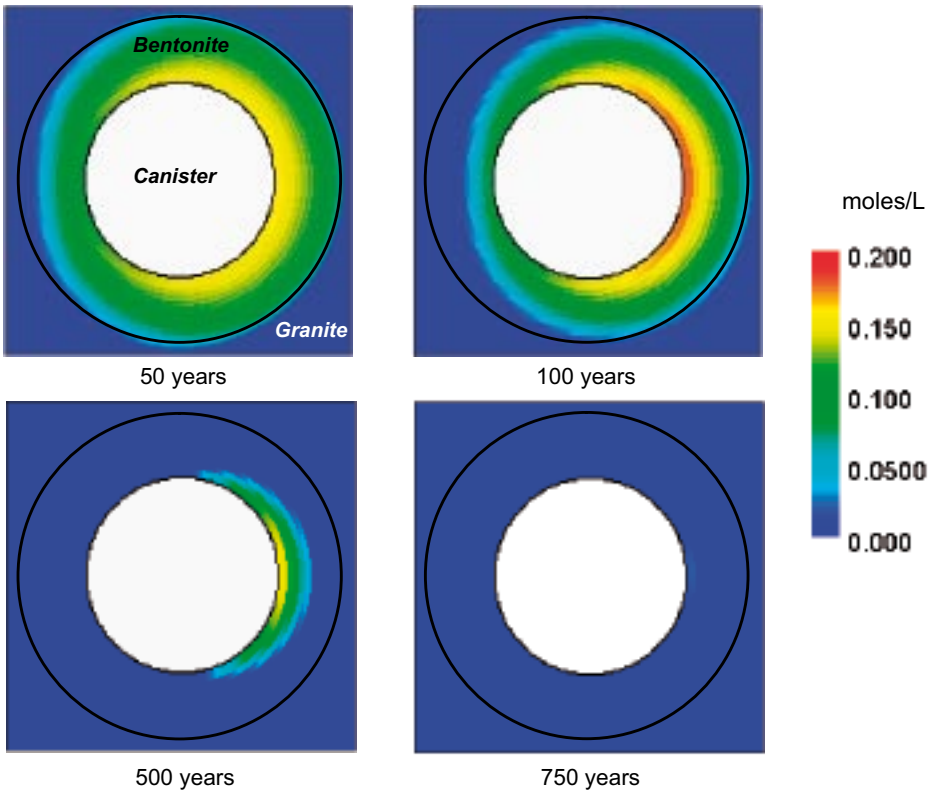

Figure 5-69. *Predicted evolution of anhydrite content in the bentonite buffer during the thermal stage. Note the coeval dissolution and precipitation of this mineral in different parts of the bentonite in the first 100 years. Afterwards, anhydrite dissolves to disappear in less than 800 years.*

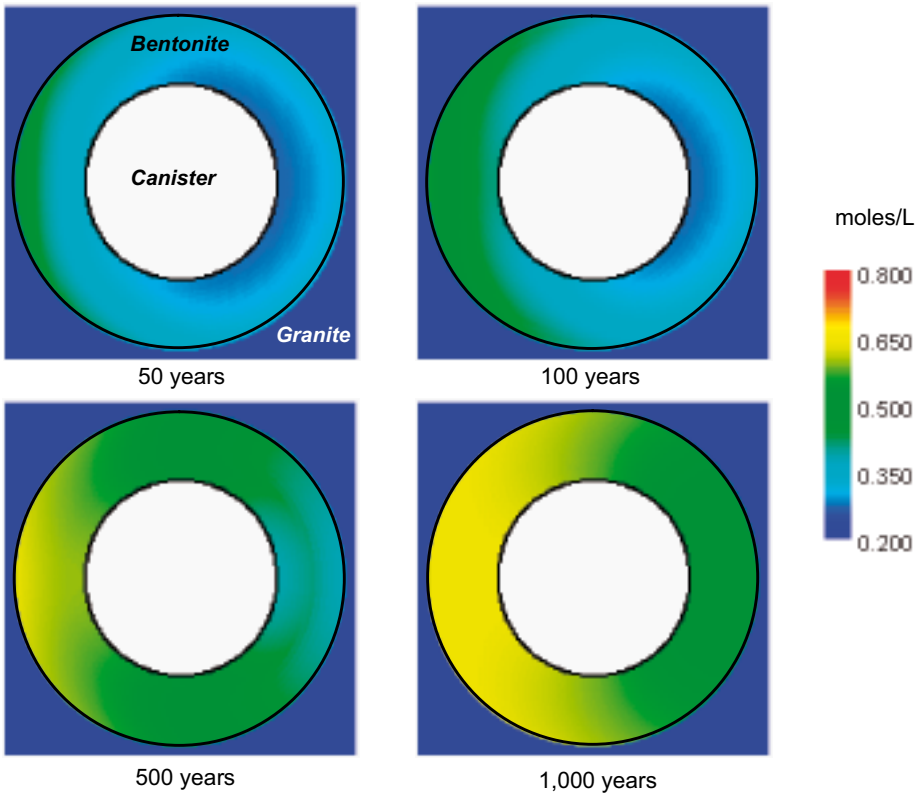

Figure 5-70. *Evolution of [CaX_2] in the bentonite buffer during the thermal stage. The lower increase in the calcium occupancy in the right hand side of the buffer, especially during the initial 250 years, is due to the precipitation of anhydrite that fixes the calcium available in pore water.*

Related to the silica phases, there is a general dissolution of silica phases in the bentonite, which is more pronounced in the warmest part, close to the canister (Figure 5-71). The only exception is found at the coolest zone in the right hand side of the domain, where quartz precipitates during the entire period of simulation. Initial content is 3.03 moles/L, and after 1,000 years, the concentration of silica drops down to 2.98 moles/L in the warmer part of the bentonite.

Finally, the model also predicts the precipitation of small amounts of hematite in the bentonite close to the canister, in amounts smaller than 10^{-7} mol/L after 1,000 years of simulation.

5.5.4.2 MX-80 bentonite far from the fracture level

The inflowing groundwater through the fracture plane causes significant changes on the chemistry of bentonite pore water. From results in CASE-I, it has been concluded that the influence of the groundwater flow on bentonite sections at some distance from the fracture level could be negligible during the first thousand years of simulation. Therefore, the variations in the pore water chemistry are mainly caused by lateral diffusive flow following concentration gradients existing between different thermal zones.

The results obtained when simulating the pore water evolution in a MX-80 buffer indicate that pH variations are smaller than in the case of a section close to the fracture plane (Figure 5-72). As expected, the lowest pH is found of the warmer zones, although the difference with the cooler ones is only of 0.20 pH-units. Major changes in pH occur in the warmer zones during the initial 50 years, from 7.02 to 6.92 due to the predicted precipitation of up to 0.0020 moles/L of dolomite. Anhydrite progressively dissolves in the cooler zones, allowing calcium and sulphate to diffuse to higher temperature zones where re-precipitated as anhydrite (Figure 5-73). The precipitation of both anhydrite and dolomite in warmest part of the system, near the canister, represents the major sink for calcium, and therefore, Na by Ca exchange is not a significant process as it was predicted in the previous case.

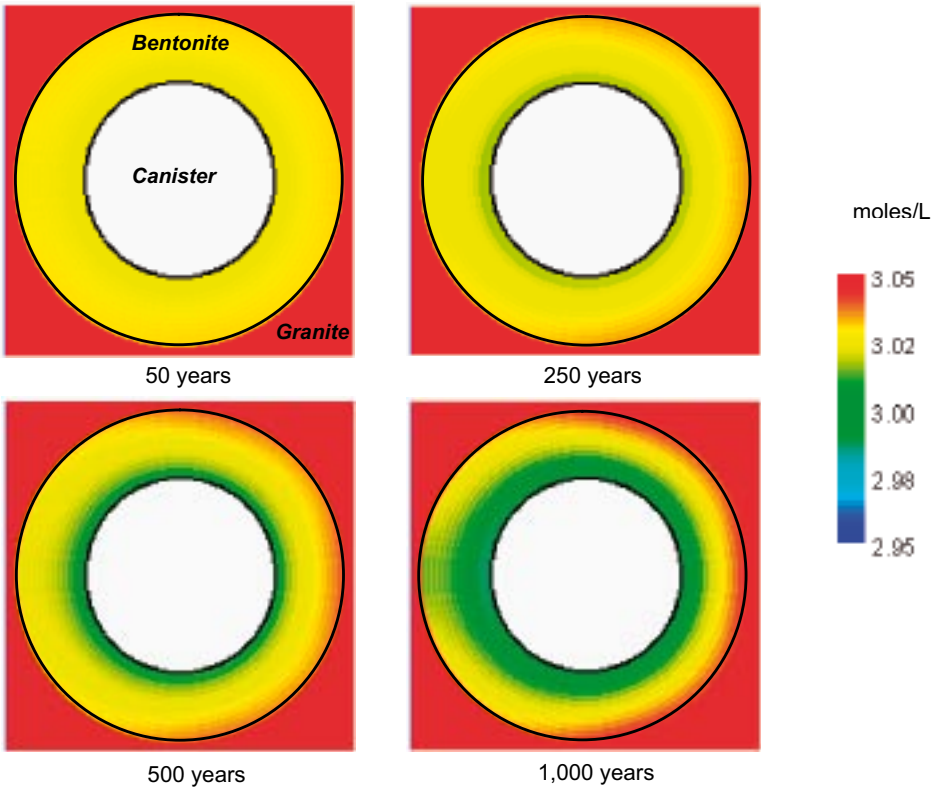

Figure 5-71. *Predicted evolution of quartz content in the bentonite buffer during the thermal stage.*

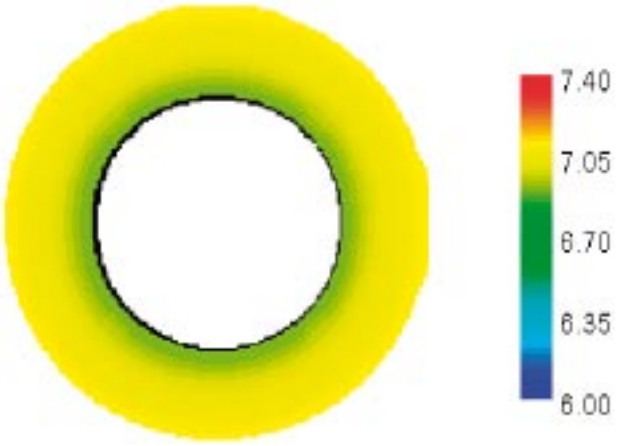

Figure 5-72. *pH of MX-80 bentonite pore water after 1,000 years simulation. Note the small variation in pH, especially when compared with Figure 5-67.*

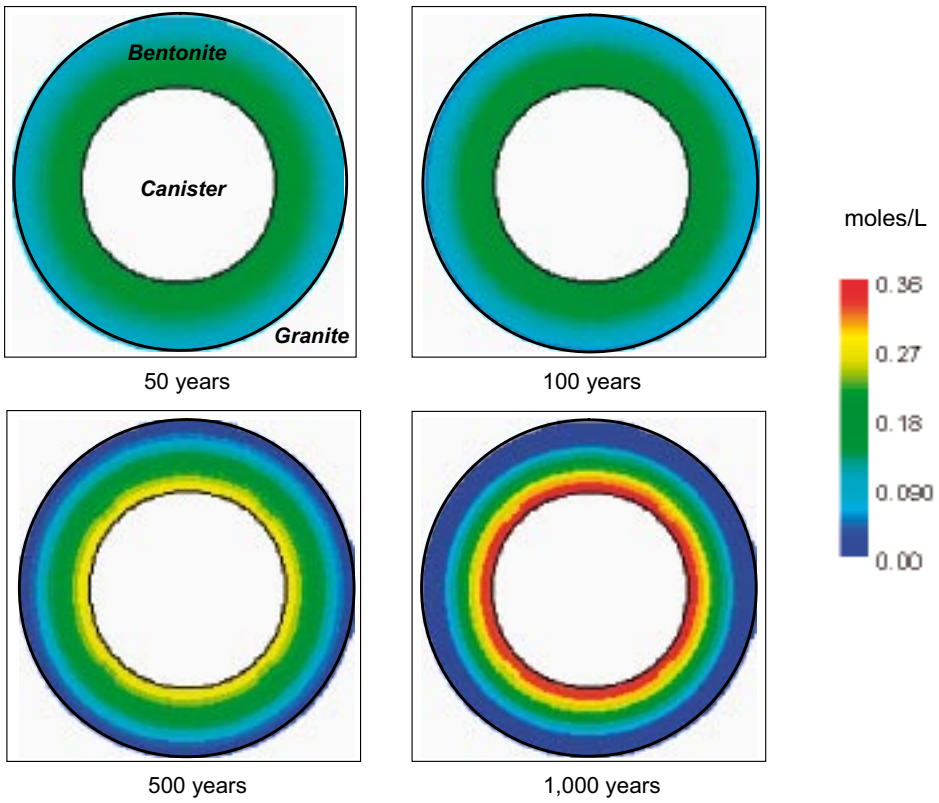

Figure 5-73. *Predicted evolution of anhydrite content in the bentonite buffer during the thermal stage in a section located away from a hydraulically conductive fracture. Note the symmetric changes in the modelled domain. Diffusive transport of calcium and sulphate leads to dissolution of anhydrite in the outer (cooler) parts of the section and subsequent re-precipitation in the inner (warmer) zones. Compare the different evolution with Figure 5-69.*

The evolution of quartz concentration shows the reverse behaviour than anhydrite, as quartz is predicted to dissolve in the warmer part of the system (near the canister) and re-precipitates in the cooler zones at the granite-bentonite boundary (Figure 5-74).

5.5.4.3 Deponit CA-N bentonite buffer at fracture level

The obtained data from simulations in the CASE-III using the Deponit CA-N bentonite show significant differences in the evolution of mineral and ion behaviour, caused by the existence of accessory minerals that are not present in the MX-80 bentonite, such as siderite, calcite and dolomite. Nevertheless, the resulting evolution of pH does not differ substantially than the evolution when considering the MX-80 bentonite (Figure 5-75).

Compared to MX-80, the Deponit CA-N bentonite contains 4 times more calcium sulphate. This mineral tends to dissolve in the cooler zones and re-precipitate in the warmer ones (Figure 5-76), but it is not exhausted at the end of the simulation. This evolution controls the precipitation and/or dissolution of other Ca-bearing minerals such as dolomite and calcite (Figure 5-77), which in turn determines the evolution of pH, although, in the present simulation, calcite is being replaced by dolomite in the warmer part of the system and the contrary occurs in the cooler part of the system.

On the other hand, evolution of quartz concentration follows a very similar pattern to that predicted when considering MX-80 as the bentonite buffer.

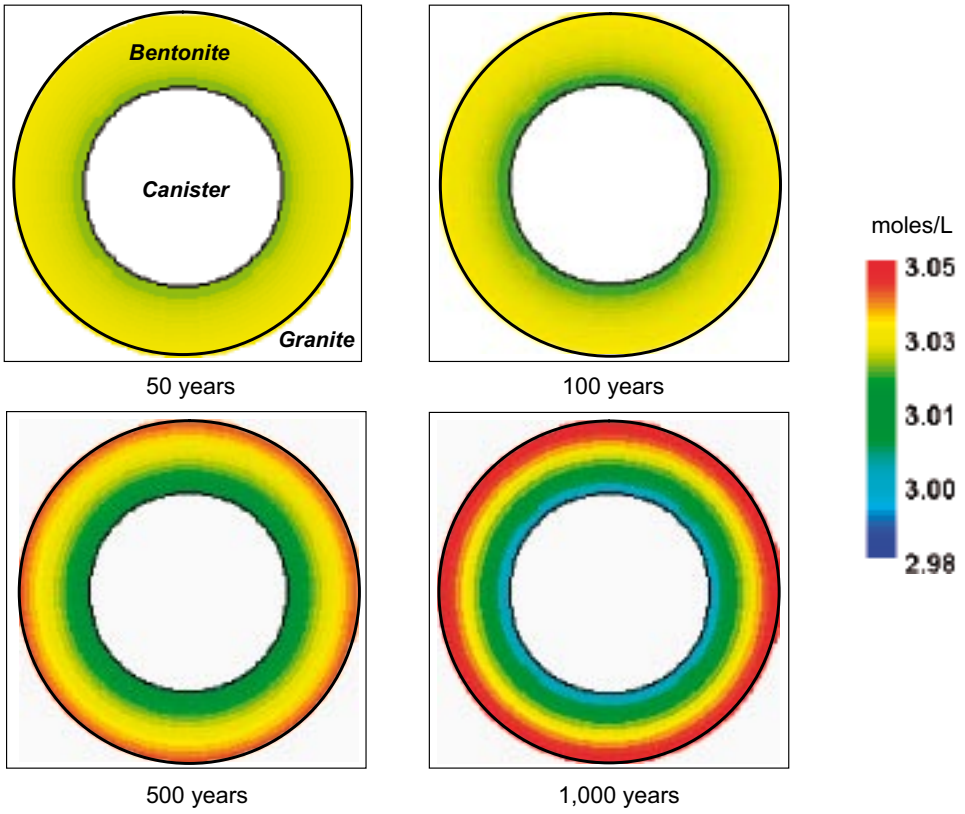

Figure 5-74. *Evolution of quartz concentration in the bentonite buffer. It is clearly observable the mobilization of silica from warmer zones to cooler zones through time. Quartz progressively dissolves in the areas closer to canister and re-precipitates in the outer rims of the bentonite sections. Solute transport and reaction from granite to bentonite is not allowed in the simulations.*

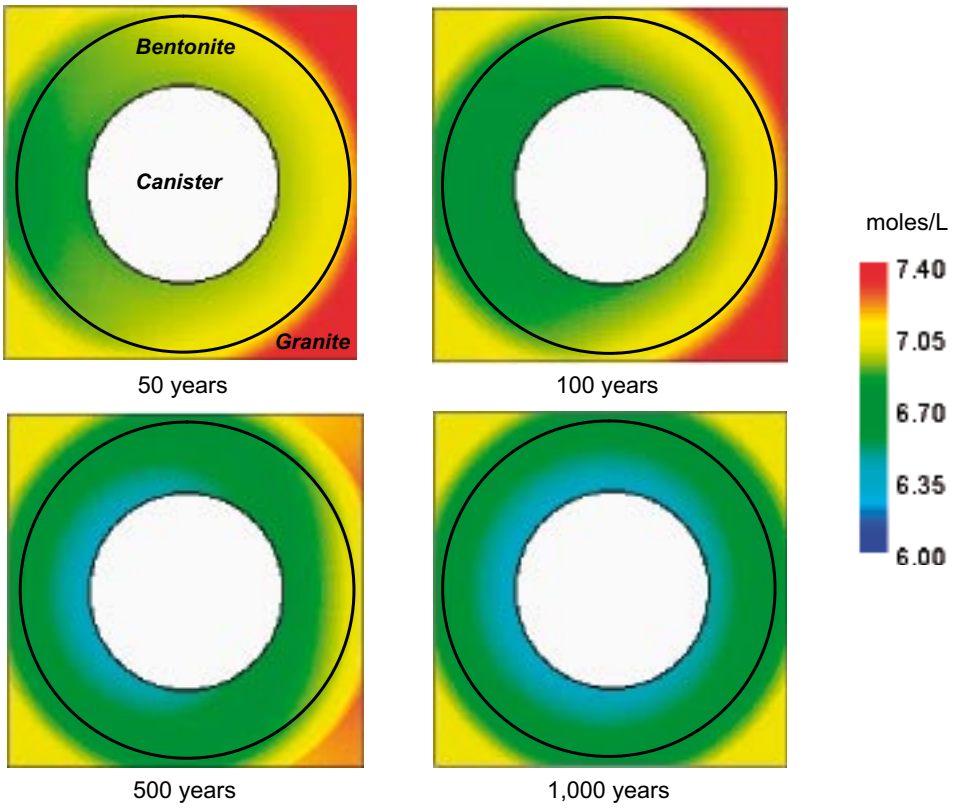

Figure 5-75. *Predicted pH evolution of the system during the thermal stage. Deponit CA-N is used as a bentonite buffer.*

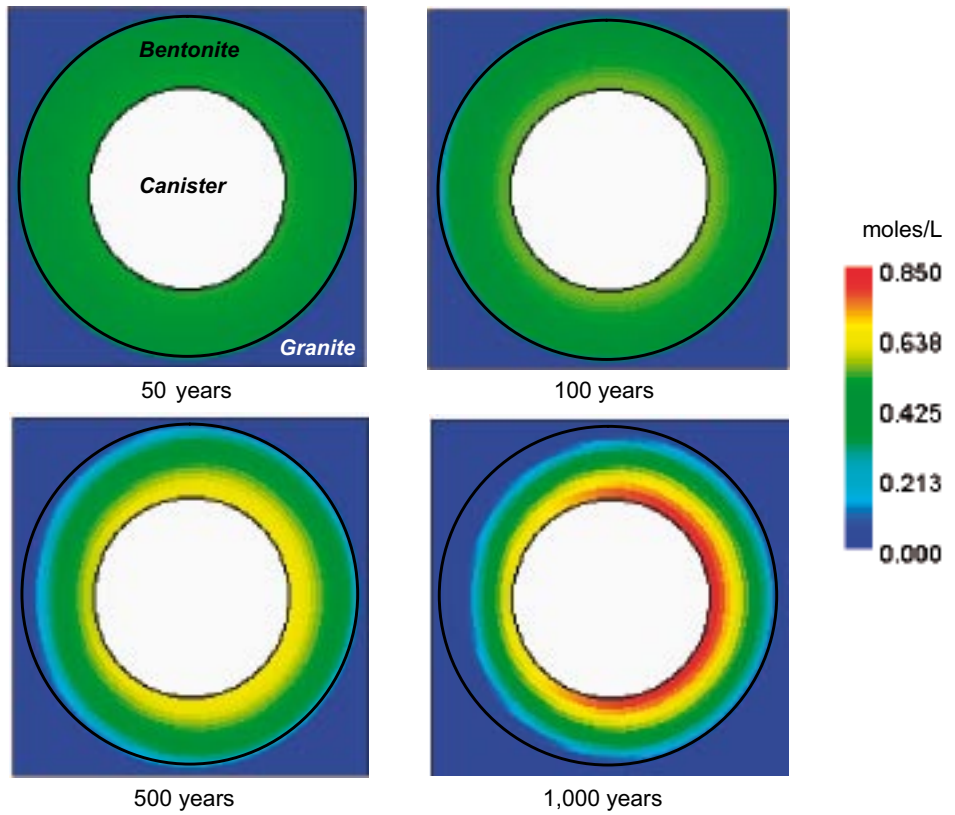

Figure 5-76. *Predicted evolution of anhydrite content in the bentonite buffer during the thermal stage when Deponit CA-N is used as the bentonite buffer.*

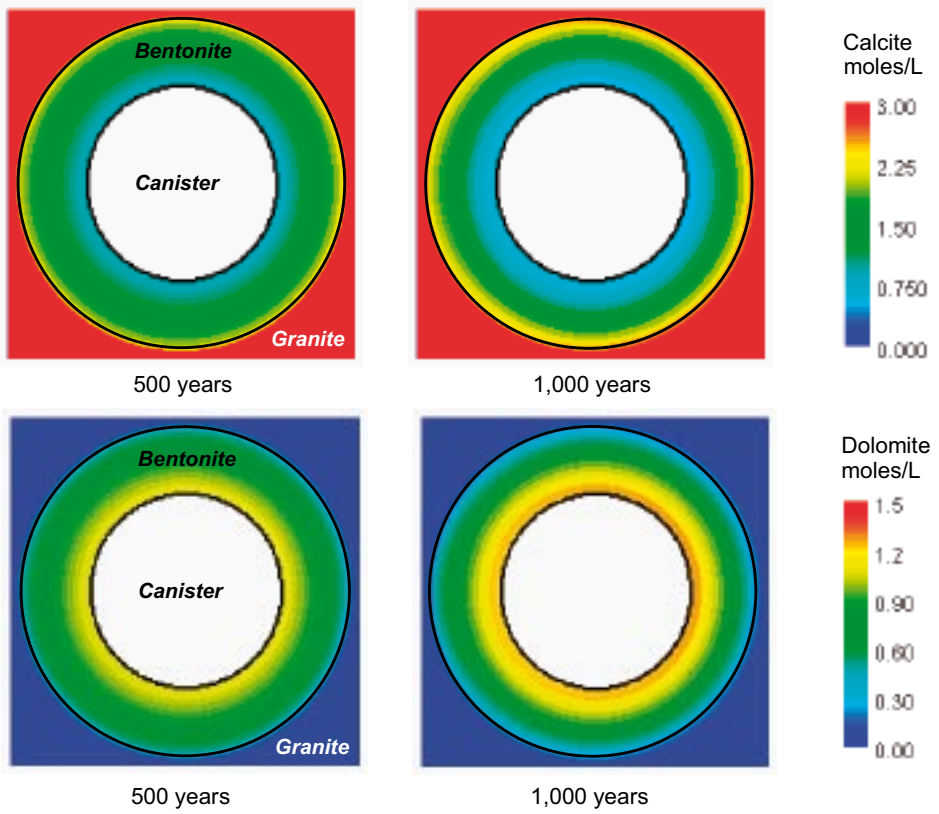

Figure 5-77. *Predicted evolution of calcite (upper graphics) and dolomite (lower graphics) in the bentonite buffer during the thermal stage when Deponit CA-N is used as the bentonite buffer. Note than dolomite replaces calcite close to the canister and the reverse occurs in the cooler part of the system, near the granite-bentonite boundary.*

5.5.4.4 Deponit CA-N bentonite far from the fracture level

The results obtained when considering a section far from any conductive fracture and the Deponit CA-N bentonite as the buffer material, are close to those with MX-80. pH evolution is very similar reaching minimum values in the warmer zones down to 6.85 after 1,000 years of simulation. Such an evolution is caused by coupled replacement between carbonate minerals as occurred in the previous case where a buffer section of Deponit CA-N bentonite was assumed to be close to a conductive fracture. In the cooler zones, calcite dissolves and dolomite and siderite precipitate. Contrary to that, in the warmer zones, calcite replaces dolomite and siderite. The result of this process is a net gain of protons in the pore water, especially at the initial times, and, consequently, a reduction of pH.

The behaviour of anhydrite and quartz is the same as for the case of MX-80 bentonite far from the fracture, where anhydrite is being dissolved from the cooler parts of the system (granite-bentonite boundary) and precipitates at the warmer part of the system (near the canister). Whereas, quartz is predicted to have a reverse behaviour, dissolving from the warmer part of the system and precipitating near the granite-bentonite boundary.

5.5.5 Final remarks of CASE-III

The most relevant results of CASE-III simulations are the following:

- A very different behaviour is predicted when comparing the evolution of the section close to the hydraulic conductive fracture in the granite and the section far from the fracture (no influence of granitic groundwater).
- No significant differences have been predicted ob the basis of different bentonite type considered as buffer material.
- pH is predicted to decrease in the warmer parts of the bentonite buffer (close to canister). This decrease is more pronounced in the section close to the fracture (pH = 6.35), despite the bentonite type considered as the buffer material.
- pH is controlled by the precipitation of carbonate minerals in the bentonite, which is more significant close to the canister (warmer part) and in the section close to the fracture.
- Gypsum transforms in anhydrite, a more stable phase at the temperatures considered in the system. During the simulation, anhydrite dissolves from the outer part of the bentonite and precipitates in the warmer part. However, when groundwater can contact the bentonite buffer, calcium and sulphate diffuse out of the buffer, enhancing the complete dissolution of anhydrite.
- Ca by Na replacement in the exchanger is enhanced by calcium availability due to anhydrite dissolution.
- Silica phases (i.e. quartz) dissolves from the warmer part of the system (close to canister) and precipitates in the outer rim of the bentonite.

6 Conclusions

The modelling results indicate that the interaction of present-day groundwater with the bentonite buffer has minor effects on the pH evolution of the system, despite the type of bentonite considered in the model (MX-80 or Deponit CA-N). The pH buffering capacity is exerted by carbonate minerals if they are present. Whereas in the case that carbonate minerals are not present in the bentonite, pH is then controlled by surface acidity reactions in the clay fraction, although the buffering capacity is not as strong as the equilibrium with carbonate minerals. The redox state of the system seems to be controlled by the regional groundwater, which is in equilibrium with pyrite and siderite.

The most relevant changes predicted are the increase in calcium occupancy in the cation exchanger of the bentonite and the dissolution of gypsum. In addition, in the presence of carbonate minerals the dissolution-precipitation behaviour of these minerals depends on the competition between the in-diffusion of calcium and the out-diffusion of aqueous carbonate in the bentonite. However, minor dissolution or precipitation occurs when considering the interaction with present-day Forsmark groundwater.

The intrusion of high-salinity water into the system has no significant effect on the pH evolution. However, changes in the cation exchange occupancy, and carbonate minerals and gypsum dissolution-precipitation differs from the reference case due to the highest concentration of calcium in the high-salinity water when compared with present-day groundwater.

The most significant changes in the evolution of the system are predicted when an ice-melting derived water, which is very diluted and alkaline, enters into the system. Then the dissolution of carbonate minerals is enhanced, increasing pH in the bentonite pore water. However, if no carbonate minerals are present in the bentonite (reference composition of the MX-80 bentonite), then surface acidity reactions have a certain pH buffer capacity, minimising the pH increase due to the interaction with the ice-melting water. In addition, the intrusion of this type of water enhances the dissolution of gypsum and the calcium occupancy in the exchanger of the bentonite. The last effect is due to the fast out-diffusion of sodium from the bentonite.

The variation in pH due to the intrusion of ice-melting water is less important if groundwater flows through the backfill before reaching the bentonite buffer instead of directly contacting the buffer through an existing hydraulically conductive fracture intersecting the deposition hole. The reason for this effect is that the backfill exerts an additional buffering capacity on the water composition previously to contact the bentonite buffer.

Finally, the effect of a thermal gradient in the system, results in a general decrease of pH, although there is not acidification of the system, as the neutral pH decreases as temperature increases. This effect is more pronounced when direct contact with regional groundwater is allowed (i.e. section close to a hydraulic conductive fracture intersecting the deposition hole). However, the high temperature results in the precipitation of calcite and hematite in the buffer. However, one of the important effects due to the thermal gradient is the dissolution of some accessory minerals in certain parts of the buffer and their precipitation in other parts. The most important of these dissolution-precipitation effects is that of anhydrite and silica phases. Anhydrite dissolves in the outer cooler rim of bentonite and precipitates in the warmer part, close to the canister, whereas silica phases follow the opposite behaviour, dissolving from the inner part of the bentonite and precipitating in the outer rim.

7 References

Allison J D, Brown D V, Novo-Gradac K J, 1991. MINTEQA2/ PRODEFA2. A geochemical assessment model for environmental systems: version 3.0 user's manual. EPA/600/3-91/021.

Arcos D, Bruno J, Karnland O, 2003. Geochemical model of the granite–bentonite–groundwater interaction at Äspö HRL (LOT experiment). Applied Clay Science, 23/1-4: 219–228.

Bein A, Arad A, 1992. Formation of saline groundwaters in the Baltic region through freezing of seawater during glacial periods. Journal of Hydrology, 140, 75–87.

Benbow S, Savage D, Wersin P, Johnson L H, 2000. Modelling thermal alteration of bentonite barriers in Opalinus Clay. Silica migration-SiO_2 and smectite kinetics, NAGRA internal report.

Börgesson L, Fälth B, 2004. Water saturation phase of the tunnel backfill in the KBS-3V concept and its influence on the wetting of the buffer. Preliminary Report. Clay Technology AB. June 2004.

Bradbury M H, Baeyens B, 2002. Pore water chemistry in compacted re-saturated MX-Bentonite. Physico-chemical characterisation and geochemical modelling. PSI Bericht, Nr. 02–10.

Bruno J, Arcos D, Duro L, 1999. Processes and features affecting the near field hydrochemistry. Groundwater-bentonite interaction. SKB TR-99-29, Svensk Kärnbränslehantering AB.

Cama J, Ganor J, Ayora C, Lasaga A C, 2000. Smectite dissolution kinetics at 80°C and pH 8.8. Geochimica et Cosmochimica Acta, 64, 2701–2717.

Carlson L, 2004. Bentonite Mineralogy. Part 1: Methods of investigation – a literature review. Part2: Mineralogical research of selected bentonites. POSIVA Working Report 2004-02.

Dershowitz W, Winberg A, Hermansson J, Byegard J, Tullborg E-L, Andersson P, Mazurek M, 2003. Äspö Hard Rock Laboratory. Äspö Task Force on modelling of groundwater flow and transport of solutes. Task 6C. A semi-synthetic model of block scale conductive structures at the Äspö HRL. SKB IPR-03-13, Svensk Kärnbränslehantering AB.

Domènech C, Arcos D, Bruno J, Karnland O, Muurinen A, 2004. Geochemical model of the granite-bentonite-groundwater at Äspö (LOT experiment). Mat. Res. Soc. Symp. Proc., 807: 855–859.

Falck W E, Read D, Thomas J B, 1996. Chemval 2. Thermodynamic database EUR16897 EN.

Gunnarsson D, Börgesson L, Keto P, Tolppanen P, Hansen J, 2004. Backfilling and closure of the deep repository. Assessment of backfill concepts. SKB R-04-53, Svensk Kärnbränslehantering AB.

Hartley L, Cox I, Holton D, Hunter F, Joyce S, Gylling B, Lindgren M, 2004. Groundwater flow and radionuclide transport modelling using CONNECTFLOW in support of the SR Can assessment. SKB R-04-61, Svensk Kärnbränslehantering AB.

Hoehn E, Eikenberg J, Fierz T, Drost W, Reichlmayr E, 1998. The Grimsel Migration Experiment: field injection-withdrawal experiments in fractured rock with sorbing tracers. Journal of Contaminant Hydrology, 34, 85–106.

Huertas F J, Caballero E, Jiménez de Cisneros C, Huertas F, Linares J, 2001. Kinetics of montmorillonite dissolution in granitic solutions. Applied Geochemistry, 16 (4), 397–407.

Jacobsson A, Pusch R, 1978. Egenskaper hos bentonitbaserat buffermaterial. KBS TR 32, Svensk Kärnbränslehantering AB.

Johannesson L-E, Nilsson U, 2006. Geotechnical properties of candidate backfill material for the deep repository, SKB TR (in prep.), Svensk Kärnbränslehantering AB.

Johnson J, 2000. Llnl.dat Lawrence Livermore National Laboratory thermodynamic database.

Karnland O, 1995. Salt redistribution and enrichment in compacted bentonite exposed to a thermal gradient. SKB AR-95-31, Svensk Kärnbränslehantering AB.

Karnland O, Sandén T, Johannesson L E, Erikssen T, Jansson M, Wold S, Pedersen K, Motamedi M, Rosborg B, 2000. Long Term test buffer material. Final report on the pilot parcels. SKB TR-00-22, Svensk Kärnbränslehantering AB.

Kipp K L, 1997. Guide to the revised heat and solute transport simulator, HST3D-version 2. U.S. Geological Survey Water Resources Investigations report 97-4157, 149 pp.

Laaksoharju M, Smellie J, Nilsson A C, Skårman C, 1995. Groundwater sampling and chemical characterisation of the Laxemar deep borehole KLX02. SKB TR-95-05, Svensk Kärnbränslehantering AB.

Laaksoharju M, 1999. Groundwater characterisation and modelling: problems, facts and possibilities. SKB TR-99-42, Svensk Kärnbränslehantering AB.

Laaksoharju M, Gimeno M, Auqué L, Gómez J, Smellie J, Tullborg E-L, Gurban I, 2004. Hydrogeochemical evaluation of the Forsmark site, model version, 1.1. SKB R-04-05, Svensk Kärnbränslehantering AB.

Lindgren M, Lindström F, 1999. SR-97. Radionuclide transport calculations. SKB TR-99-23, Svensk Kärnbränslehantering AB.

Ludvigson J-E, Jönsson S, 2003. Forsmark site investigation. Hydraulic interference test. Boreholes HFM01, HFM02 and HFM03. SKB P-03-35, Svensk Kärnbränslehantering AB.

Moreno L, Gylling B, 1998. Equivalent flow rate concept in near field transport model COMP23, SKB R-98-53, Svensk Kärnbränslehantering AB.

Nordman C, 2003. Forsmark site investigation. Boremap mapping of percussion boreholes HFM01-03. SKB P-03-20, Svensk Kärnbränslehantering AB.

Ochs M, Lothenbach B, Wanner H, Sato H, Yui M, 2001. An integrated sorption-diffusion model for the calculation of consistent distribution and diffusion coefficients in compacted bentonite. Journal of Contaminant Hydrology, 47, 283–296.

Ochs M, Talerico C, 2004. SR-Can. Data and uncertainty assessment. Migration parameters for the bentonite buffer in the KBS-3 concept. SKB TR-04-18, Svensk Kärnbränslehantering AB.

Ochs M, 2006. SR-Can. Data and uncertainty assessment. Migration parameters for a backfill of Friedland Clay in the KBS-3 concept. SKB TR (in prep.), Svensk Kärnbränslehantering AB.

Parkhurst D L, Appelo C A J, 1999. User's guide to PHREEQC (version 2) – A computer program for speciation, batch-reaction, one-dimensional transport and inverse geochemical calculations. U.S. Geological Survey Water Resources investigations report 99-4259.

Parkhurst D L, Kipp K L, Engesgaard P, Charlton S R, 2004. PHAST – A program for simulating ground-water flow, solute transport, and multicomponent geochemical reactions. U.S. Geological Survey, Techniques and Methods 6-A8, 154 pp.

Pedersen K, 2000. Microbial processes in radioactive waste disposal. SKB TR-00-04, Svensk Kärnbränslehantering AB.

Petersson J, Berglund J, Danielsson P, Wängnerud A, Tullborg E-L, Mattsson H, Thunehed H, Isaksson H, Lindroos H, 2004. Forsmark site investigation. Petrography, geochemistry, petrophysics and fracture mineralogy of boreholes KFM01A, KFM02A and KFM03A+B. SKB P-04-103, Svensk Kärnbränslehantering AB.

Pusch R, 1998. Backfilling with mixtures of bentonite/ballast materials or natural smectitic clay? SKB TR-98-16, Svensk Kärnbränslehantering AB.

Pusch R, Schomburg J, 1999. Impact of microstructure on the hydraulic conductivity of undisturbed and artificially prepared smectitic clay. Engineering Geology, 54, 167–172.

Pusch R, 2001. Experimental study of the effect of high porewater salinity on the physical properties of a natural smectitic clay. SKB TR-01-07, Svensk Kärnbränslehantering AB.

Pusch R, Zwahr H, Gerber R, Schomburg J, 2003. Interaction of cement and smectitic clay – theory and practice. Applied Clay Science, 23, 203–210.

Sandström B, Savolainen M, Tullorg E-L, 2004. Forsmark site investigation. Fracture mineralogy. Results from fracture minerals and wall rock alteration in boreholes KFM01A, KFM02A, KFM03A and KFM03B. SKB P-04-149, Svensk Kärnbränslehantering AB.

SKB, 1999. Deep repository for spent nuclear fuel; SR 97 – Post Closure safety; Main report. SKB TR-99-06, Svensk Kärnbränslehantering AB.

SKB, 2002. Forsmark – site descriptive model version 0. SKB R-02-32, Svensk Kärnbränslehantering AB.

SKB, 2004a. Preliminary site description. Forsmark area-version 1.1. SKB R-04-15, Svensk Kärnbränslehantering AB.

SKB, 2004b. Interim main report of the safety assessment SR-Can. SKB TR-04-11, Svensk Kärnbränslehantering AB.

SKB, 2004c. Interim process report for the safety assessment SR-Can. SKB R-04-33, Svensk Kärnbränslehantering AB.

SKB, 2004d. Interim initial state report for the safety assessment SR-Can. SKB R-04-35, Svensk Kärnbränslehantering AB.

SKB, 2006. Preliminary assessment of long-term safety for KBS-3 repositories at Forsmark and Laxemar. Main Report of the SR-Can project. SKB TR (in prep.), Svensk Kärnbränslehantering AB.

Stephens M B, Bergman T, Andersson J, Hermansson T, Wahlgren C-H, Albrecht L, Mikko H, 2003. Bedrock mapping. Stage 1 (2002) – Outcrop data including fracture data. SKB P-03-09, Svensk Kärnbränslehantering AB.

Stumm W, Morgan J J, 1981. Aquatic chemistry, 2nd ed., Wiley-Interscience, New York.

Stumm W, 1992. Chemistry of the solid-water interface. Processes at the mineral-water and particle-water interface in natural systems. John Wiley & Sons.

Westman P, Wastegård S, Schoning K, Gustafsson B, Omstedt A, 1999. Salinity change in the Baltic sea during the last 8500 years: evidence, causes and models. SKB TR-99-38, Svensk Kärnbränslehantering AB.

Williamson M A, Rimstidt J D, 1994. The kinetics and electrochemical rate-determining step of aqueous pyrite oxidation. Geochimica et Cosmochimica Acta, 58, 5443–5454.

ISSN 1404-0344
CM Digitaltryck AB, Bromma, 2005